Supporting Information for:

Remarkable acceleration of template-directed photodimerisation of 9-phenylethynylanthracene derivatives assisted by complementary salt bridge formation

*Junki Tanabe, Daisuke Taura, Naoki Ousaka and Eiji Yashima**

Department of Molecular Design and Engineering, Graduate School of Engineering, Nagoya University, Chikusa-ku, Nagoya 464-8603, Japan
E-mail: yashima@apchem.nagoya-u.ac.jp (E.Y.)

1. Materials and Instruments

Materials. All starting materials and dehydrated solvents were purchased from Aldrich (Milwaukee, WI), Wako Pure Chemical Industries (Osaka, Japan), and Tokyo Chemical Industry (Tokyo, Japan) unless otherwise noted. Silica gel (SiO_2) and aminopropyl-modified silica gel (NH-SiO_2) for the flash chromatography were purchased from Merck and Fuji Silysia Chemical Ltd. (Kusanagi, Japan), respectively. Compounds $\mathbf{1_M}$,[S1] **C**-H,[S2] **C**-2H,[S2] $\mathbf{T_{AA}}$,[S2] and **A**[S3] were prepared according to the previously reported methods.

Instruments. The melting points were measured using a Yanaco MP-500D melting point apparatus (Kyoto, Japan) and were uncorrected. The NMR spectra were measured on a Varian UNITY INOVA 500AS spectrometer operating at 500 MHz for ^{1}H and 125 MHz for ^{13}C using a Teflon-valved NMR tube (5-mm (i.d.)) (Norell Inc.). Chemical shifts are reported in parts per million (δ) downfield from tetramethylsilane (TMS) in $CDCl_3$ or in benzene-d_6 using a solvent residual peak as the internal standard. The recycling preparative HPLC was performed with an LC-928R liquid chromatograph (Japan Analytical Industry, Tokyo, Japan) equipped with two SEC columns (JAIGEL-1H (1 x 60 cm) and JAIGEL-2H (1 x 60 cm)) in series and a UV-visible detector (254 nm, JAI UV-310), and $CHCl_3$ was used as the eluent. The ESI-MS spectra were recorded on a JEOL JMS-T100CS spectrometer (Akishima, Japan). The matrix-assisted laser desorption/ionisation time-of-flight mass (MALDI-TOF-MS) spectra were taken on a Shimadzu AXIMA-CFR plus spectrometer (Kyoto, Japan) equipped with a 337 nm N_2 laser using 1,8,9-anthracene triol (dithranol) as the matrix. The elemental analyses were performed by the laboratory of elemental analyses in the Department of Agriculture, Nagoya University. The IR

spectra were recorded using a JASCO Fourier Transform IR-680 spectrophotometer (Hachioji, Japan). The absorption and CD spectra were measured in a 0.1-, 1-, or 10-mm quartz cell on a JASCO V-570 spectrophotometer and a JASCO J-820 spectropolarimeter, respectively. The fluorescence spectra were measured in a 10-mm quartz cell on a JASCO FP-6500 spectrofluorometer. The size-exclusion chromatography (SEC) measurements were carried out using a JASCO PU-2080 liquid chromatograph equipped with a UV–Visible (254 nm; JASCO UV-2070) detector. Two Tosoh TSKgel Multipore HXL-M (30 cm) SEC columns (Tosoh, Tokyo, Japan) were connected in series using THF containing tetrabutylammonium bromide (TBAB) (0.1 wt %) as the eluent at a flow rate of 1.0 mL min^{-1}. The single-crystal X-ray data were collected on a Rigaku Saturn 724+ CCD diffractometer with Mo K*a* radiation (λ = 0.71075 Å) at 103 K. The photoirradiation (λ > 400 nm) was performed using a 500 W xenon lamp (Ushio Optical Modulex SX-UI500XQ) through a cut-off filter (SIGMAKOKI Co., Ltd.).

2. Synthetic Procedures

Scheme S1. Synthesis of photodimers ([4+4]-*anti*-**2$_{MM}$** and [4+2]-*anti*-**2$_{MM}$**)

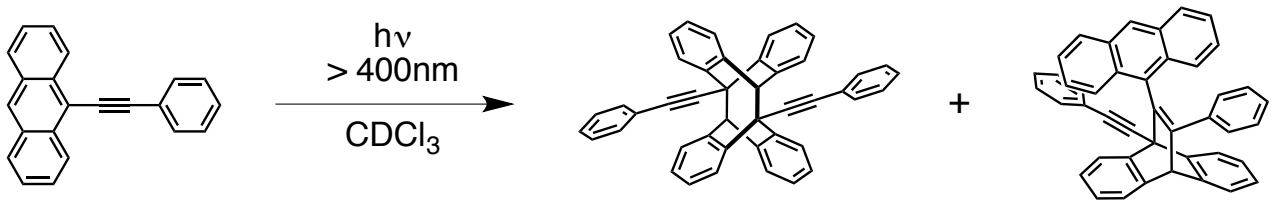

1$_M$ [4+4]-*anti*-**2$_{MM}$** [4+2]-*anti*-**2$_{MM}$**

A solution of **1$_M$** (55.9 mg, 0.201 mmol) in $CDCl_3$ (25 mL) was irradiated with light (> 400 nm) at ambient temperature for 5 h using a cut-off filter. After evaporating the solvent, the residue was recrystallised from CH_2Cl_2 in the presence of methanol to give a mixture of [4+4]-*anti*-**2$_{MM}$** and [4+2]-*anti*-**2$_{MM}$** (30.0 mg), which were further separated by column chromatography (SiO_2, *n*-hexane/$CHCl_3$ = 1/0 to 5/1 (v/v)) into pure [4+4]-*anti*-**2$_{MM}$** (2.5 mg, 4.5% yield) as a white solid and [4+2]-*anti*-**2$_{MM}$** (20.4 mg, 36.5% yield) as a yellow solid, respectively. The structures were determined by single-crystal X-ray analyses (see ***Figs. S3*** and ***S4***, respectively).

[4+4]-*anti*-2$_{MM}$. Mp: 155–157 °C. ^{1}H NMR (500 MHz, $CDCl_3$, 25 °C): δ 7.73 (dd, *J* = 7.9, 1.7 Hz, 4H, ArH), 7.66 (dd, *J* = 7.5, 1.5 Hz, 4H, ArH), 7.47–7.43 (m, 6H, ArH), 7.03 (dd, *J* = 7.5, 1.5 Hz, 4H, ArH), 6.96 (ddd, *J* = 7.5, 7.5, 1.5 Hz, 4H, ArH), 6.90 (ddd, *J* = 7.5, 7.5, 1.5 Hz, 4H, ArH), 4.91 (s, 2H, CH). ^{13}C NMR (125 MHz, $CDCl_3$, 25 °C): δ 142.59, 140.39, 131.91, 128.55, 128.46, 127.95, 126.33, 126.21, 126.06, 123.45, 92.37, 89.14, 64.90, 54.31. IR (KBr, cm^{-1}): 3065 (ν_{ArC-H}), 3018

(ν_{ArC-H}), 1489 (ν_{ArC-C}), 1472 (ν_{ArC-C}), 1453 (ν_{ArC-C}). MALDI-TOF-MS: $[M(C_{44}H_{28})+Na]^+$ (calcd. 579.2): found. 579.0. Anal. Calcd for $C_{44}H_{28}$: C, 94.93; H, 5.07. Found: C, 94.77; H, 5.02.

[4+2]-*anti*-2_{MM}. Mp: 310 °C (dec.). ^{1}H NMR (500 MHz, $CDCl_3$, 25 °C): δ 8.34 (s, 1H, ArH), 7.92 (d, J = 8.5 Hz, 2H, ArH), 7.72 (dd, J = 7.0, 1.0 Hz, 2H, ArH), 7.59 (dd, J = 7.0, 1.0 Hz, 2H, ArH), 7.32–7.29 (m, 2H, ArH), 7.21 (ddd, J = 7.5, 7.0, 1.0 Hz, 2H, ArH), 7.21 (ddd, J = 7.5, 7.0, 1.0 Hz, 2H, ArH), 7.12–6.98 (m, 9H, ArH), 6.90–6.89 (m, 3H, ArH), 6.47 (dd, J = 8.0, 1.0 Hz, 2H, ArH), 5.73 (s, 1H, CH). ^{13}C NMR (125 MHz, $CDCl_3$, 25 °C): δ 148.80, 145.41, 144.77, 144.44, 138.07, 133.00, 131.40, 131.35, 130.63, 128.32, 127.92, 127.80, 127.78, 127.03, 126.89, 126.48, 126.33, 125.57, 125.23, 125.18, 124.98, 122.99, 122.83, 122.64, 91.16, 84.71, 58.41, 56.50. IR (KBr, cm^{-1}): 3053 (ν_{ArC-H}), 1492 (ν_{ArC-C}), 1456 (ν_{ArC-C}), 1442 (ν_{ArC-C}), 1359 (ν_{ArC-C}). UV-vis ($CDCl_3$): λ_{max} (ε [M^{-1} cm^{-1}]) = 395 (8,900), 374 (9,250), 355 (5,630) nm. MALDI-TOF-MS: $[M(C_{44}H_{28})+Na]^+$ (calcd. 579.2): found. 578.9. Anal. Calcd for $C_{44}H_{28}$: C, 94.93; H, 5.07. Found: C, 94.79; H, 4.97.

Scheme S2. Synthesis of endoperoxide ($\mathbf{1_M}$-O_2)

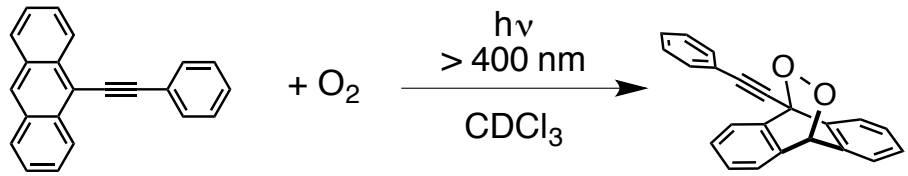

$\mathbf{1_M}$ $\mathbf{1_M}$-O_2

A solution of $\mathbf{1_M}$ (9.1 mg, 0.033 mmol) in $CDCl_3$ (10 mL) was saturated with oxygen by bubbling the gas using a stainless steel needle for 30 min. The solution was then irradiated with light over 400 nm at ambient temperature for 15 min using a cut-off filter. The solvent was removed under reduced pressure to give a mixture of $\mathbf{1_M}$ (10%) and $\mathbf{1_M}$-O_2 (90%) (9.0 mg) as a yellow solid. The spectroscopic data of $\mathbf{1_M}$-O_2 were immediately taken without further purification because $\mathbf{1_M}$-O_2 was not stable and thermally decomposed back to the monomer $\mathbf{1_M}$ (see ***Fig. S7***). Mp: 93–95 °C. ^{1}H NMR (500 MHz, $CDCl_3$, 25 °C): δ 7.81 (d, J = 5.0 Hz, 2H, ArH), 7.73 (d, J = 5.0 Hz, 2H, ArH), 7.47–7.44 (m, 5H, ArH), 7.38–7.34 (m, 4H, ArH), 6.08 (s, 1H, CH). ^{13}C NMR (125 MHz, $CDCl_3$, 25 °C): δ 138.52, 137.44, 132.53, 129.87, 128.73, 128.47, 128.14, 123.55, 122.92, 121.47, 94.93, 80.06, 79.42, 78.42. IR (KBr, cm^{-1}): 3060 (ν_{ArC-H}), 2234 ($\nu_{C\equiv C}$), 1490 (ν_{ArC-C}), 800 (ν_{O-O}). HRMS (ESI): m/z calcd for $[M(C_{22}H_{14}O_2)-H]^-$, 309.0916; found 309.0926.

Scheme S3. Synthesis of carboxylic acid monomer ($\mathbf{1_C}$)

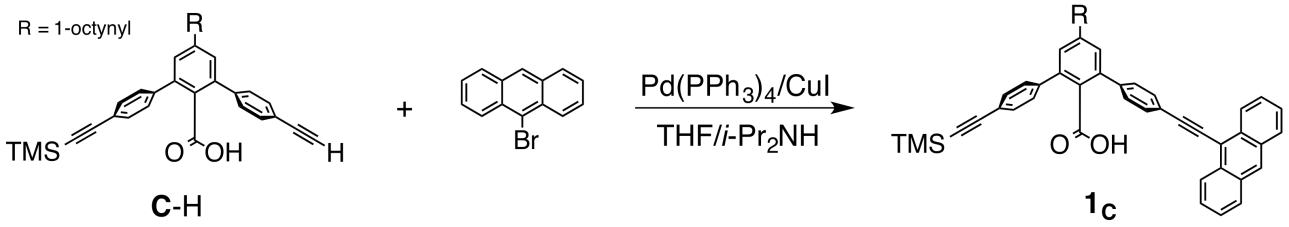

Copper (I) iodide (3.79 mg, 19.9 μmol) was added to a solution of **C**-H (200 mg, 0.398 mmol), 9-bromoanthracene (511 mg, 1.99 mmol), and tetrakis(triphenylphosphine)palladium(0) (23.0 mg, 19.9 μmol) in a THF-diisopropylamine mixture (1/1 (v/v), 15 mL) and the mixture was stirred at 65 °C for 17 h. After evaporating the solvents, the residue was purified by column chromatography (SiO_2, *n*-hexane/EtOAc = 1/0 to 3/1 (v/v)) to give pure $\mathbf{1_C}$ (77.4 mg, 57.3% yield) as a yellow solid. Mp: 98–100 °C. ^{1}H NMR (500 MHz, $CDCl_3$, 25 °C): δ 8.65 (d, J = 8.5 Hz, 2H, ArH), 8.42 (s, 1H, ArH), 8.01 (d, J = 8.5 Hz, 2H, ArH), 7.82 (d, J = 8.5 Hz, 2H, ArH), 7.59–7.56 (m, 2H, ArH), 7.54–7.49 (m, 6H, ArH), 7.45 (d, J = 1.5 Hz, 1H, ArH), 7.41 (d, J = 1.5 Hz, 1H, ArH), 7.37 (d, J = 8.5 Hz, 2H, ArH), 2.43 (t, J = 7.0 Hz, 2H, C≡CCH_2), 1.64–1.59 (m, 2H, CH_2), 1.48–1.44 (m, 2H, CH_2), 1.34–1.31 (m, 4H, CH_2), 0.90 (t, J = 7.0 Hz, 3H, CH_3), 0.25 (s, 9H, TMS). ^{13}C NMR (125 MHz, $CDCl_3$, 25 °C): δ 172.40, 140.28, 140.16, 139.93, 139.88, 132.77, 132.13, 132.08, 132.00, 131.84, 131.28, 130.52, 128.80, 128.77, 128.51, 127.93, 126.92, 126.80, 126.14, 125.81, 123.48, 122.98, 117.24, 104.88, 100.48, 95.56, 93.30, 87.50, 79.62, 31.49, 28.77, 28.70, 22.69, 19.61, 14.22, 0.15. IR (KBr, cm^{-1}): 2157 ($\nu_{C\equiv C}$), 1701 ($\nu_{C=O}$). UV-vis ($CDCl_3$): λ_{max} (ε [$M^{-1}cm^{-1}$]) = 426 (23,700), 404 (26,500), 385 (18,200) nm. HRMS (ESI): m/z calcd for [M($C_{48}H_{42}O_2Si$)−H]$^-$, 677.2876; found 677.2889.

Scheme S4. Synthesis of carboxylic acid photodimers ([4+2]-*anti*-$\mathbf{2_{CC}}$ and [4+4]-*anti*-$\mathbf{2_{CC}}$)

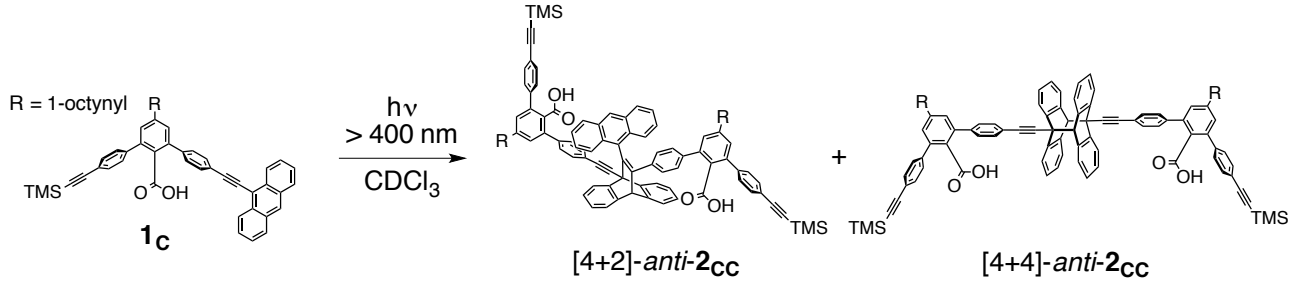

A solution of $\mathbf{1_C}$ (16 mg, 0.024 mmol) in $CDCl_3$ (0.80 mL) was degassed five times by means of freeze-pump out-thaw (nitrogen) cycles, and then irradiated with light (> 400 nm) at 25 °C for

150 min under nitrogen using a cut-off filter. After evaporating the solvent, the residue was purified by column chromatography (SiO_2, *n*-hexane/EtOAc = 1/0 to 10/1 (v/v)) to afford [4+4]-*anti*-$\mathbf{2_{CC}}$ (3.4 mg, 21% yield) and [4+2]-*anti*-$\mathbf{2_{CC}}$ (9.7 mg, 61% yield), respectively, as yellow solids.

[4+4]-*anti*-$\mathbf{2_{CC}}$. Mp: 98–100 °C. ^{1}H NMR (500 MHz, $CDCl_3$, 25 °C): δ 7.77 (d, J = 8.5 Hz, 4H, ArH), 7.66 (d, J = 7.5 Hz, 4H, ArH), 7.54–7.50 (m, 10H, ArH), 7.46 (d, J = 1.4 Hz, 2H, ArH), 7.42 (d, J = 1.4 Hz, 2H, ArH), 7.39 (d, J = 8.0 Hz, 4H, ArH), 7.03 (d, J = 7.5 Hz, 4H, ArH), 6.97–6.94 (m, 4H, ArH), 6.90–6.88 (m, 4H, ArH), 4.91 (s, 2H, CH), 2.44 (t, J = 7.0 Hz, 4H, C≡CCH_2), 1.64–1.60 (m, 4H, CH_2), 1.49–1.43 (m, 4H, CH_2), 1.34–1.32 (m, 8H, CH_2), 0.91 (t, J = 7.0 Hz, 6H, CH_3), 0.26 (s, 18H, TMS). ^{13}C NMR (125 MHz, $CDCl_3$, 25 °C): δ 170.26, 142.59, 140.43, 140.34, 140.32, 139.95, 139.92, 132.19, 132.07, 130.23, 128.80, 128.53, 128.10, 126.50, 126.37, 126.22, 126.15, 123.23, 123.02, 117.24, 104.82, 95.48, 93.47, 93.40, 88.91, 79.62, 65.00, 54.43, 31.50, 28.79, 28.71, 22.70, 19.64, 14.22, 0.14. IR (KBr, cm^{-1}): 2157 ($\nu_{C\equiv C}$), 1702 ($\nu_{C=O}$). HRMS (ESI): m/z calcd for $[M(C_{96}H_{84}O_4Si_2)-H]^-$, 1355.5830; found 1355.5815.

[4+2]-*anti*-$\mathbf{2_{CC}}$. Mp: 159–161 °C. ^{1}H NMR (500 MHz, $CDCl_3$, 25 °C): δ 8.31 (s, 1H, ArH), 7.89 (d, J = 8.5 Hz, 2H, ArH), 7.73 (d, J = 7.0 Hz, 2H, ArH), 7.60 (d, J = 7.0 Hz, 2H, ArH), 7.45 (d, J = 8.0 Hz, 2H, ArH), 7.42 (d, J = 8.0 Hz, 2H, ArH), 7.32–7.26 (m, 5H, ArH), 7.25–7.20 (m, 6H, ArH), 7.19–7.15 (m, 2H, ArH), 7.13 (d, J = 1.5 Hz, 1H, ArH), 7.10–7.00 (m, 6H, ArH), 6.97 (d, J = 8.5, 2H, ArH), 6.90 (d, J = 8.5, 2H, ArH), 6.48 (d, J = 8.0, 2H, ArH), 5.78 (s, 1H, CH), 2.41 (t, J = 7.0 Hz, 2H, C≡CCH_2), 2.33 (t, J = 7.0 Hz, 2H, C≡CCH_2), 1.61–1.57 (m, 2H, CH_2), 1.55–1.50 (m, 2H, CH_2), 1.45–1.34 (m, 4H, CH_2), 1.33–1.24 (m, 8H, CH_2), 0.90 (t, J = 7.0 Hz, 3H, CH_3), 0.87 (t, J = 7.0 Hz, 3H, CH_3), 0.25 (s, 9H, TMS), 0.23 (s, 9H, TMS). ^{13}C NMR (125 MHz, $CDCl_3$, 25 °C): δ 169.98, 169.58, 148.59, 145.33, 145.21, 144.75, 140.31, 140.23, 140.18, 139.94, 139.29, 138.30, 137.65, 132.92, 132.12, 132.04, 131.95, 131.86, 131.63, 131.49, 130.68, 130.14, 130.09, 128.54, 128.46, 128.44, 128.05, 126.97, 126.88, 126.41, 125.59, 125.78, 125.74, 125.45, 125.37, 125.08, 123.20, 122.95, 122.89, 122.77, 122.36, 104.87, 104.83, 95.38, 95.25, 93.21, 92.92, 91.02, 85.81, 79.58, 79.55, 76.59, 58.57, 56.20, 31.49, 31.45, 29.52, 28.77, 28.71, 28.65, 19.59, 19.52, 14.22, 14.19, 0.14. IR (KBr, cm^{-1}): 2157 ($\nu_{C\equiv C}$), 1701 ($\nu_{C=O}$). UV-vis ($CDCl_3$): λ_{max} (ε [M^{-1} cm^{-1}]) = 396 (10,100), 376 (10,100), 356 (7,500) nm. HRMS (ESI): m/z calcd for $[M(C_{96}H_{84}O_4Si_2)-H]^-$, 1355.5830; found 1355.5865.

Scheme S5. Synthesis of carboxylic acid monomer ($\mathbf{3_C}$)

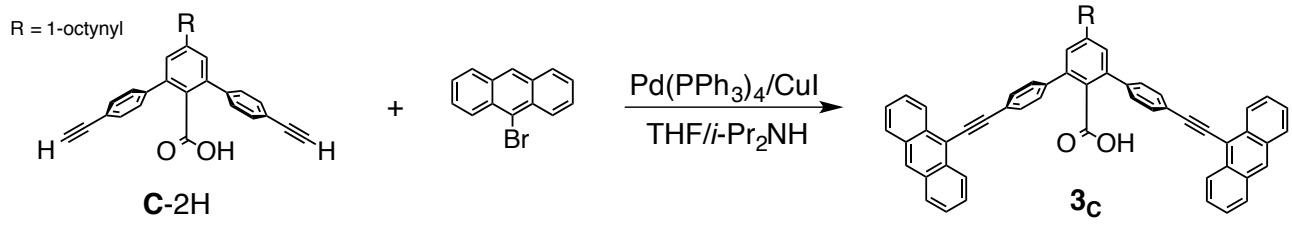

C-2H $\qquad\qquad$ $\mathbf{3_C}$

Copper (I) iodide (4.57 mg, 24.0 μmol) was added to a solution of **C**-2H (100 mg, 0.232 mmol), 9-bromoanthracene (309 mg, 1.20 mmol), and tetrakis(triphenylphosphine)palladium(0) (27.7 mg, 24.0 μmol) in a THF-diisopropylamine mixture (1/1 (v/v), 10 mL) and the mixture was stirred at 70 °C for 13 h. After evaporating the solvents, the residue was purified by column chromatography (SiO_2, *n*-hexane/EtOAc = 1/0 to 3/1 (v/v)) and preparative recycling HPLC ($CHCl_3$) to give pure $\mathbf{3_C}$ (74.0 mg, 39.4% yield) as a yellow solid. Mp: 218–220 °C. ^{1}H NMR (500 MHz, $CDCl_3$, 25 °C): δ 8.61 (d, J = 8.5 Hz, 4H, ArH), 8.37 (s, 2H, ArH), 7.99 (d, J = 8.5 Hz, 4H, ArH), 7.84 (d, J = 8.0 Hz, 4H, ArH), 7.56–7.53 (m, 8H, ArH), 7.50–7.47 (m, 6H, ArH), 2.45 (t, J = 7.0 Hz, 2H, C≡CCH_2), 1.67–1.61 (m, 2H, CH_2), 1.50–1.44 (m, 2H, CH_2), 1.35–1.32 (m, 4H, CH_2), 0.91 (t, J = 7.0 Hz, 3H, CH_3). ^{13}C NMR (125 MHz, $CDCl_3$, 25 °C): δ 170.87, 140.35, 139.94, 132.76, 132.20, 131.89, 131.27, 130.34, 128.85, 128.81, 127.92, 126.86, 126.76, 126.28, 125.81, 123.56, 117.22, 100.45, 93.41, 87.51, 79.66, 31.52, 28.80, 28.73, 22.71, 19.66, 14.23. IR (KBr, cm^{-1}): 2170 ($\nu_{C\equiv C}$), 1700 ($\nu_{C=O}$). UV-vis ($CDCl_3$): λ_{max} (ε [M^{-1} cm^{-1}]) = 427 (45,000), 405 (48,300), 388 (32,000) nm. HRMS (ESI): m/z calcd for $[M(C_{59}H_{42}O_2)-H]^-$, 781.3107; found 781.3102.

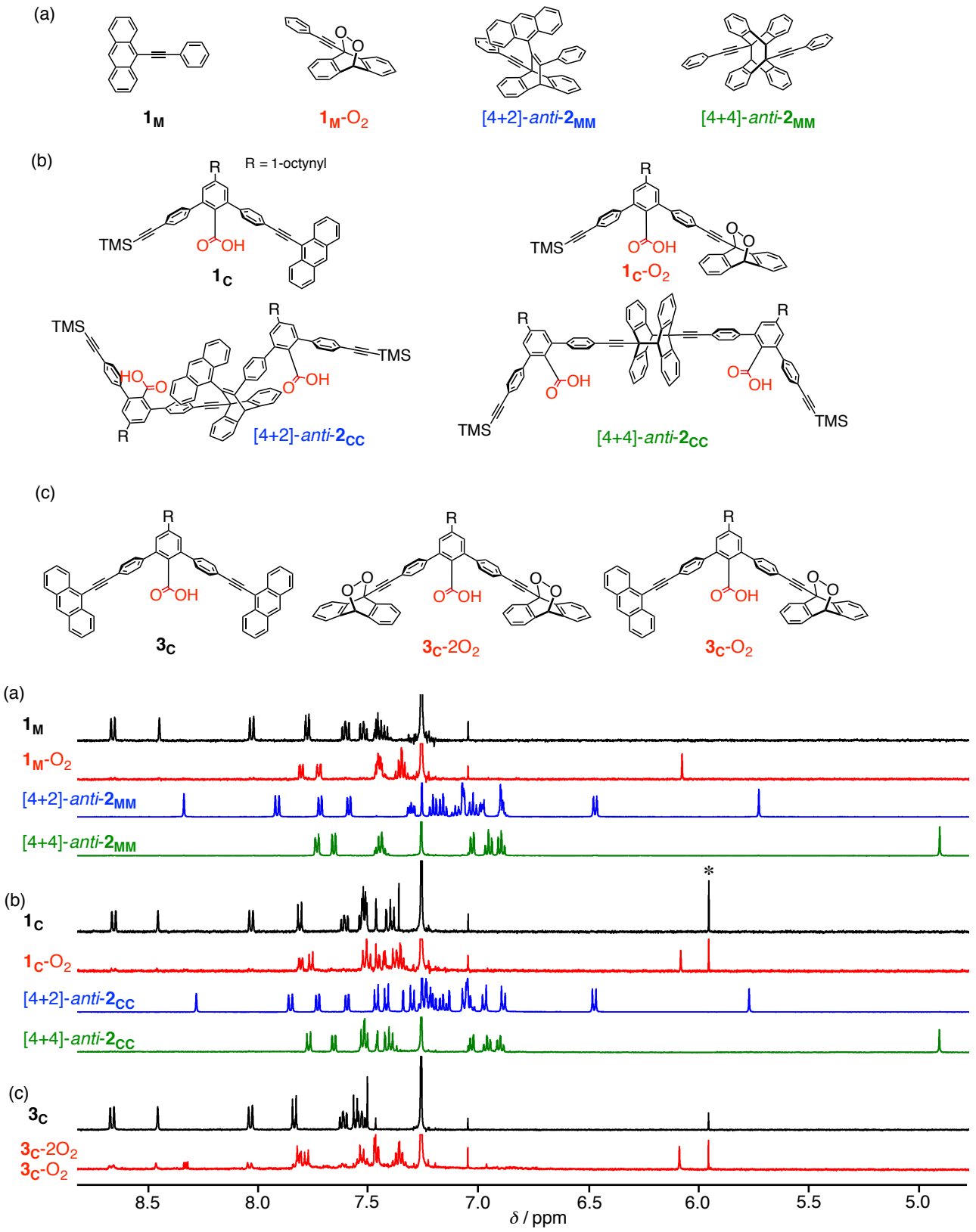

Fig. S1. ^{1}H NMR spectra of (a) $\mathbf{1}_{\mathbf{M}}$ (0.50 mM), $\mathbf{1}_{\mathbf{M}}$-O_2 (0.45 mM), [4+2]-*anti*-$\mathbf{2}_{\mathbf{MM}}$ (5.0 mM), [4+4]-*anti*-$\mathbf{2}_{\mathbf{MM}}$ (1.5 mM), (b) $\mathbf{1}_{\mathbf{C}}$ (0.50 mM), $\mathbf{1}_{\mathbf{C}}$-O_2 (0.45 mM), [4+2]-*anti*-$\mathbf{2}_{\mathbf{CC}}$ (4.6 mM), [4+4]-*anti*-$\mathbf{2}_{\mathbf{CC}}$ (0.32 mM), (c) $\mathbf{3}_{\mathbf{C}}$ (0.50 mM) and a mixture of $\mathbf{3}_{\mathbf{C}}$-$2O_2$ and $\mathbf{3}_{\mathbf{C}}$-O_2 (0.25 mM) in $CDCl_3$ at 25 °C. ∗ denotes the peak of 1,1,2,2-tetrachloroethane used as an internal standard.

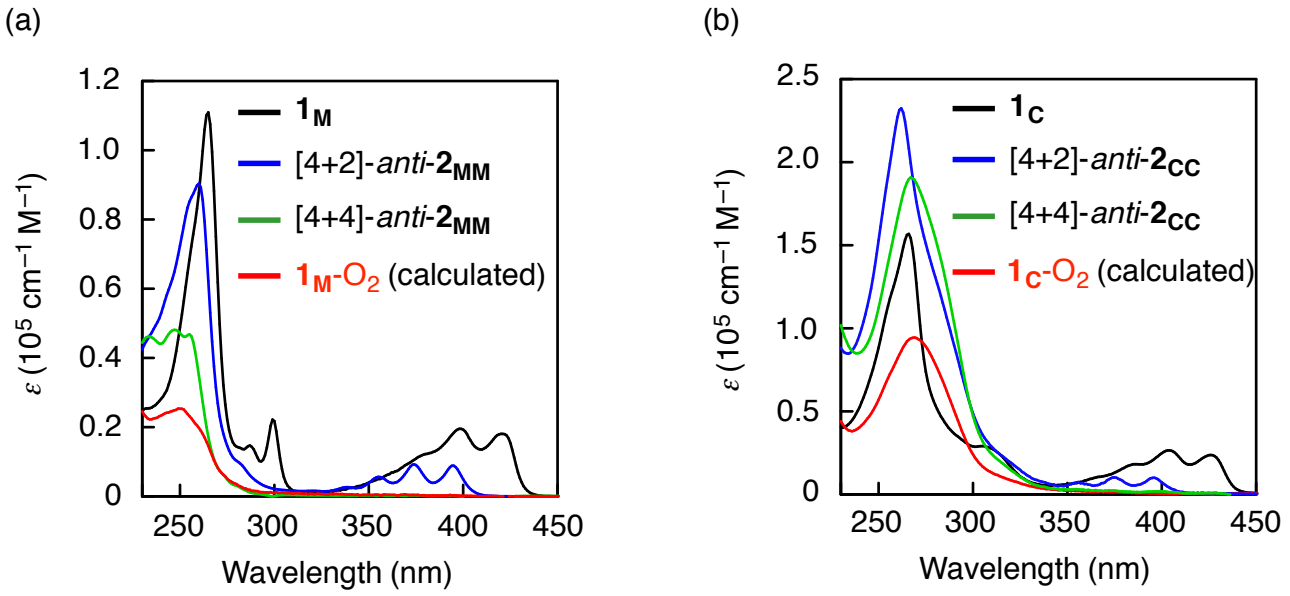

Fig. S2. Absorption spectra of (a) $\mathbf{1}_{\mathbf{M}}$ (0.50 mM), [4+2]-*anti*-$\mathbf{2}_{\mathbf{MM}}$ (0.19 mM), [4+4]-*anti*-$\mathbf{2}_{\mathbf{MM}}$ (0.11 mM), $\mathbf{1}_{\mathbf{M}}$-O_2 (calculated, 0.45 mM), (b) $\mathbf{1}_{\mathbf{C}}$ (0.50 mM), [4+2]-*anti*-$\mathbf{2}_{\mathbf{CC}}$ (0.45 mM), [4+4]-*anti*-$\mathbf{2}_{\mathbf{CC}}$ (0.32 mM), and $\mathbf{1}_{\mathbf{C}}$-O_2 (calculated, 0.45 mM) in $CDCl_3$ at ambient temperature. The absorption spectra of $\mathbf{1}_{\mathbf{M}}$-O_2 and $\mathbf{1}_{\mathbf{C}}$-O_2 were calculated based on the absorption spectra of $\mathbf{1}_{\mathbf{M}}$ and $\mathbf{1}_{\mathbf{C}}$ which remained unreacted (ca. 10%) whose contribution were subtracted from the observed spectra of a mixture of $\mathbf{1}_{\mathbf{M}}$ (0.05 mM) and $\mathbf{1}_{\mathbf{M}}$-O_2 (0.45 mM) (see ***Fig. S6b***) and a mixture of $\mathbf{1}_{\mathbf{C}}$ (0.05 mM) and $\mathbf{1}_{\mathbf{C}}$-O_2 (0.45 mM) (see ***Fig. S16b***), respectively.

3. General Procedures of Photoirradiation

3-1. Photoreaction in Undegassed Solution. A typical experimental procedure: Stock solutions of $\mathbf{1_M}$ (8.0 mM; solution I) and 1,1,2,2-tetrachloroethane (5.2 mM; solution II) in dry $CDCl_3$ were prepared. Aliquots of solutions I (0.40 μmol, 50 μL) and II (0.26 μmol, 50 μL), and dry $CDCl_3$ (700 μL) were added into a Teflon-valved NMR tube (5-mm (i.d.)) by a syringe. The solution was then irradiated with light (> 400 nm) at 25 °C for 180 s using a cut-off filter. The reaction progress was monitored by ^{1}H NMR spectroscopy (***Fig. S6a***).

3-2. Photoreaction in Degassed Solution. A typical experimental procedure: Stock solutions of $\mathbf{1_M}$ (8.0 mM; solution I) and 1,1,2,2-tetrachloroethane (7.6 mM; solution II) in dry $CDCl_3$ were prepared. Aliquots of solutions I (0.40 μmol, 50 μL) and II (0.38 μmol, 50 μL), and dry $CDCl_3$ (700 μL) were added into a Teflon-valved NMR tube (5-mm (i.d.)) by a syringe. The solution was degassed five times by means of freeze-pump out-thaw (nitrogen) cycles, and then irradiated with light (> 400 nm) at 25 °C for 30 min under nitrogen using a cut-off filter. The reaction progress was monitored by ^{1}H NMR spectroscopy (***Fig. S11a***).

3-3. Isolation of [4+2]-*anti*-$\mathbf{2_{CC}}$ and [4+4]-*anti*-$\mathbf{2_{CC}}$. A mixture of $\mathbf{1_C}$ (0.50 mM) and **A** (0.50 mM) in degassed $CDCl_3$ (0.80 mL) was irradiated with light (> 400 nm) for 90 min using a cut-off filter at 25 °C. The ^{1}H NMR spectral changes were shown in ***Fig. S22a***. After evaporating the solvent, the residue was purified by column chromatography (NH-SiO_2, *n*-hexane/EtOAc/AcOH = 1/1/0 to 1/1/0.1 (v/v/v)) to afford a mixture of carboxylic acids ($\mathbf{1_C}$, [4+2]-*anti*-$\mathbf{2_{CC}}$, and [4+4]-*anti*-$\mathbf{2_{CC}}$) and the monomeric amidine (**A**). The mixture was then dissolved in $CHCl_3$ (5 mL) and the solution was washed with 1 M HCl (5 mL) and evaporated to dryness and the ^{1}H NMR spectrum of the residue was measured in $CDCl_3$ (1 mL) to estimate a ratio of the photodimers ([4+2]-*anti*-$\mathbf{2_{CC}}$/[4+4]-*anti*-$\mathbf{2_{CC}}$) as shown in ***Fig. S22b***.

3-4. Isolation of [4+2]-*anti*-$\mathbf{4_{CC}}$ and [4+4]-*anti*-$\mathbf{4_{CC}}$. A mixture of $\mathbf{3_C}$ (0.50 mM) and $\mathbf{T_{AA}}$ (0.25 mM) in degassed $CDCl_3$ (0.80 mL) was irradiated with light (> 400 nm) for 120 s using a cut-off filter at 25 °C. The ^{1}H NMR spectral changes were shown in ***Fig. S36a***. After evaporating the solvent, the residue was purified by column chromatography (NH-SiO_2, $CHCl_3$/MeOH/AcOH = 50/1/0 to 10/1/0.1 (v/v/v)) to afford a mixture of carboxylic acids and the amidine template ($\mathbf{T_{AA}}$). The carboxylic acid mixtures were then dissolved in $CHCl_3$ (5 mL) and the solution was washed with 1 M HCl (5 mL) and evaporated to dryness. The ^{1}H NMR spectrum of the residue was measured in $CDCl_3$ (1 mL) to estimate a ratio of the photodimers ([4+2]-*anti*-$\mathbf{4_{CC}}$/[4+4]-*anti*-$\mathbf{4_{CC}}$) as shown in ***Fig. S37g***.

4. X-ray Crystallographic Data

Crystallographic Data of [4+4]-*anti*-$\mathbf{2_{MM}}$. X-ray diffraction data set for [4+4]-*anti*-$\mathbf{2_{MM}}$ was collected on a Rigaku Saturn 724+ CCD diffractometer with Mo Kα radiation (λ = 0.71075 Å) at 103 K. Single crystals of [4+4]-*anti*-$\mathbf{2_{MM}}$ [$C_{22}H_{14}$, MW = 278.33] suitable for X-ray analysis were obtained by slow diffusion of methanol into a CH_2Cl_2 solution of [4+4]-*anti*-$\mathbf{2_{MM}}$, and a single colorless crystal with dimensions of 0.08 × 0.04 × 0.02 mm^3 was selected for intensity measurements. The unit cell was monoclinic with the space group $P2_1/c$. The lattice constants with Z = 4, ρ_{calcd} = 1.264 g cm^{-3}, $\mu(Mo_{K\alpha})$ = 0.072 mm^{-1}, $F(000)$ = 584.0, $2\theta_{max}$ = 54.84° were a = 11.819(5) Å, b = 10.742(3) Å, c = 12.543(5) Å, and V = 1,463.1(9) $Å^3$. A total of 11,613 reflections was collected, of which 3,334 reflections were independent (R_{int} = 0.0306). The structure was refined to final R_1 = 0.0603 for 2,933 data [$I>2\sigma(I)$] with 199 parameters and wR_2 = 0.1403 for all data, GOF = 1.122, and residual electron density max/min = 0.253/–0.222 e $Å^{-3}$. The ORTEP drawing is shown in ***Fig. S3***, and the crystal data and structure refinement are listed in ***Table S1***.

Data collection and processing were conducted using the Rigaku CrystalClear software package.[S4] The structure was solved by direct methods using Sir2004[S5] and refined by full-matrix least squares methods on F^2 with SHELXL-97 program[S6,S7] using Yadokari-XG 2009.[S8,S9] All non-hydrogen atoms were refined anisotropically. All hydrogen atoms were calculated geometrically and refined using the riding model. Crystallographic data have been deposited at the CCDC (12 Union Road, Cambridge CB2 1EZ, UK) and copies can be obtained on request, free of charge, by quoting the publication citation and the deposition number 1503774.

Table S1. Crystal Data and Structure Refinement for [4+4]-*anti*-$\mathbf{2_{MM}}$

Empirical formula	$C_{22}H_{14}$	
Formula weight	278.33	
Temperature	103 K	
Wavelength	0.71075 Å	
Crystal system	Monoclinic	
Space group	$P2_1/c$	
Unit cell dimensions	a = 11.819(5) Å	α = 90°
	b = 10.742(3) Å	β = 113.260(5)°
	c = 12.543(5) Å	γ = 90°
Volume	1,463.1(9) Å^3	
Z	4	
Density (calculated)	1.264 g/cm^3	
Absorption coefficient	0.072 mm^{-1}	
F(000)	584.0	
Crystal size	0.08 × 0.04 × 0.02 mm^3	
Theta range for data collection	3.28 to 27.44°	
Index ranges	$-15 \le h \le 15, -13 \le k \le 9, -16 \le l \le 16$	
Reflections collected	11,613	
Independent reflections	3,334 [R_{int} =0.0306]	
Completeness to theta = 27.44°	99.6 %	
Absorption correction	Semi-empirical from equivalents	
Max. and min. transmission	1.0000 and 0.9233	
Refinement method	Full-matrix least-squares on F^2	
Data / restraints / parameters	3,334 / 0 / 199	
Goodness-of-fit on F^2	1.122	
Final R indices [I>2sigma(I)]	R_1 = 0.0603, wR_2 = 0.1340	
R indices (all data)	R_1 = 0.0694, wR_2 = 0.1403	
Largest diff. peak and hole	0.253 and –0.222 eÅ^{-3}	

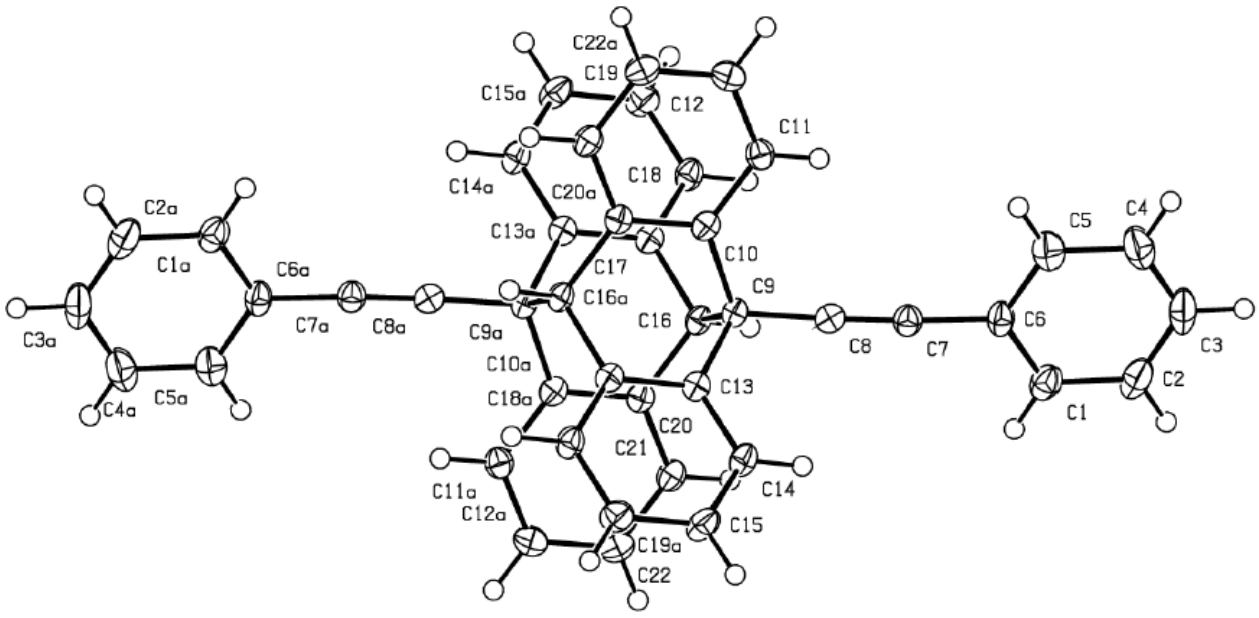

Fig. S3. ORTEP drawing of the crystal structure of [4+4]-*anti*-$\mathbf{2_{MM}}$ with thermal ellipsoids at 50% probability.

Crystallographic Data of [4+2]-*anti*-$\mathbf{2_{MM}}$. X-ray diffraction data set for [4+2]-*anti*-$\mathbf{2_{MM}}$ was collected on a Rigaku Saturn 724+ CCD diffractometer with Mo Kα radiation (λ = 0.71075 Å) at 103 K. Single crystals of [4+2]-*anti*-$\mathbf{2_{MM}}$ [$C_{44}H_{28}$, MW = 556.66] suitable for X-ray analysis were obtained by slow diffusion of methanol into a CH_2Cl_2 solution of [4+2]-*anti*-$\mathbf{2_{MM}}$, and a single colorless crystal with dimensions of 0.20 × 0.15 × 0.09 mm^3 was selected for intensity measurements. The unit cell was monoclinic with the space group $P2_1/c$. The lattice constants with Z = 4, ρ_{calcd} = 1.253 g cm^{-3}, $\mu(Mo_{K\alpha})$ = 0.071 mm^{-1}, $F(000)$ = 1168.0, $2\theta_{max}$ = 55.04° were a = 10.616(4) Å, b = 18.469(7) Å, c = 15.306(6) Å, and V = 2950(2) $Å^3$. A total of 23,660 reflections was collected, of which 6,719 reflections were independent (R_{int} = 0.0443). The structure was refined to final R_1 = 0.0491 for 6,406 data [$I>2\sigma(I)$] with 397 parameters and wR_2 = 0.1236 for all data, *GOF* = 1.072, and residual electron density max/min = 0.359/–0.222 e $Å^{-3}$. The ORTEP drawing is shown in ***Fig. S4***, and the crystal data and structure refinement are listed in ***Table S2***.

Data collection and processing were conducted using the Rigaku CrystalClear software package.[S4] The structure was solved by direct methods using Sir2004[S5] and refined by full-matrix least squares methods on F^2 with SHELXL-97 program[S6,S7] using Yadokari-XG 2009.[S8,S9] All non-hydrogen atoms were refined anisotropically. All hydrogen atoms were calculated geometrically and refined using the riding model. Crystallographic data have been deposited at the CCDC (12 Union Road, Cambridge CB2 1EZ, UK) and copies can be obtained on request, free of charge, by quoting the publication citation and the deposition number 1503775.

Table S2. Crystal Data and Structure Refinement for [4+2]-*anti*-$\mathbf{2_{MM}}$

Empirical formula	$C_{44}H_{28}$	
Formula weight	556.66	
Temperature	103(2) K	
Wavelength	0.71075 Å	
Crystal system	Monoclinic	
Space group	$P2_1/c$	
Unit cell dimensions	a = 10.616(4) Å	α = 90°
	b = 18.469(7) Å	β = 100.612(7)°
	c = 15.306(6) Å	γ = 90°
Volume	2,950(2) Å^3	
Z	4	
Density (calculated)	1.253 g/cm^3	
Absorption coefficient	0.072 mm^{-1}	
F(000)	1168.0	
Crystal size	0.20 × 0.15 × 0.09 mm^3	
Theta range for data collection	3.03 to 27.48°	
Index ranges	$-13 \le h \le 13, -23 \le k \le 23, -18 \le l \le 19$	
Reflections collected	23,660	
Independent reflections	6,719 [R_{int} = 0.1236]	
Completeness to theta = 27.48°	99.5 %	
Absorption correction	Semi-empirical from equivalents	
Max. and min. transmission	1.0000 and 0.9192	
Refinement method	Full-matrix least-squares on F^2	
Data / restraints / parameters	6,719 / 0 / 397	
Goodness-of-fit on F^2	1.125	
Final R indices [I>2sigma(I)]	R_1 = 0.0491, wR_2 = 0.1214	
R indices (all data)	R_1 = 0.0516, wR_2 = 0.1236	
Largest diff. peak and hole	0.359 and –0.222 eÅ^{-3}	

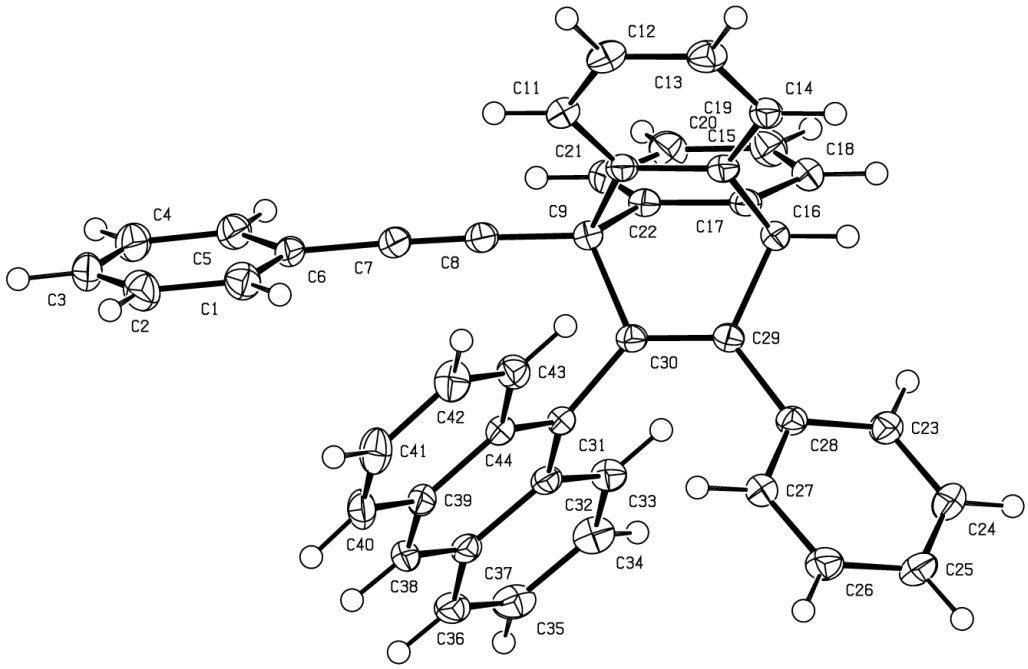

Fig. S4. ORTEP drawing of the crystal structure of [4+2]-*anti*-$\mathbf{2_{MM}}$ with thermal ellipsoids at 50% probability.

5. Theoretical Studies of the Photodimers [4+4]-*anti*-$\mathbf{2}_{MM}$, [4+4]-*syn*-$\mathbf{2}_{MM}$, [4+2]-*anti*-$\mathbf{2}_{MM}$, and [4+2]-*syn*-$\mathbf{2}_{MM}$

The molecular modelling was performed on a Windows XP PC with the ArgusLab software.[S10] The initial model structures were constructed based on the crystal structure of [4+4]-*anti*-$\mathbf{2}_{MM}$ or [4+2]-*anti*-$\mathbf{2}_{MM}$. The initial models were then fully optimised by semi-empirical molecular orbital (MO) calculations (PM6 method[S11] in MOPAC2012[S12]) and further density functional theory (DFT) calculations at the B3LYP level and the 6-31G* basis set in *Gaussian 09* software (Gaussian, Inc., Pittsburgh, PA).[S13] Computer resources for the DFT calculations were provided by the Information Technology Center of Nagoya University. The resultant energy-minimised structures with their total energies are depicted in ***Fig. S5***.

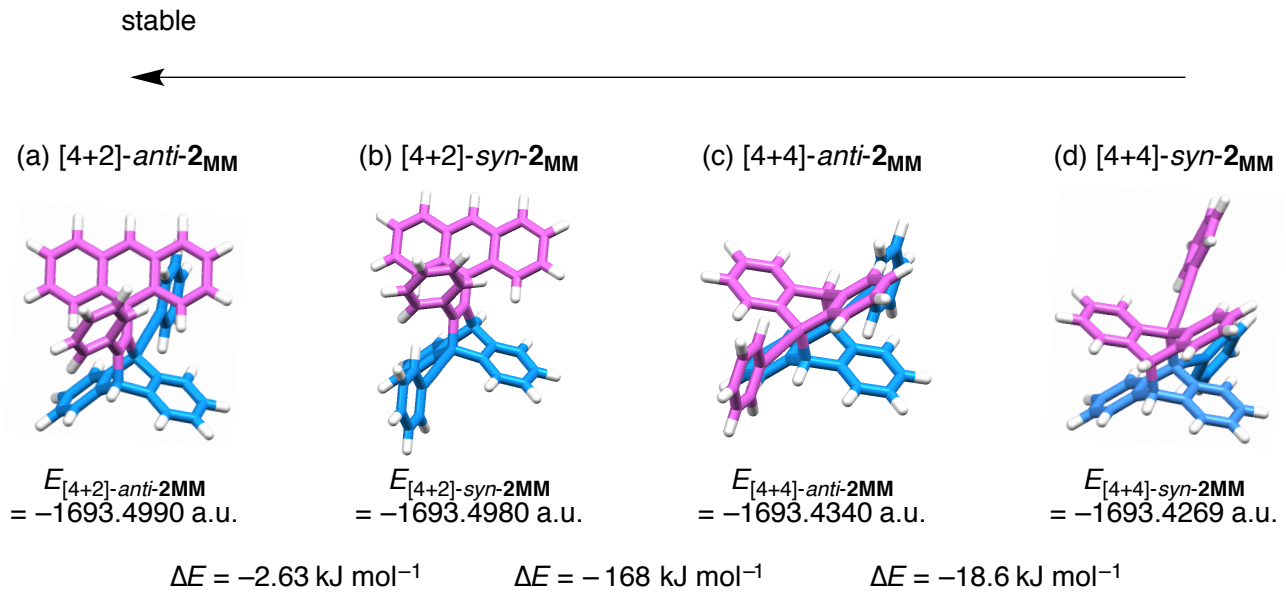

Fig. S5. Capped-stick drawings of the structures of (a) [4+2]-*anti*-$\mathbf{2}_{MM}$, (b) [4+2]-*syn*-$\mathbf{2}_{MM}$, (c) [4+4]-*anti*-$\mathbf{2}_{MM}$, and (d) [4+4]-*syn*-$\mathbf{2}_{MM}$ optimised by DFT calculations. DFT-calculated energies (E) and energy differences (ΔE) are also shown in the bottom.

6. Photoreaction of Model Anthracene Monomer $\mathbf{1}_M$ in the Presence of Oxygen

6-1. Photoreaction of $\mathbf{1}_M$ in Undegassed $CDCl_3$ (0.50 mM)

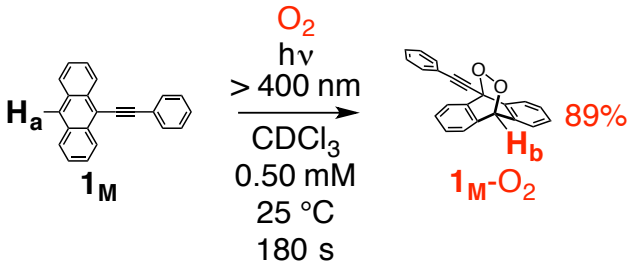

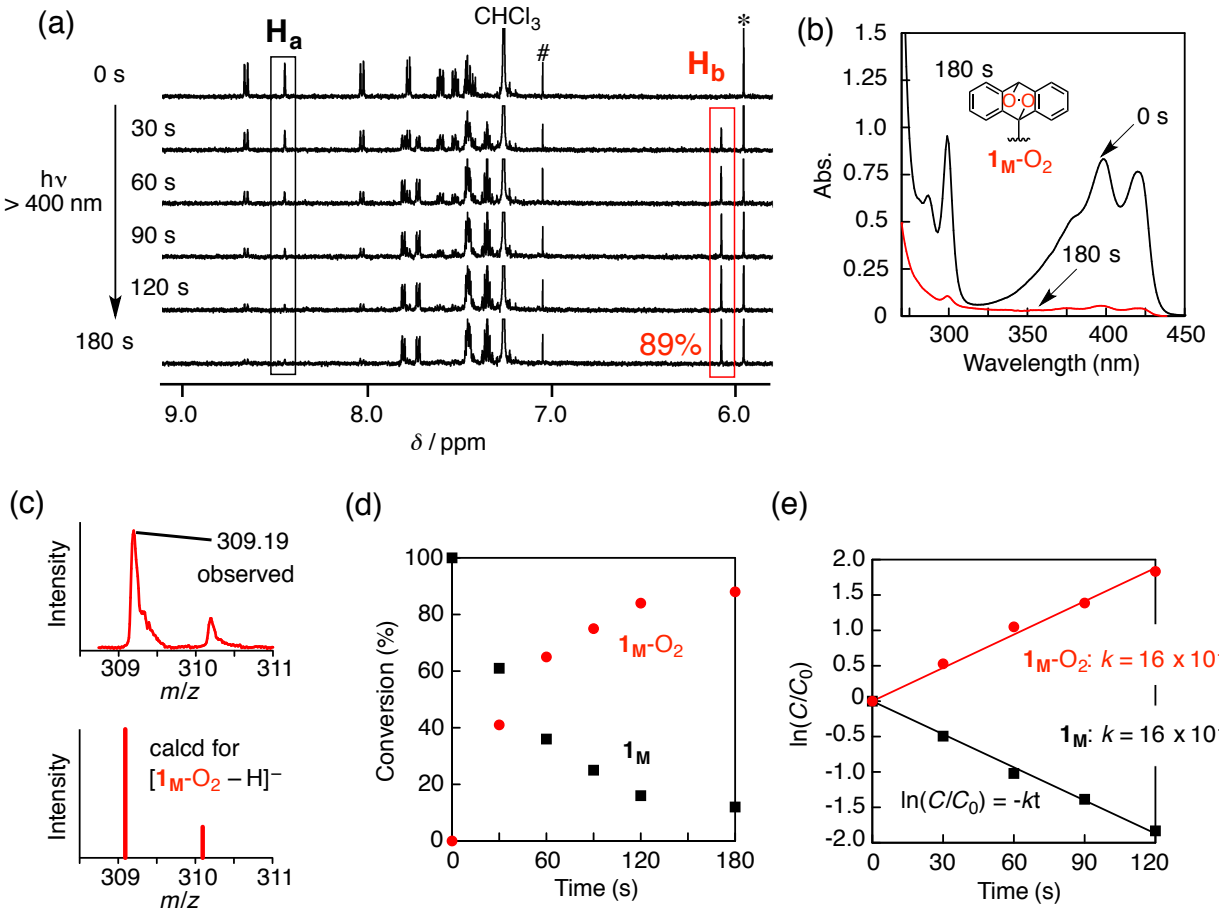

Fig. S6. (a) Time-dependent ^{1}H NMR spectral changes of $\mathbf{1}_M$ (500 MHz, undegassed $CDCl_3$, 25 °C, 0.50 mM) upon irradiation of light (> 400 nm). # and ∗ denote the ^{13}C satellite peaks of the solvent and the peak of 1,1,2,2-tetrachloroethane (0.32 mM) used as an internal standard, respectively. (b) Time-dependent absorption spectral changes of $\mathbf{1}_M$ (0.50 mM) in undegassed $CDCl_3$ before (0 s) and after (180 s) irradiation of light (> 400 nm). Cell length = 1 mm. (c) Negative mode ESI-MS spectrum (CH_3CN/CH_3OH = 1/1 (*v*/*v*)) of $\mathbf{1}_M$ after irradiation of light (> 400 nm) for 180 s in undegassed $CDCl_3$. (d) Time-conversion relationships and (e) kinetic plots of the photooxidation of $\mathbf{1}_M$ (undegassed $CDCl_3$, 25 °C, 0.50 mM) estimated from the integral ratios of the peaks for H_a ($\mathbf{1}_M$), H_b ($\mathbf{1}_M$-O_2), and the internal standard (1,1,2,2-tetrachloroethane) based on the ^{1}H NMR spectral changes shown in (a).

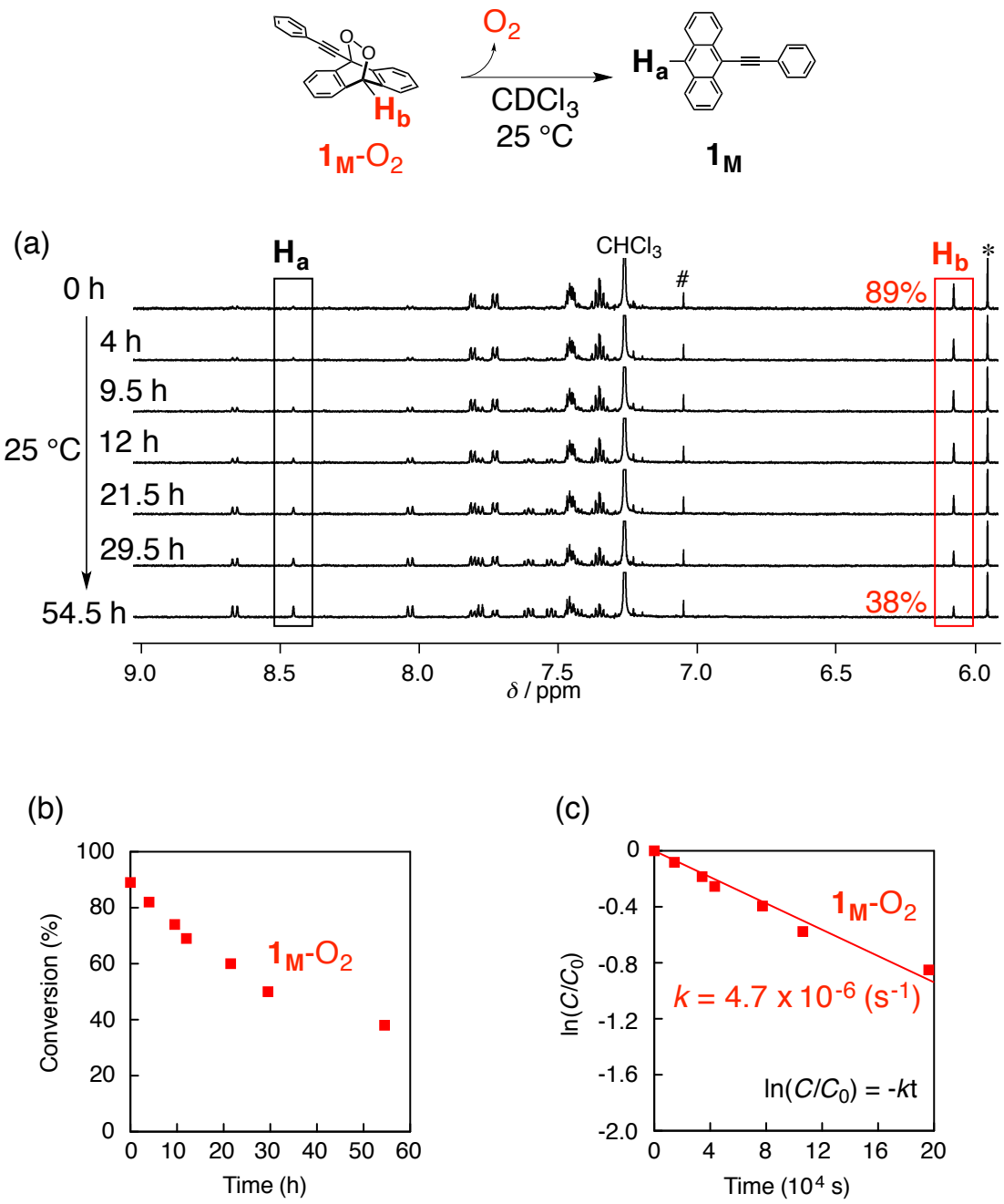

Fig. S7. (a) Time-dependent ^{1}H NMR spectral changes of $\mathbf{1_M}$-O_2 at 25 °C under shielded light in $CDCl_3$. # and ∗ denote the ^{13}C satellite peaks of the solvent and the peak of 1,1,2,2-tetrachloroethane (0.32 mM) used as an internal standard, respectively. The photooxidised $\mathbf{1_M}$-O_2 was obtained in an undegassed $CDCl_3$ solution of $\mathbf{1_M}$ (0.50 mM) upon irradiation of light (> 400 nm) for 180 s (see ***Fig. S6a***). (b) Time-conversion relationships and (c) kinetic plots of the thermal reverse reaction of $\mathbf{1_M}$-O_2 ($CDCl_3$, 25 °C, 0.50 mM) estimated from the integral ratios of the peaks for H_a ($\mathbf{1_M}$), H_b ($\mathbf{1_M}$-O_2), and the internal standard (1,1,2,2-tetrachloroethane) based on the ^{1}H NMR spectral changes shown in (a).

6-2. Photoreaction of $\mathbf{1}_M$ in Undegassed $CDCl_3$ (8.0 mM)

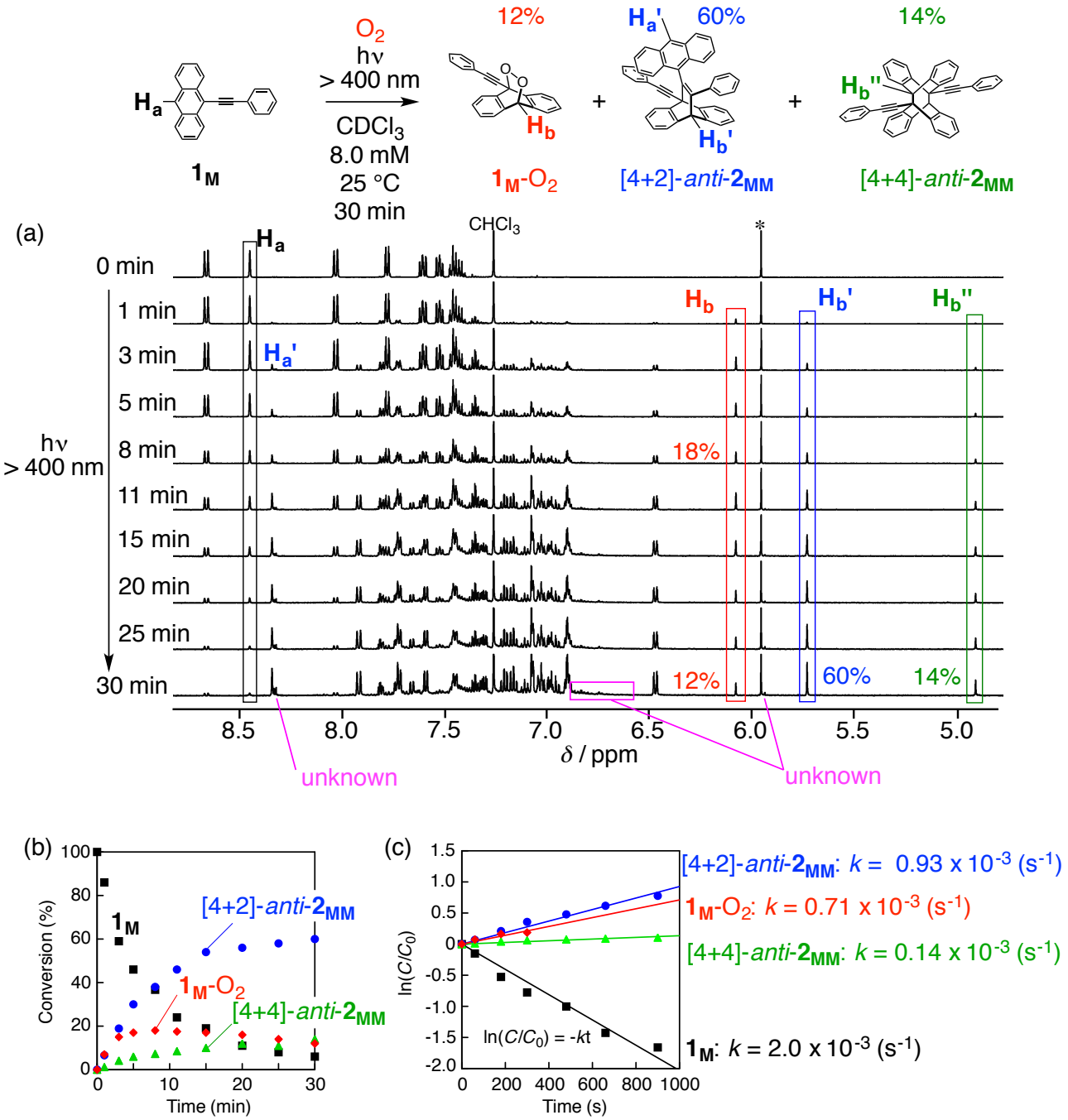

Fig. S8. (a) Time-dependent ^{1}H NMR spectral changes of $\mathbf{1}_M$ (500 MHz, undegassed $CDCl_3$, 25 °C, 8.0 mM) upon irradiation of light (> 400 nm). ∗ denotes the peak of 1,1,2,2-tetrachloroethane (2.8 mM) used as an internal standard. The unknown peaks are probably due to photolysis products of $\mathbf{1}_M$-O_2. (b) Time-conversion relationships and (c) kinetic plots of the photodimerisation of $\mathbf{1}_M$ (undegassed $CDCl_3$, 25 °C, 8.0 mM) estimated from the integral ratios of the peaks for H_a ($\mathbf{1}_M$), H_b ($\mathbf{1}_M$-O_2), H_b' ([4+2]-*anti*-$\mathbf{2}_{MM}$), H_b'' ([4+4]-*anti*-$\mathbf{2}_{MM}$), and the internal standard (1,1,2,2-tetrachloroethane) based on the ^{1}H NMR spectral changes shown in (a).

6-3. Photoreaction of $\mathbf{1}_M$ in Undegassed Benzene-d_6 (0.50 mM)

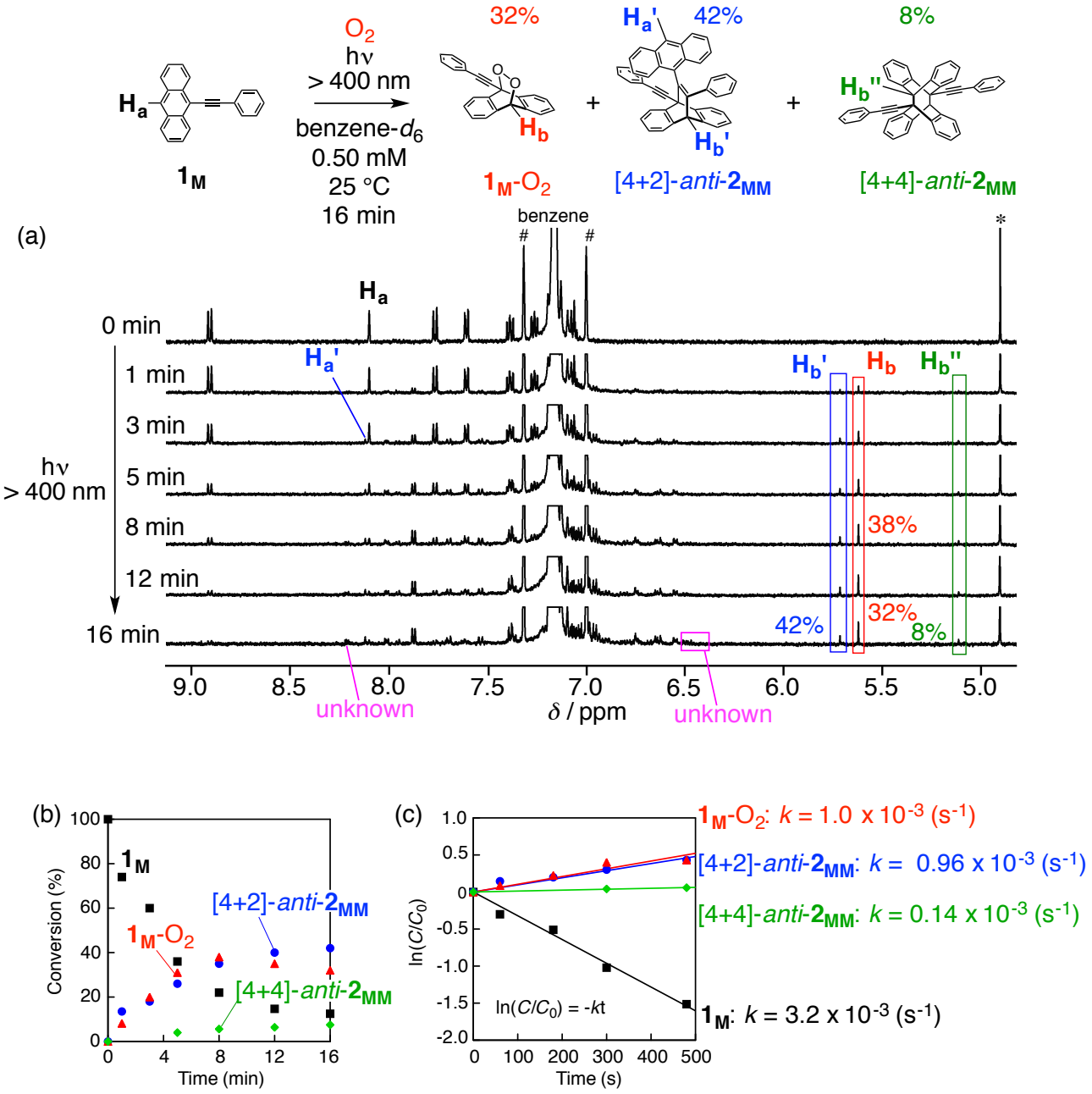

Fig. S9. (a) Time-dependent ^{1}H NMR spectral changes of $\mathbf{1}_M$ (500 MHz, undegassed benzene-d_6, 25 °C, 0.50 mM) upon irradiation of light (> 400 nm). # and ∗ denote the ^{13}C satellite peaks of the solvent and the peak of 1,1,2,2-tetrachloroethane (0.75 mM) used as an internal standard, respectively. The unknown peaks are probably due to photolysis products of $\mathbf{1}_M$-O_2. (b) Time-conversion relationships and (c) kinetic plots of the photodimerisation of $\mathbf{1}_M$ (undegassed benzene-d_6, 25 °C, 0.50 mM) estimated from the integral ratios of the peaks for H_a ($\mathbf{1}_M$), H_b ($\mathbf{1}_M$-O_2), H_b' ([4+2]-*anti*-$\mathbf{2}_{MM}$), H_b'' ([4+4]-*anti*-$\mathbf{2}_{MM}$), and the internal standard (1,1,2,2-tetrachloroethane) based on the ^{1}H NMR spectral changes shown in (a).

6-4. Photoreaction of $\mathbf{1_M}$ in Undegassed Benzene-d_6 (8.0 mM)

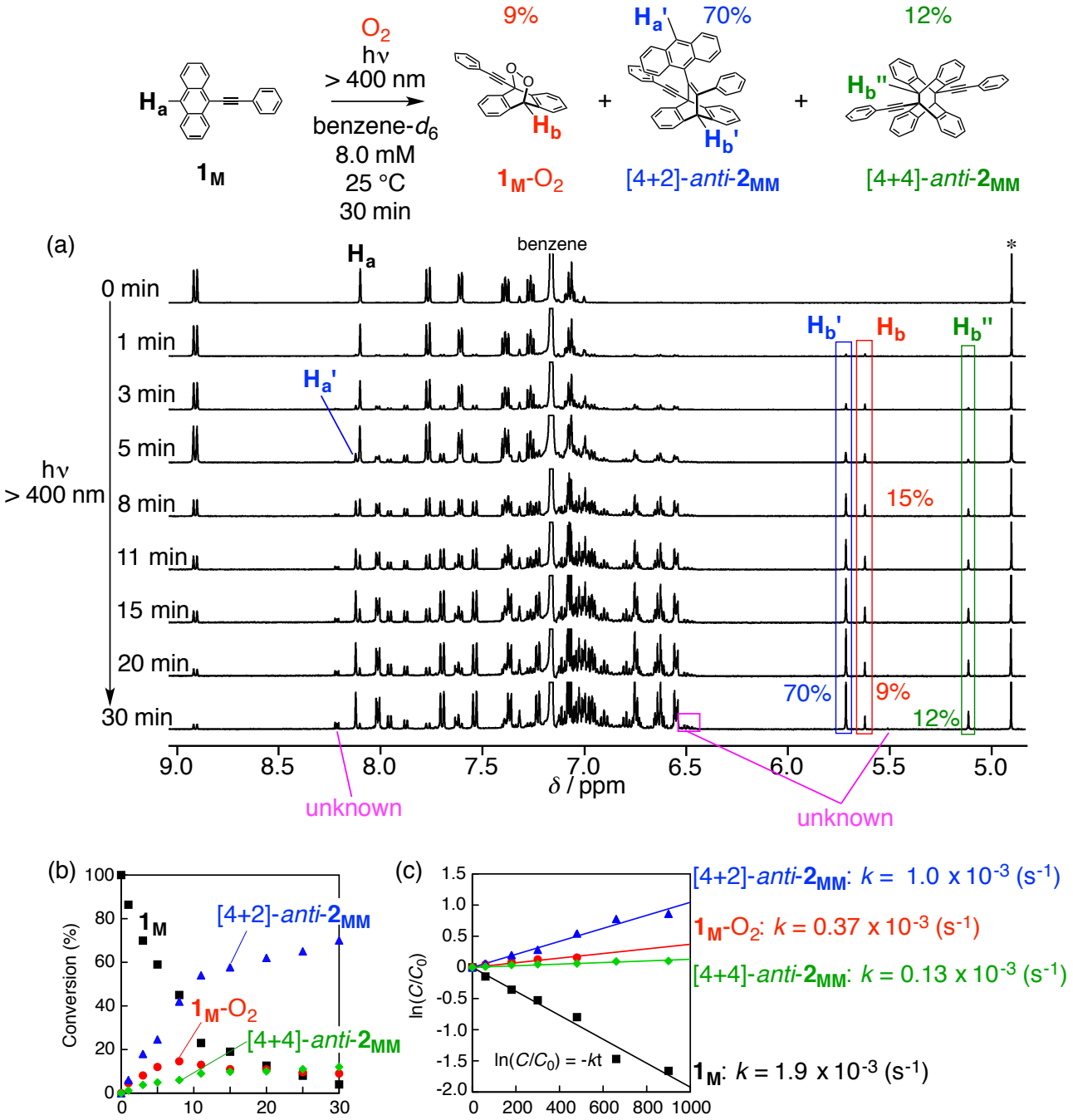

Fig. S10. (a) Time-dependent ^{1}H NMR spectral changes of $\mathbf{1_M}$ (500 MHz, undegassed benzene-d_6, 25 °C, 8.0 mM) upon irradiation of light (> 400 nm). ∗ denotes the peak of 1,1,2,2-tetrachloroethane (3.8 mM) used as an internal standard. The unknown peaks are probably due to photolysis products of $\mathbf{1_M}$-O_2. (b) Time-conversion relationships and (c) kinetic plots of the photodimerisation of $\mathbf{1_M}$ (undegassed benzene-d_6, 25 °C, 8.0 mM) estimated from the integral ratios of the peaks for H_a ($\mathbf{1_M}$), H_b ($\mathbf{1_M}$-O_2), H_b' ([4+2]-*anti*-$\mathbf{2_{MM}}$), H_b'' ([4+4]-*anti*-$\mathbf{2_{MM}}$), and the internal standard (1,1,2,2-tetrachloroethane) based on the ^{1}H NMR spectral changes shown in (a).

7. Photoreaction of Model Anthracene Monomer $\mathbf{1_M}$ in the Absence of Oxygen

7-1. Photoreaciton of $\mathbf{1_M}$ in Degassed $CDCl_3$ (0.50 mM)

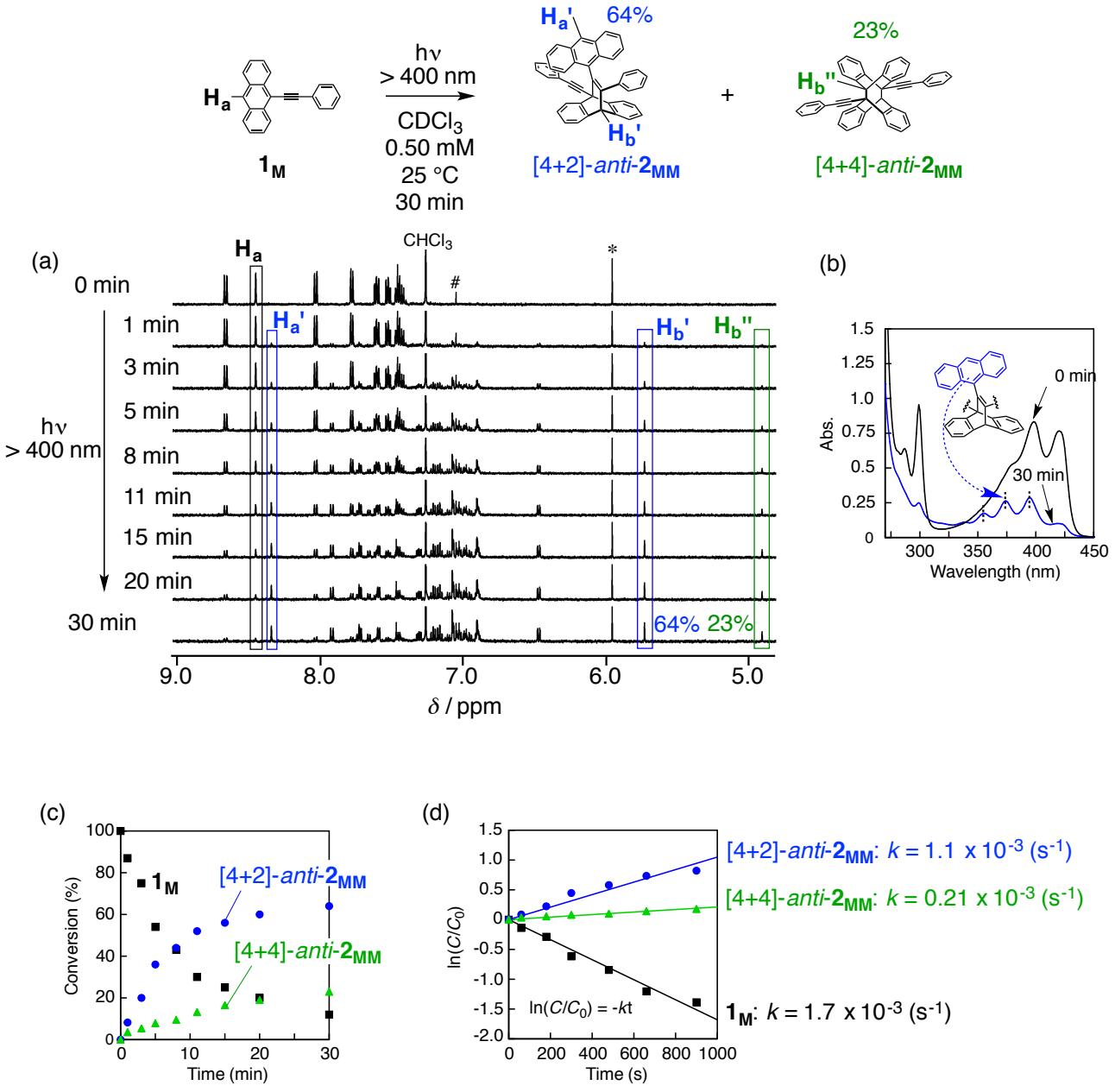

Fig. S11. (a) Time-dependent ^{1}H NMR spectral changes of $\mathbf{1_M}$ (500 MHz, degassed $CDCl_3$, 25 °C, 0.50 mM) upon irradiation of light (> 400 nm). # and ∗ denote the ^{13}C satellite peaks of the solvent and the peak of 1,1,2,2-tetrachloroethane (0.48 mM) used as an internal standard, respectively. (b) Time-dependent absorption spectral changes of $\mathbf{1_M}$ (0.50 mM) in degassed $CDCl_3$ before (0 min) and after (30 min) irradiation of light (> 400 nm). Cell length = 1 mm. (c) Time-conversion relationships and (d) kinetic plots of the photodimerisation of $\mathbf{1_M}$ (degassed $CDCl_3$, 25 °C, 0.50 mM) estimated from the integral ratios of the peaks for H_a ($\mathbf{1_M}$), H_b' ([4+2]-*anti*-$\mathbf{2_{MM}}$), H_b'' ([4+4]-*anti*-$\mathbf{2_{MM}}$), and the internal standard (1,1,2,2-tetrachloroethane) based on the ^{1}H NMR spectral changes shown in (a).

7-2. Photoreaction of $\mathbf{1}_M$ in Degassed $CDCl_3$ (8.0 mM)

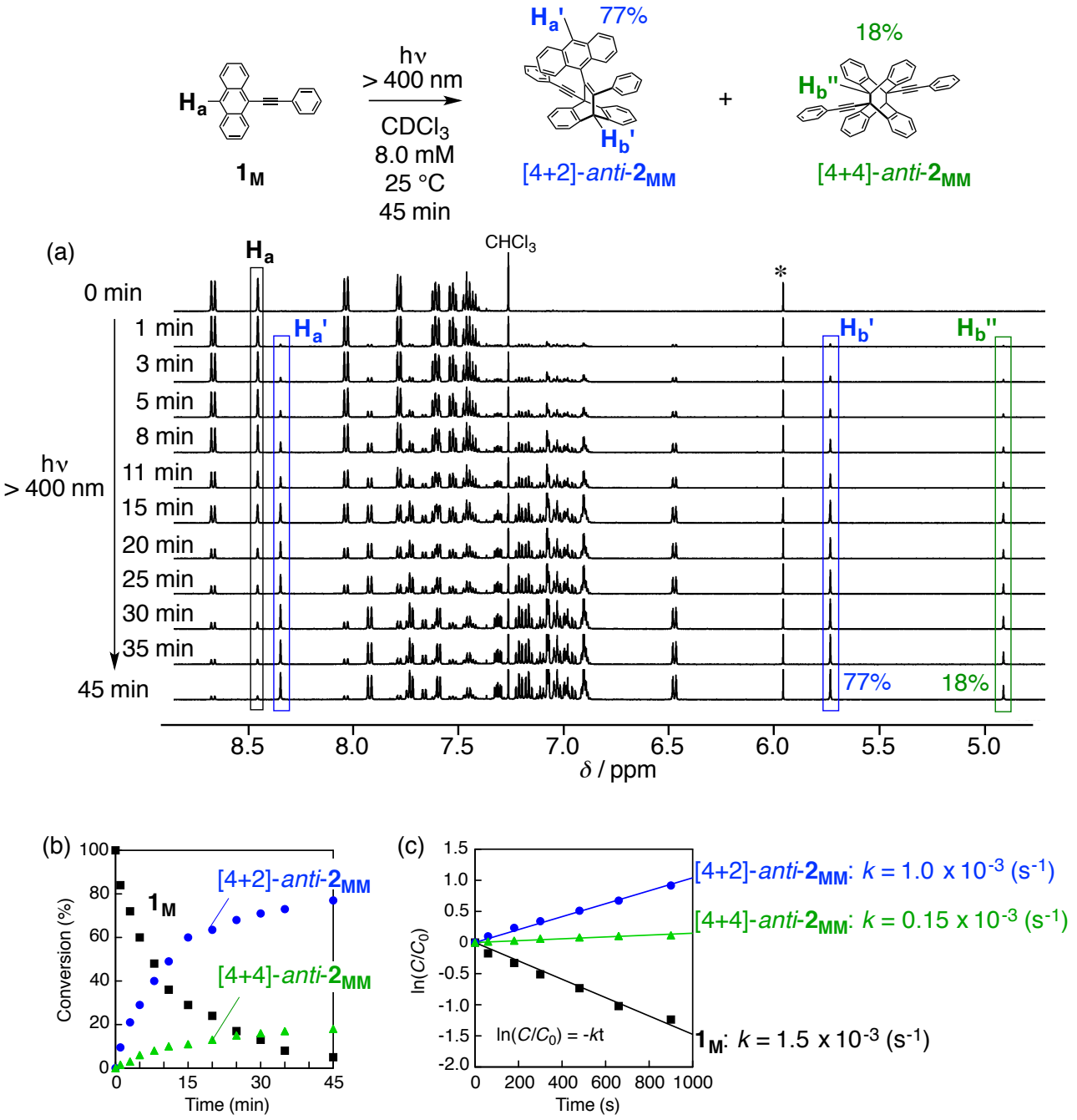

Fig. S12. (a) Time-dependent ^{1}H NMR spectral changes of $\mathbf{1}_M$ (500 MHz, degassed $CDCl_3$, 25 °C, 8.0 mM) upon irradiation of light (> 400 nm). ∗ denotes the peak of 1,1,2,2-tetrachloroethane (1.3 mM) used as an internal standard. (b) Time-conversion relationships and (c) kinetic plots of the photodimerisation of $\mathbf{1}_M$ (degassed $CDCl_3$, 25 °C, 8.0 mM) estimated from the integral ratios of the peaks for H_a ($\mathbf{1}_M$), H_b' ([4+2]-*anti*-$\mathbf{2}_{MM}$), H_b'' ([4+4]-*anti*-$\mathbf{2}_{MM}$), and the internal standard (1,1,2,2-tetrachloroethane) based on the ^{1}H NMR spectral changes shown in (a).

7-3. Photoreaction of $\mathbf{1}_M$ in Degasssed Benzene-d_6 (0.50 mM)

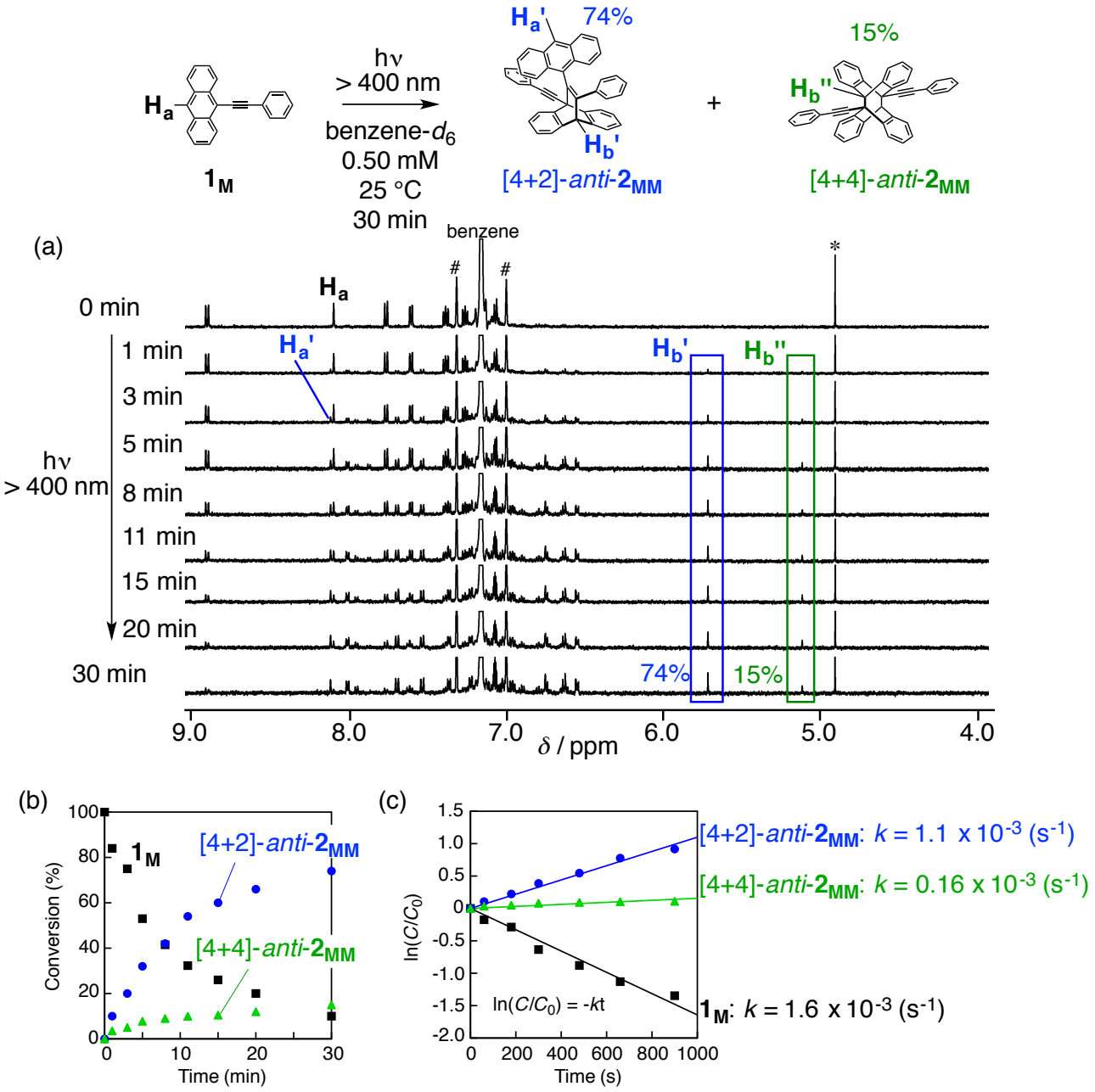

Fig. S13. (a) Time-dependent ^{1}H NMR spectral changes of $\mathbf{1}_M$ (500 MHz, degassed benzene-d_6, 25 °C, 0.50 mM) upon irradiation of light (> 400 nm). # and ∗ denote the ^{13}C satellite peaks of the solvent and the peak of 1,1,2,2-tetrachloroethane (0.25 mM) used as an internal standard, respectively. (b) Time-conversion relationships and (c) kinetic plots of the photodimerisation of $\mathbf{1}_M$ (degassed benzene-d_6, 25 °C, 0.50 mM) estimated from the integral ratios of the peaks for H_a ($\mathbf{1}_M$), H_b' ([4+2]-*anti*-$\mathbf{2}_{MM}$), H_b'' ([4+4]-*anti*-$\mathbf{2}_{MM}$), and the internal standard (1,1,2,2-tetrachloroethane) based on the ^{1}H NMR spectral changes shown in (a).

7-4. Photoreaction of $\mathbf{1}_M$ in Degassed Benzene-d_6 (8.0 mM)

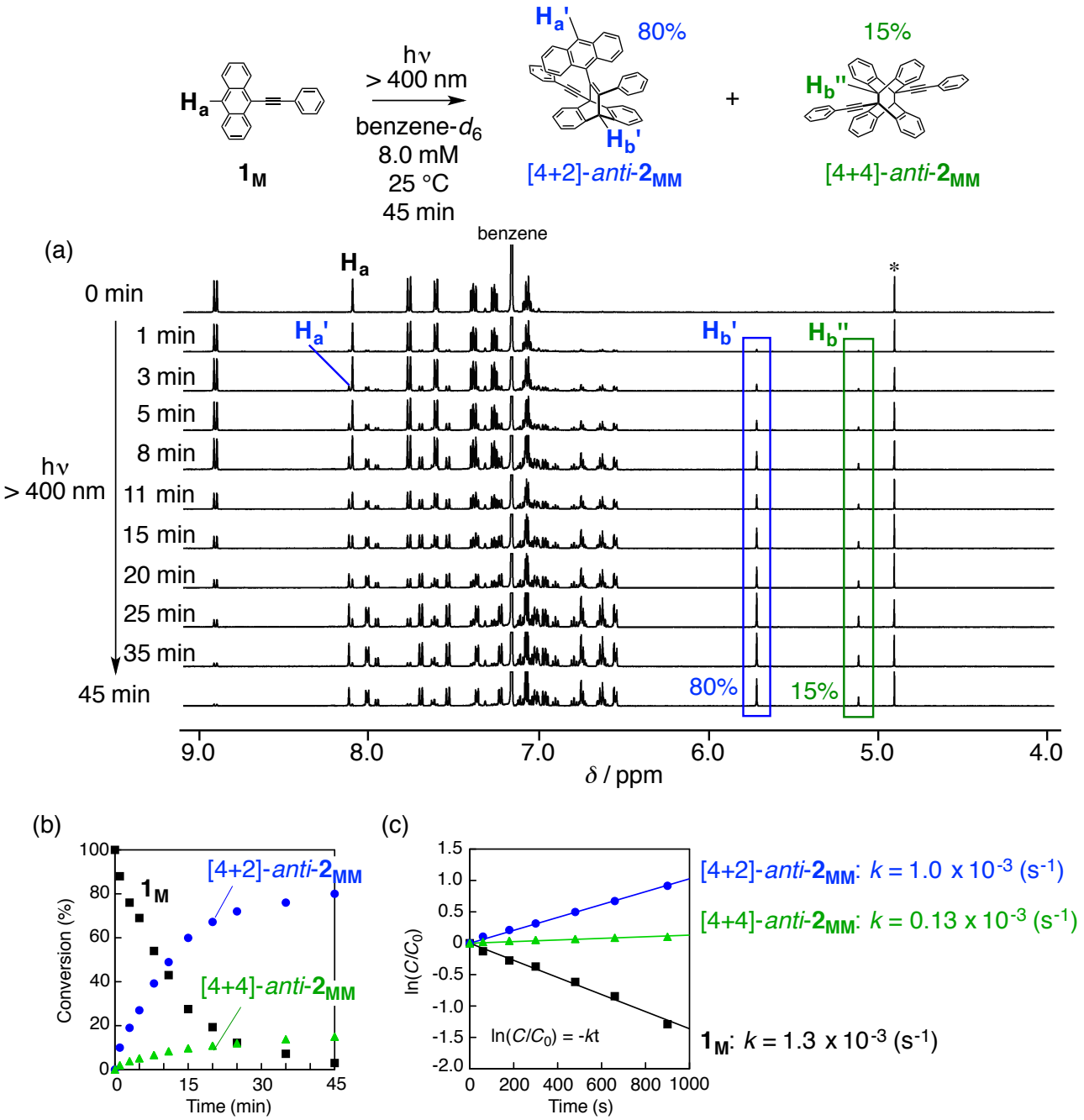

Fig. S14. (a) Time-dependent ^{1}H NMR spectral changes of $\mathbf{1}_M$ (500 MHz, degassed benzene-d_6, 25 °C, 8.0 mM) upon irradiation of light (> 400 nm). ∗ denotes the peak of 1,1,2,2-tetrachloroethane (1.4 mM) used as an internal standard. (b) Time-conversion relationships and (c) kinetic plots of the photodimerisation of $\mathbf{1}_M$ (degassed benzene-d_6, 25 °C, 8.0 mM) estimated from the integral ratios of the peaks for H_a ($\mathbf{1}_M$), H_b' ([4+2]-*anti*-$\mathbf{2}_{MM}$), H_b'' ([4+4]-*anti*-$\mathbf{2}_{MM}$), and the internal standard (1,1,2,2-tetrachloroethane) based on the ^{1}H NMR spectral changes shown in (a).

8. Raman Experiments

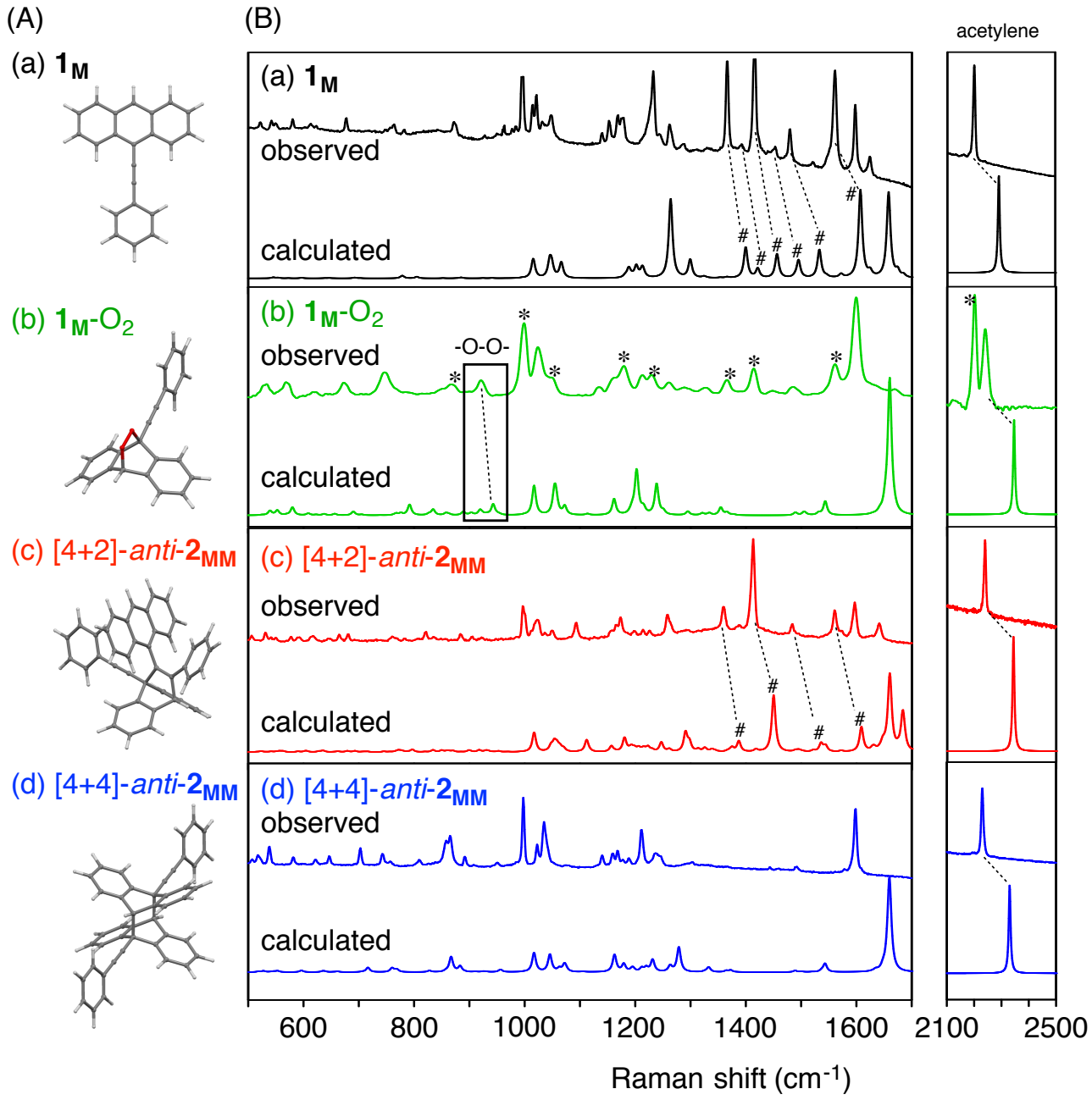

Fig. S15. (A) Capped-stick drawings of the structures of (a) $\mathbf{1}_{M}$, (b) $\mathbf{1}_{M}$-O_2, (c) [4+2]-*anti*-$\mathbf{2}_{MM}$, and (d) [4+4]-*anti*-$\mathbf{2}_{MM}$ optimised by DFT calculations and (B) Experimental (top) and DFT simulated (bottom) Raman spectra of (a) $\mathbf{1}_{M}$, (b) $\mathbf{1}_{M}$-O_2, (c) [4+2]-*anti*-$\mathbf{2}_{MM}$, and (d) [4+4]-*anti*-$\mathbf{2}_{MM}$. ∗, #, and -O-O- denote the peaks due to $\mathbf{1}_{M}$, the in-plane anthracene breathing modes, and O-O stretching vibration bands, respectively. DFT calculations were performed at the B3LYP level and the 6-31G* basis set in *Gaussian* 09 software (Gaussian, Inc., Pittsburgh, PA).[S13] The Raman spectra of $\mathbf{1}_{M}$, [4+2]-*anti*-$\mathbf{2}_{MM}$, and [4+4]-*anti*-$\mathbf{2}_{MM}$ were measured on a confocal Raman microscope (Renishaw inVia Raman system, Renishaw, Inc.) using a laser beam at 785 nm for exicitation and an exposure time of 10 s. The Raman spectrum of $\mathbf{1}_{M}$-O_2 was measured on a confocal Raman microscope (NRS-5100, JASCO) using a laser beam at 1064 nm for exitation and an exposure time of 60 s.

9. Photoreaction of Mono-9-Phenylethynylanthracene-Bound Carboxylic Acid Monomer in the Presence of Oxygen

9-1. Photoreaction of $\mathbf{1_C}$ in Undegassed $CDCl_3$

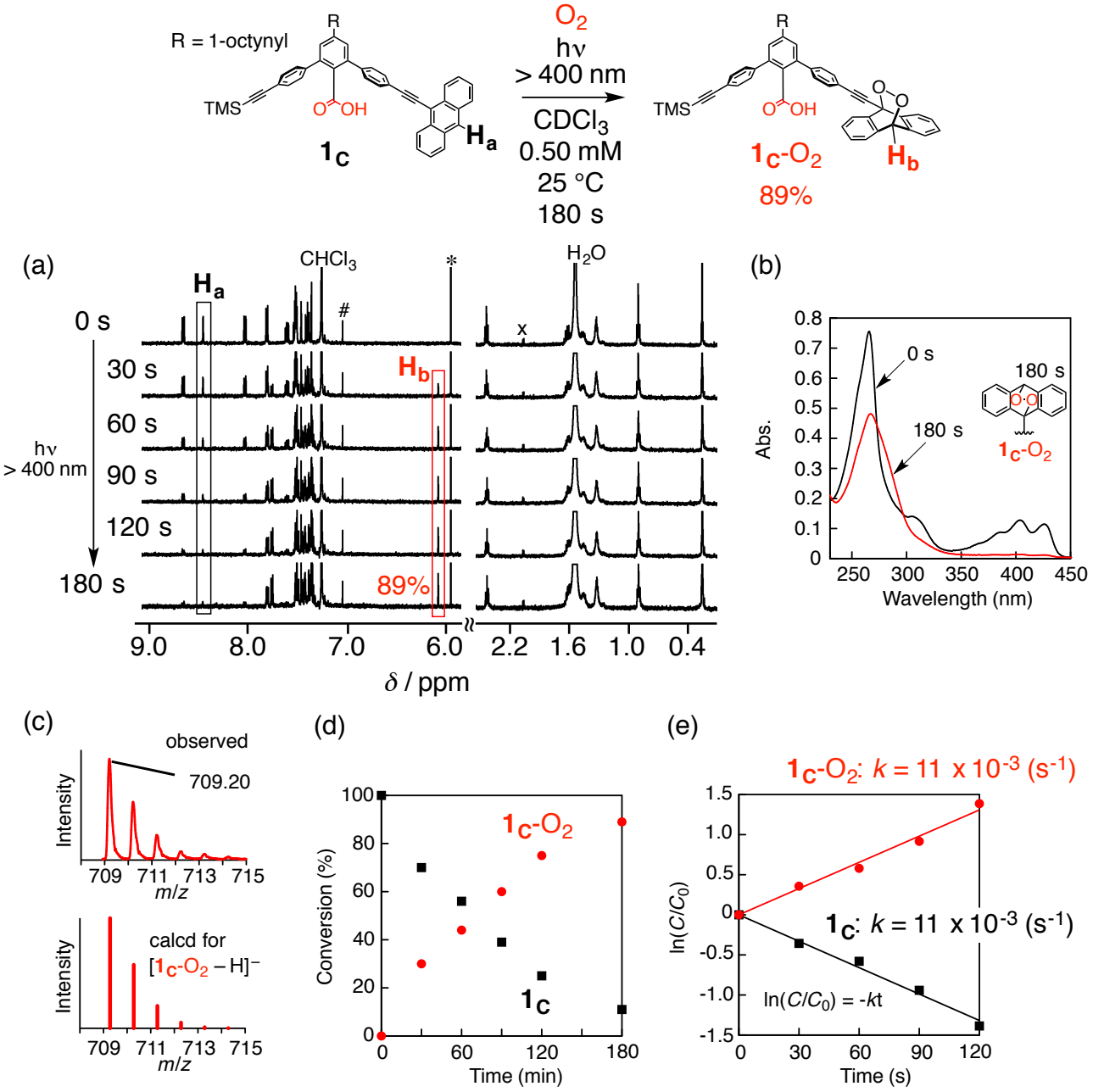

Fig. S16. (a) Time-dependent ^{1}H NMR spectral changes of $\mathbf{1_C}$ (500 MHz, undegassed $CDCl_3$, 25 °C, 0.50 mM) upon irradiation of light (> 400 nm). #, ∗, and x denote the ^{13}C satellite peaks of the solvent, the peak of 1,1,2,2-tetrachloroethane (0.25 mM) used as an internal standard, and impurities contained in $CDCl_3$, respectively. (b) Time-dependent absorption spectral changes of $\mathbf{1_C}$ (0.50 mM) in undegassed $CDCl_3$ before (0 s) and after (180 s) irradiation of light (> 400 nm). Cell length = 0.1 mm. (c) Negative mode ESI-MS spectrum (CH_3CN/CH_3OH = 1/1 (*v*/*v*)) of $\mathbf{1_C}$ after irradiation of light (> 400 nm) for 180 s in undegassed $CDCl_3$. (d) Time-conversion relationships and (e) kinetic plots of the photooxidation of $\mathbf{1_C}$ (undegassed $CDCl_3$, 25 °C, 0.50 mM) estimated from the integral ratios of the peaks for H_a ($\mathbf{1_C}$), H_b ($\mathbf{1_C}$-O_2), and the internal standard (1,1,2,2-tetrachloroethane) based on the ^{1}H NMR spectral changes shown in (a).

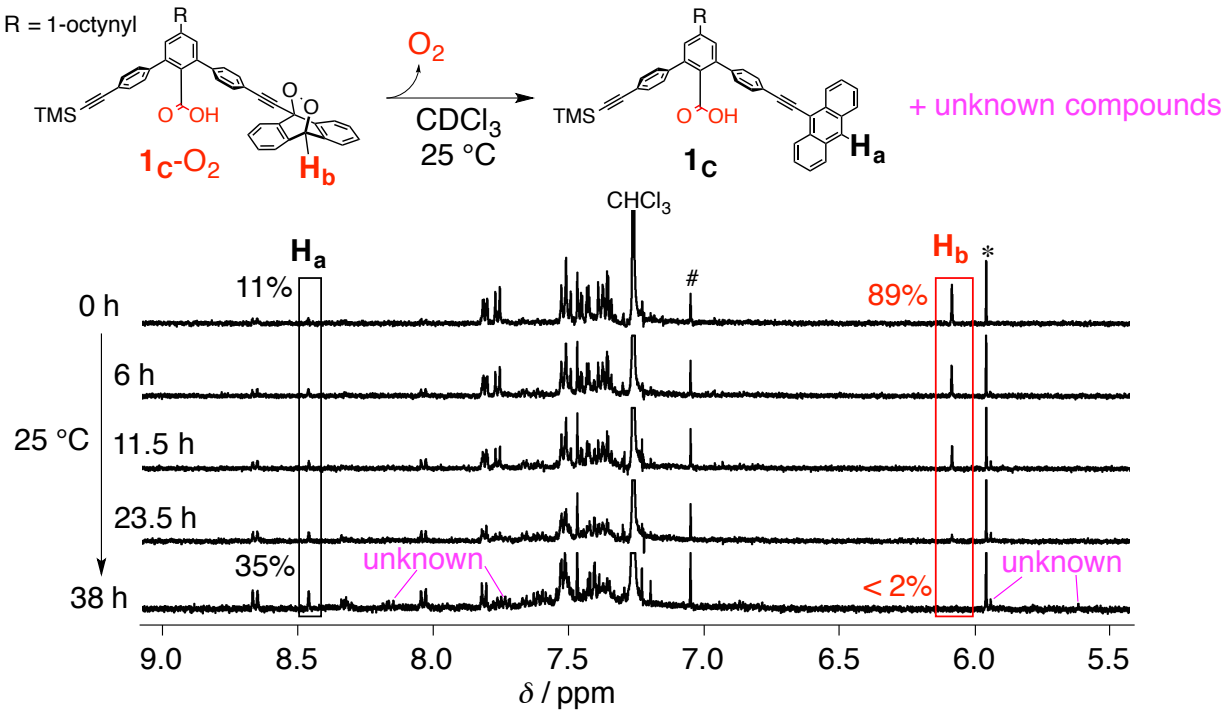

Fig. S17. Time-dependent ^{1}H NMR spectral changes of $\mathbf{1}_{C}$-O_2 (89%) at 25 °C under shielded light in $CDCl_3$. # and ∗ denote the ^{13}C satellite peaks of the solvent and the peak of 1,1,2,2-tetrachloroethane (0.32 mM) used as an internal standard, respectively. The photooxidised $\mathbf{1}_{C}$-O_2 was obtained in an undegassed $CDCl_3$ solution of $\mathbf{1}_{C}$ (0.50 mM) upon irradiation of light (> 400 nm) for 180 s (see ***Fig. S16a***). The photooxidised $\mathbf{1}_{C}$-O_2 was not stable and thermally decomposed back to the monomer $\mathbf{1}_{C}$ together with a small amount of an unkown compound.

9-2. Photoreaction of $\mathbf{1}_C$ in Undegassed $CDCl_3$ in the Presence of Monomeric Amidine A

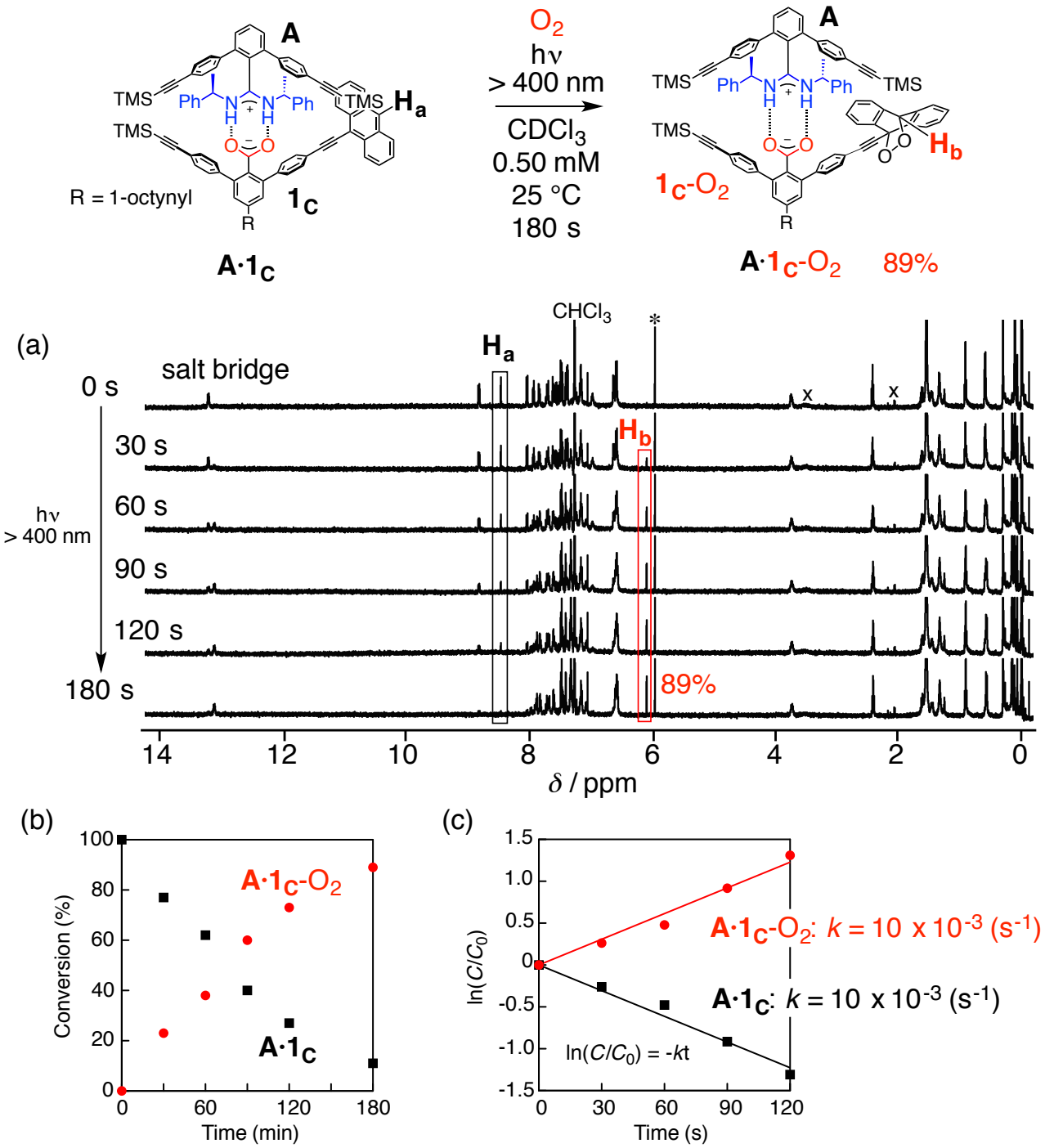

Fig. S18. (a) Time-dependent ^{1}H NMR spectral changes of $\mathbf{1}_C$ (500 MHz, undegassed $CDCl_3$, 25 °C, 0.50 mM) in the presence of **A** (0.50 mM) upon irradiation of light (> 400 nm). * and x denote the peak of 1,1,2,2-tetrachloroethane (0.20 mM) used as an internal standard and impurities contained in $CDCl_3$, respectively. The peaks were assigned on the basis of the ^{1}H NMR spectra shown in ***Fig. S27***. (b) Time-conversion relationships and (c) kinetic plots of the photooxidation of $\mathbf{1}_C$ (undegassed $CDCl_3$, 25 °C, 0.50 mM) in the presence of **A** (0.50 mM) estimated from the integral ratios of the peaks for H_a ($\mathbf{A}\cdot\mathbf{1}_C$), H_b ($\mathbf{A}\cdot\mathbf{1}_C$-$O_2$), and the internal standard (1,1,2,2-tetrachloroethane) based on the ^{1}H NMR spectral changes shown in (a).

9-3. Photoreaction of $\mathbf{1}_C$ in Undegassed $CDCl_3$ in the Presence of Amidine Template T_{AA}

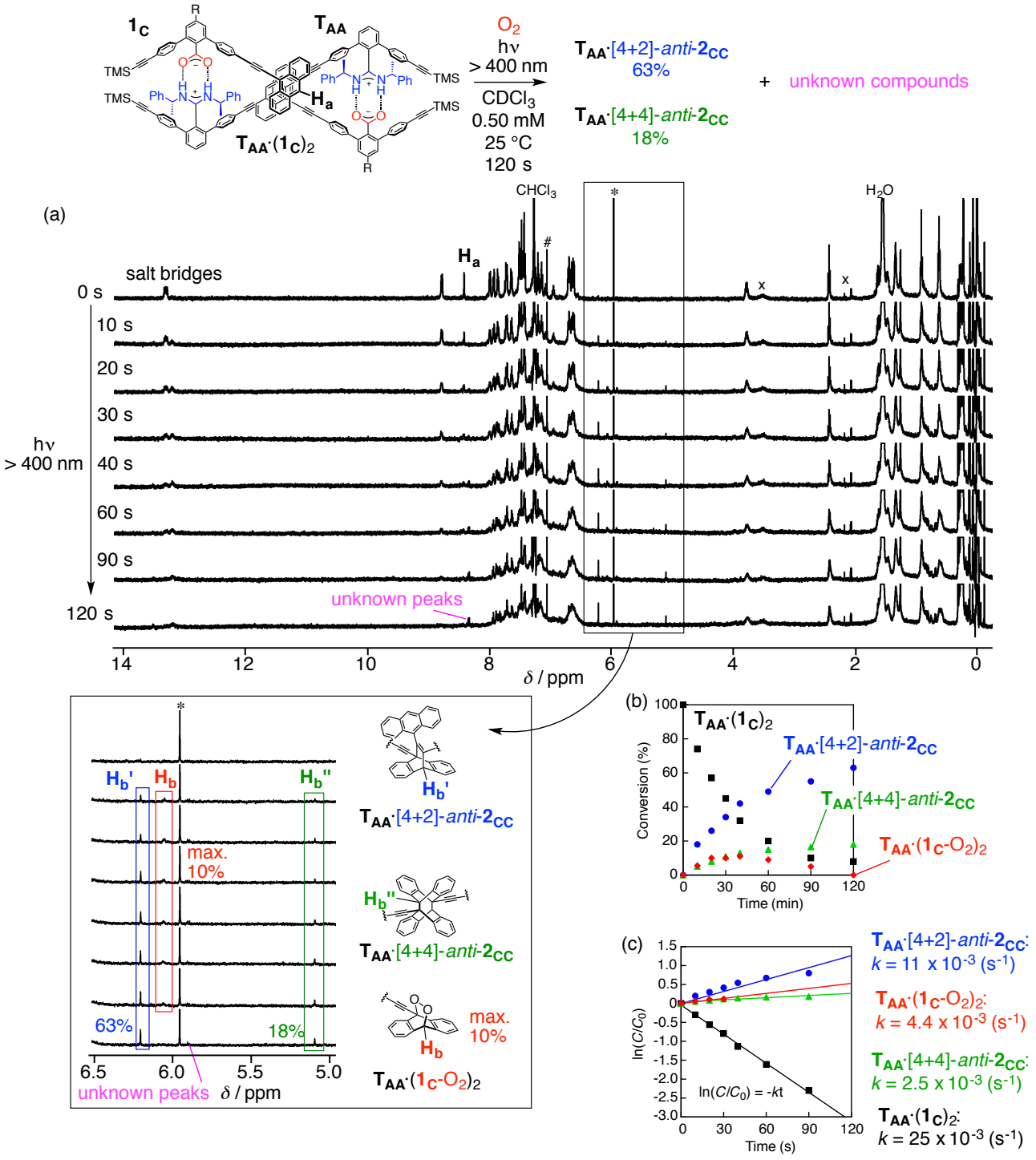

Fig. S19. (a) Time-dependent ^{1}H NMR spectral changes of $\mathbf{1}_C$ (500 MHz, undegassed $CDCl_3$, 25 °C, 0.50 mM) in the presence of T_{AA} (0.25 mM) upon irradiation of light (> 400 nm). #, ∗, and x denote the ^{13}C satellite peaks of the solvent, the peak of 1,1,2,2-tetrachloroethane (0.35 mM) used as an internal standard, and impurities contained in $CDCl_3$, respectively. The unknown peaks are probably due to photolysis products of $\mathbf{1}_C$-O_2. The peaks were assigned on the basis of the ^{1}H NMR spectra shown in ***Fig. S28***. (b) Time-conversion relationships and (c) kinetic plots of the photodimerisation of $\mathbf{1}_C$ (undegassed $CDCl_3$, 25 °C, 0.50 mM) in the presence of T_{AA} (0.25 mM) estimated from the integral ratios of the peaks for H_a (T_{AA}·($\mathbf{1}_C$)$_2$), H_b (T_{AA}·($\mathbf{1}_C$-O_2)$_2$), H_b' (T_{AA}·[4+2]-*anti*-$\mathbf{2}_{CC}$), H_b'' (T_{AA}·[4+4]-*anti*-$\mathbf{2}_{CC}$), and the internal standard (1,1,2,2-tetrachloroethane) based on the ^{1}H NMR spectral changes shown in (a).

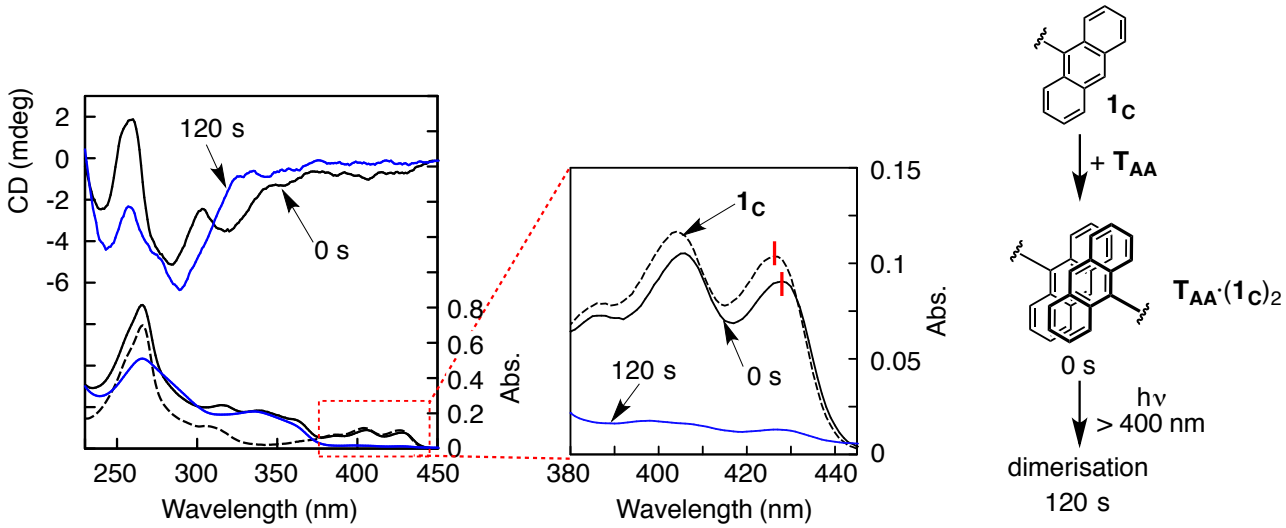

Fig. S20. Absorption spectrum of $\mathbf{1}_C$ (0.50 mM, black dotted line) in $CDCl_3$ and time-dependent absorption and CD spectral changes of $\mathbf{1}_C$ (0.50 mM) in the presence of $\mathbf{T}_{AA}$ (0.25 mM) in undegassed $CDCl_3$ before (0 s) and after (120 s) irradiation of light (> 400 nm). Cell length = 0.1 mm.

10. Photoreaction of Mono-9-Phenylethynylanthracene-Bound Carboxylic Acid Monomer in the Absence of Oxygen

10-1. Photoreaction of $\mathbf{1_C}$ in Degassed $CDCl_3$

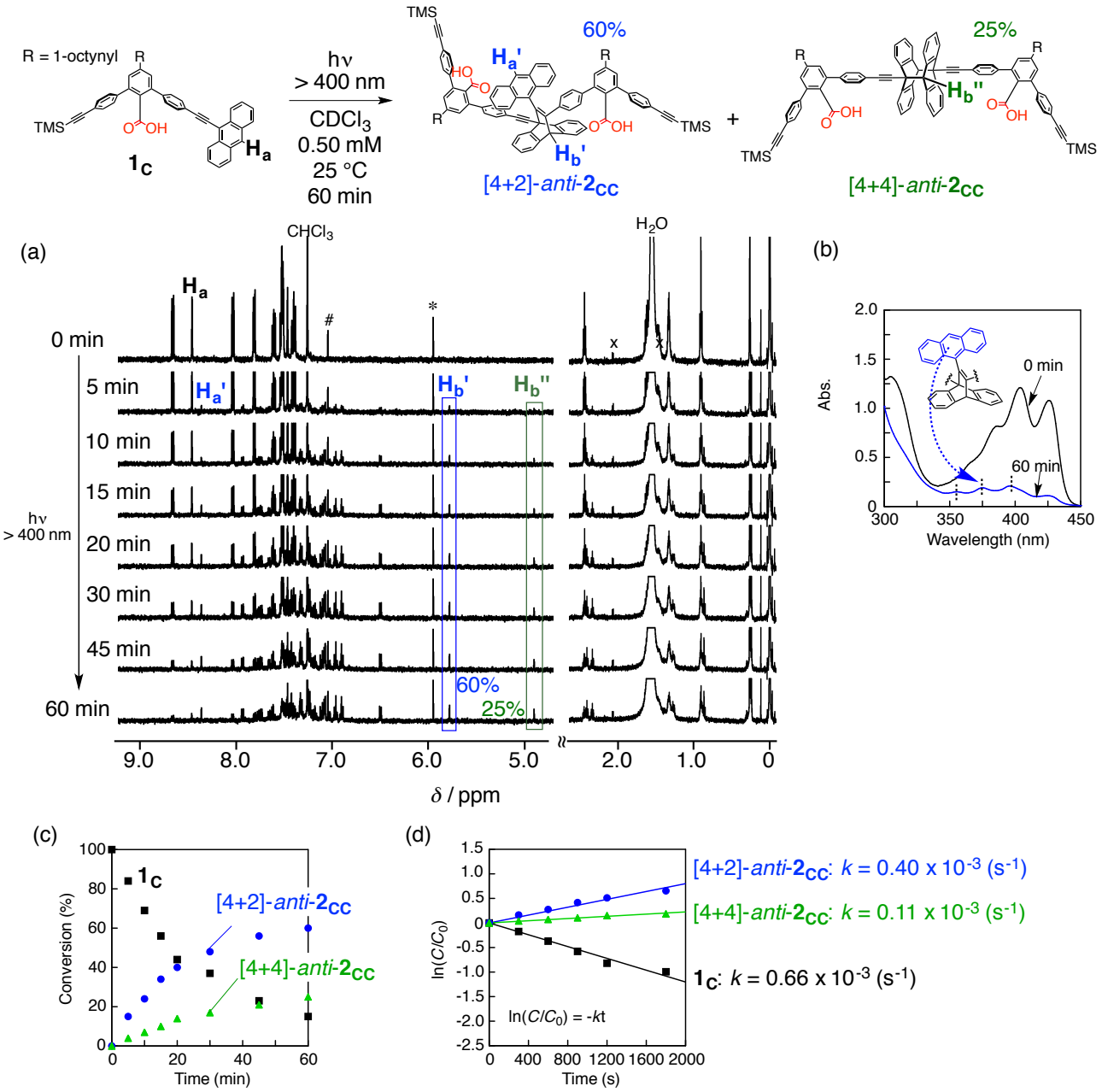

Fig. S21. (a) Time-dependent ^{1}H NMR spectral changes of $\mathbf{1_C}$ (500 MHz, degassed $CDCl_3$, 25 °C, 0.50 mM) upon irradiation of light (> 400 nm). #, ∗, and x denote the ^{13}C satellite peaks of the solvent, the peak of 1,1,2,2-tetrachloroethane (0.10 mM) used as an internal standard, and impurities contained in $CDCl_3$, respectively. (b) Time-dependent absorption spectral changes of $\mathbf{1_C}$ (0.50 mM) in degassed $CDCl_3$ before (0 min) and after (60 min) irradiation of light (> 400 nm). Cell length = 1 mm. (c) Time-conversion relationships and (d) kinetic plots of the photodimerisation of $\mathbf{1_C}$ (degassed $CDCl_3$, 25 °C, 0.50 mM) estimated from the integral ratios of the peaks for H_a ($\mathbf{1_C}$), H_b' ([4+2]-*anti*-$\mathbf{2_{CC}}$), H_b'' ([4+4]-*anti*-$\mathbf{2_{CC}}$), and the internal standard (1,1,2,2-tetrachloroethane) based on the ^{1}H NMR spectral changes shown in (a).

10-2. Photoreaction of $\mathbf{1}_C$ in Degassed $CDCl_3$ in the Presence of Monomeric Amidine A

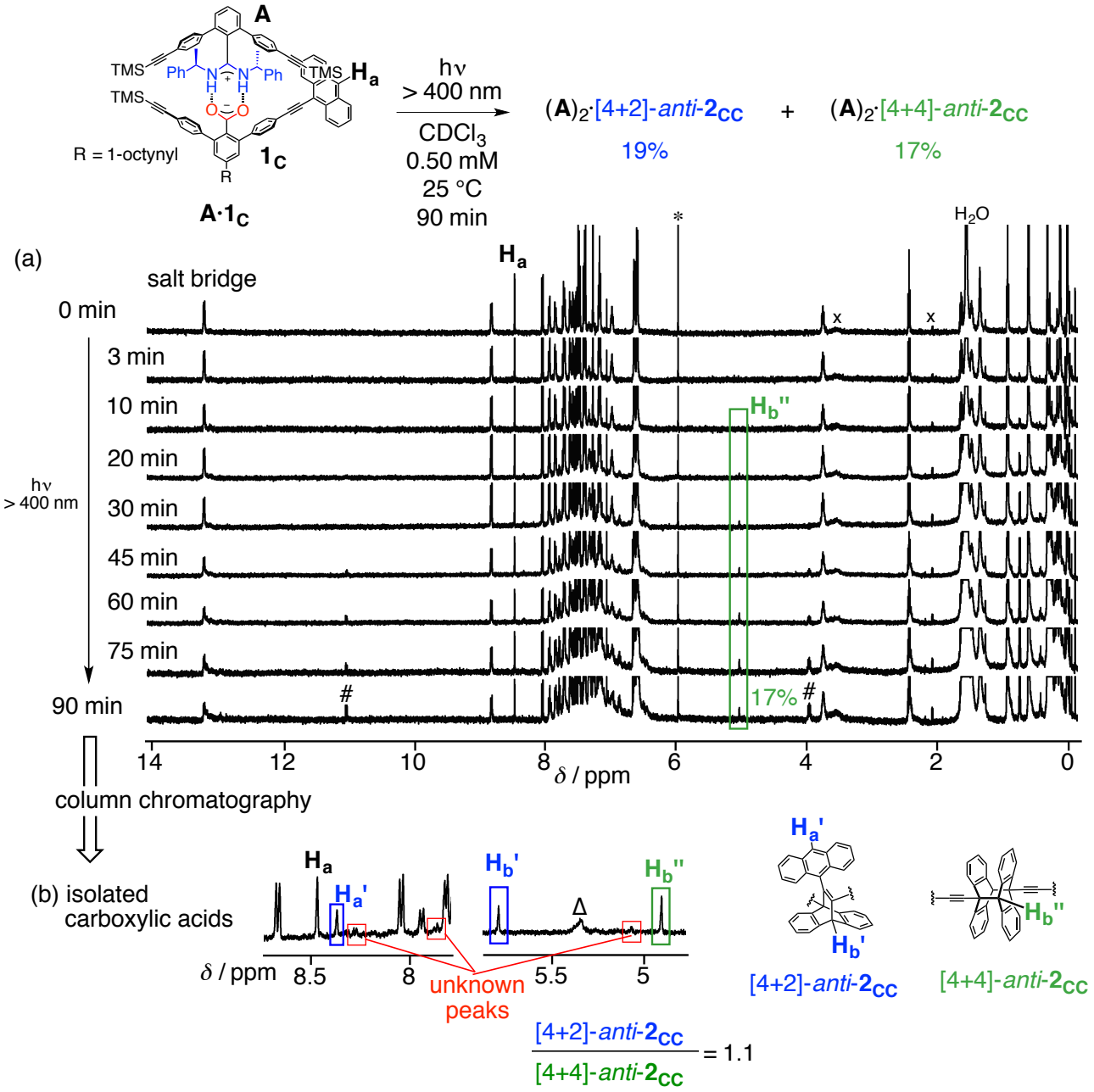

Fig. S22. (a) Time-dependent ^{1}H NMR spectral changes of $\mathbf{1}_C$ (500 MHz, degassed $CDCl_3$, 25 °C, 0.50 mM) in the presence of **A** (0.50 mM) upon irradiation of light (> 400 nm). ∗, x, and # denote the peak of 1,1,2,2-tetrachloroethane (0.23 mM) used as an internal standard, impurities contained in $CDCl_3$, and hydrochloride salt of **A** (10% after 90 min), respectively. The peaks were assigned on the basis of the ^{1}H NMR spectra shown in ***Fig. S27***. The peaks due to $(\mathbf{A})_2$·[4+2]-*anti*-$\mathbf{2}_{CC}$ were too broad to estimate its yield. The yield of $(\mathbf{A})_2$·[4+2]-*anti*-$\mathbf{2}_{CC}$ was estimated to be 19% based on the integral ratios of the peaks for isolated [4+4]-*anti*-$\mathbf{2}_{CC}$ and [4+2]-*anti*-$\mathbf{2}_{CC}$. (b) ^{1}H NMR spectrum (500 MHz, $CDCl_3$, 25 °C) of isolated carboxylic acid mixtures. The isolation procedure is described in the general procedure (3-3). Δ denotes the peak of impurities contained in eluent during evaporating the eluent.

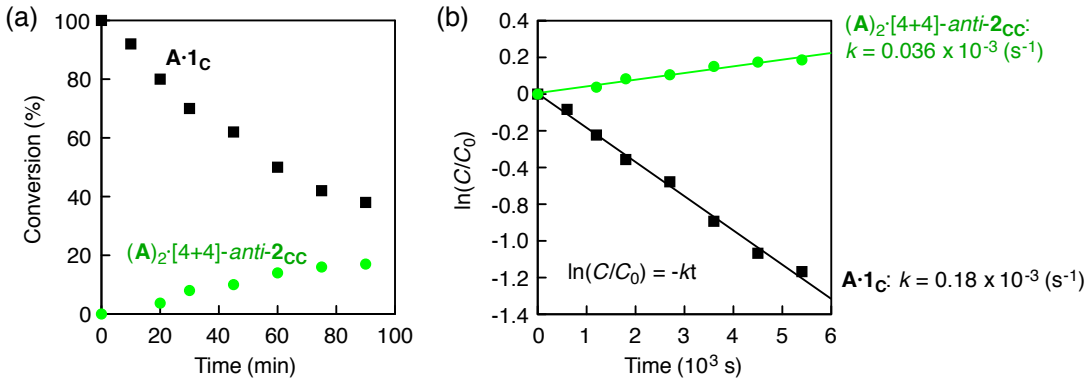

Fig. S23. (a) Time-conversion relationships and (b) kinetic plots of the photodimerisation of $\mathbf{1}_C$ (degassed $CDCl_3$, 25 °C, 0.50 mM) in the presence of **A** (0.50 mM) estimated from the integral ratios of the peaks for H_a ($\mathbf{A}\cdot\mathbf{1}_C$), H_b'' ($(\mathbf{A})_2\cdot$[4+4]-*anti*-$\mathbf{2}_{CC}$), and the internal standard (1,1,2,2-tetrachloroethane) based on the ^{1}H NMR spectral changes shown in ***Fig. S22a***.

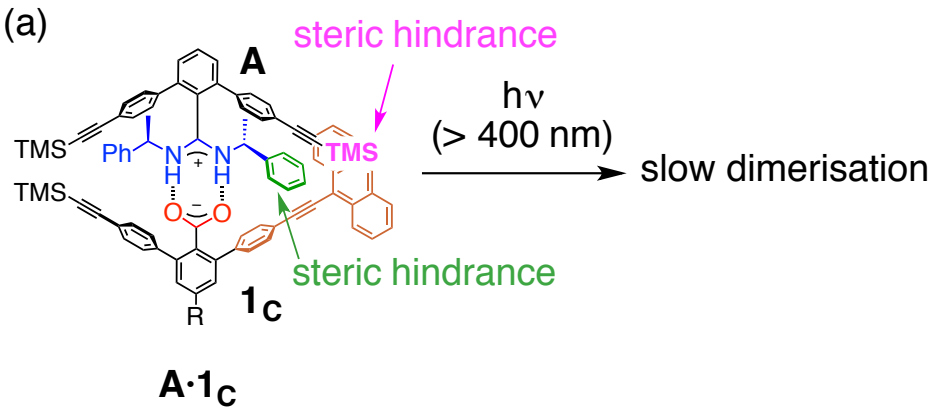

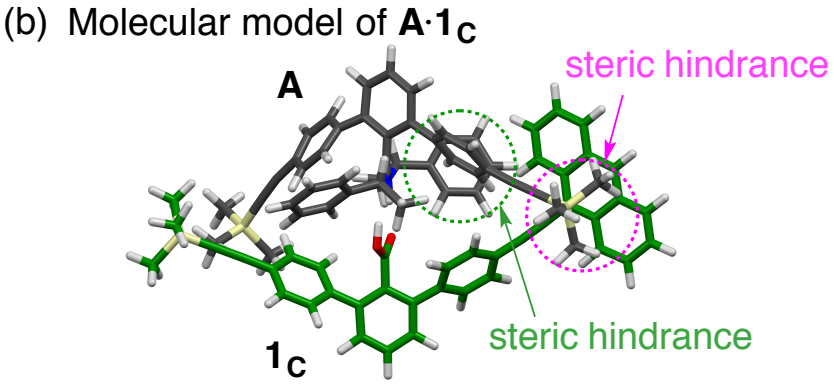

Fig. S24. (a) Possible mechanism for slow photodimerisation of $\mathbf{1}_C$ (0.50 mM) in the presence of **A** (0.50 mM) in degassed $CDCl_3$ at 25 °C. (b) An optimised structure of $\mathbf{A}\cdot\mathbf{1}_C$ by molecular mechanics (MM) calculations. The molecular modelling and MM calculations of $\mathbf{A}\cdot\mathbf{1}_C$ were performed on a Windows 7 PC using the CompassII Force Field as implemented in the Materials Studio package (Version 8.0; Accelrys Inc.). The initial structure of $\mathbf{A}\cdot\mathbf{1}_C$, in which the 1-octynyl group was replaced with a hydrogen atom, was constructed based on the crystal structure of a double-helical dimer comprising complementary amidine and carboxylic acid dimers linked by the diacetylene residues bound together through salt bridges.[S3]

10-3. Photoreaction of $\mathbf{1_C}$ in Degassed $CDCl_3$ in the Presence of Amidine Template $\mathbf{T_{AA}}$

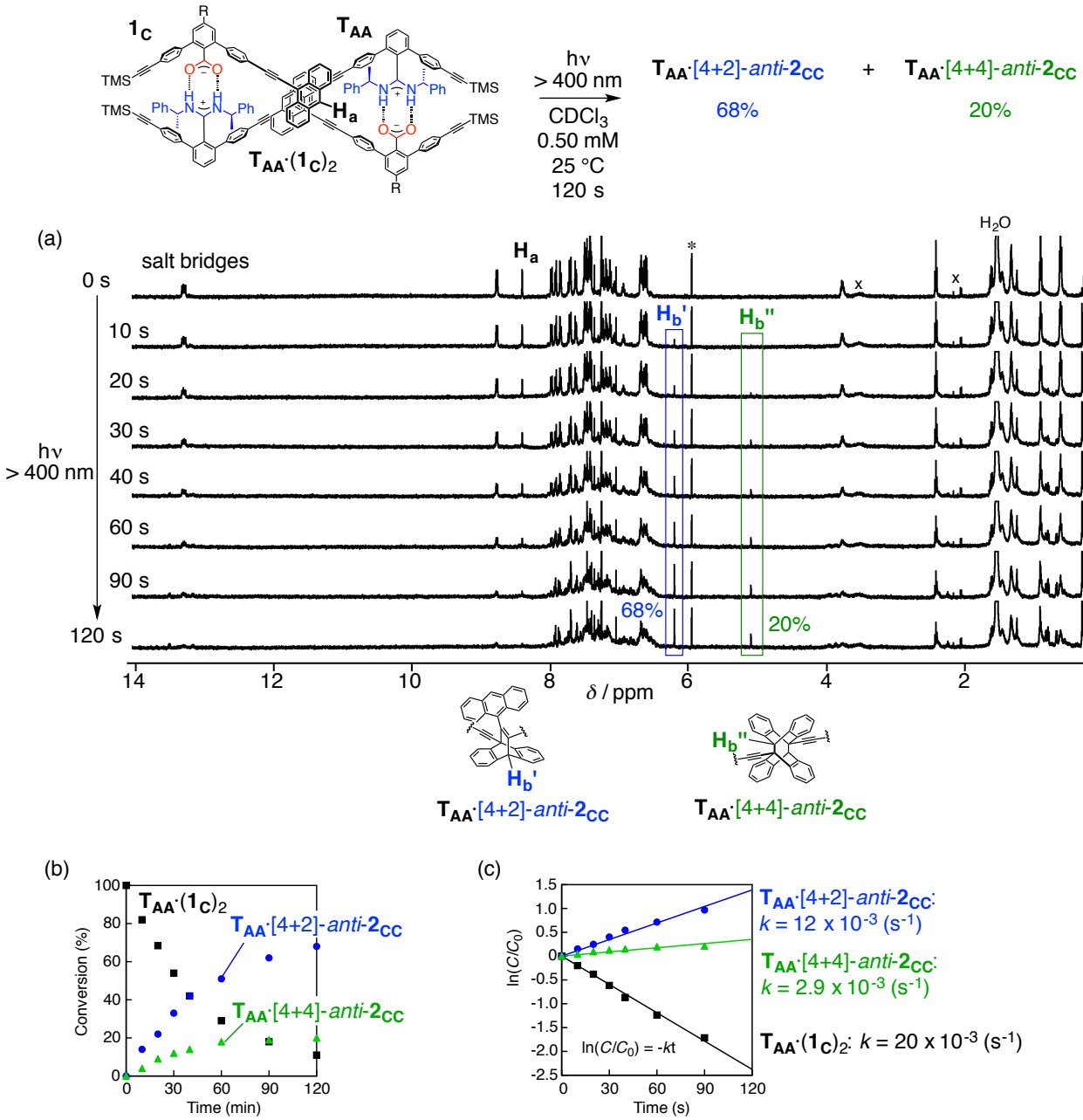

Fig. S25. (a) Time-dependent ^{1}H NMR spectral changes of $\mathbf{1_C}$ (500 MHz, degassed $CDCl_3$, 25 °C, 0.50 mM) in the presence of $\mathbf{T_{AA}}$ (0.25 mM) upon irradiation of light (> 400 nm). ∗ and **x** denote the peak of 1,1,2,2-tetrachloroethane (0.15 mM) used as an internal standard and impurities contained in $CDCl_3$, respectively. The peaks were assigned on the basis of the ^{1}H NMR spectra shown in ***Fig. S28***. (b) Time-conversion relationships and (c) kinetic plots of the photodimerisation of $\mathbf{1_C}$ (degassed $CDCl_3$, 25 °C, 0.50 mM) in the presence of $\mathbf{T_{AA}}$ (0.25 mM) estimated from the integral ratios of the peaks for H_a ($\mathbf{T_{AA}}$·($\mathbf{1_C}$)$_2$), H_b' ($\mathbf{T_{AA}}$·[4+2]-*anti*-$\mathbf{2_{CC}}$), H_b'' ($\mathbf{T_{AA}}$·[4+4]-*anti*-$\mathbf{2_{CC}}$), and the internal standard (1,1,2,2-tetrachloroethane) based on the ^{1}H NMR spectral changes shown in (a).

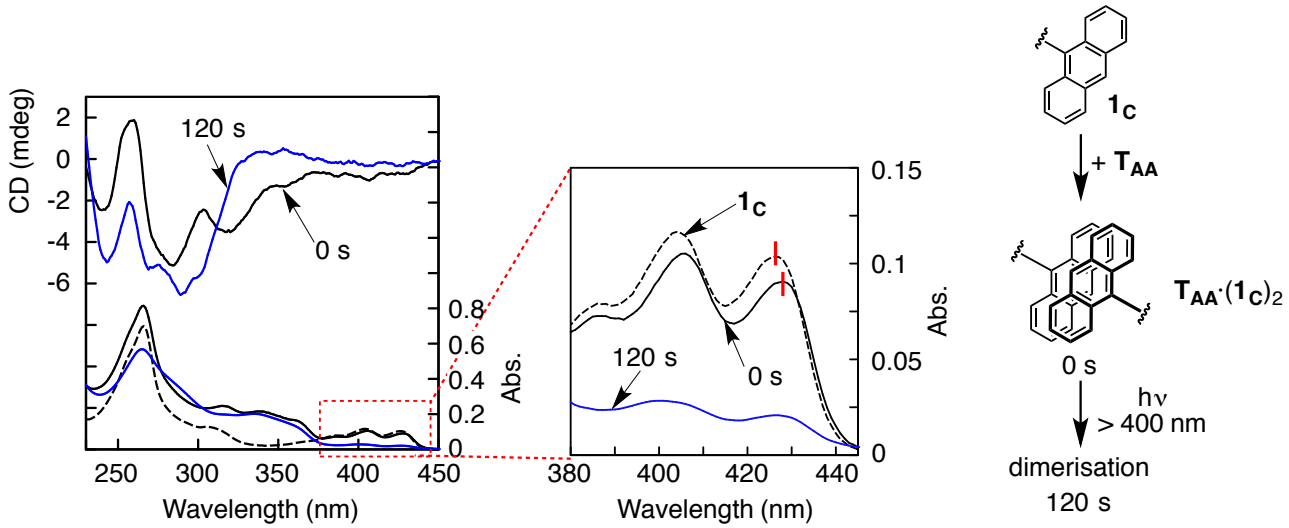

Fig. S26. Absorption spectrum of $\mathbf{1}_C$ (0.50 mM, black dotted line) in $CDCl_3$ and time-dependent absorption and CD spectral changes of $\mathbf{1}_C$ (0.50 mM) in the presence of $\mathbf{T}_{AA}$ (0.25mM) in degassed $CDCl_3$ before (0 s) and after (120 s) irradiation of light (> 400 nm). Cell length = 0.1 mm.

11. Identification of Photoreaction Products of Mono-9-Phenylethynylanthracene-Bound Carboxylic Acid Monomer

11-1. Photoreaction of $\mathbf{1}_C$ in Degassed and Undegassed $CDCl_3$ in the Presence of Monomeric Amidine A

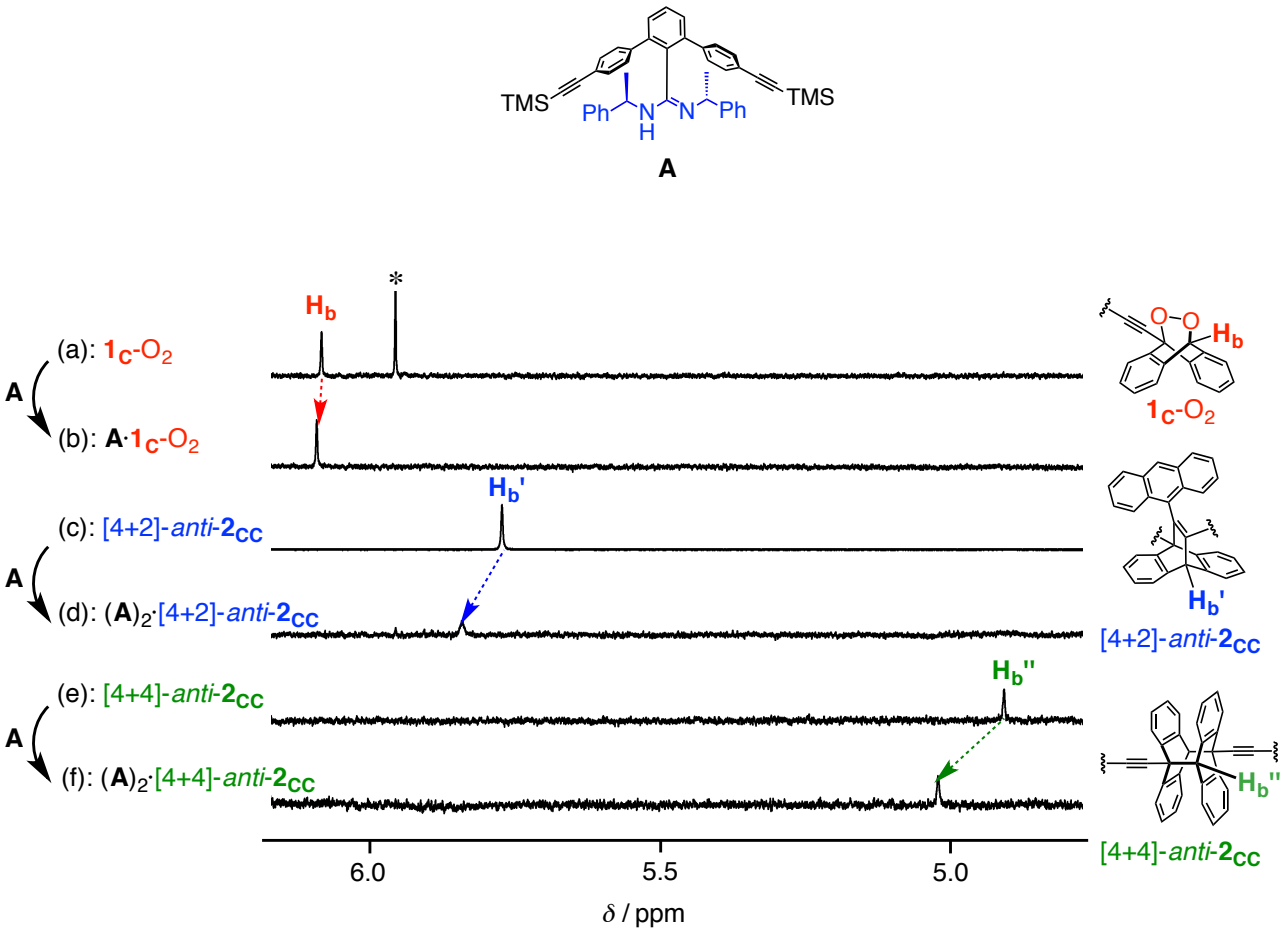

Fig. S27. ^{1}H NMR spectra (500 MHz, 25 °C) of (a) $\mathbf{1}_C$-O_2 prepared in a undegassed $CDCl_3$ solution of $\mathbf{1}_C$ (0.50 mM) upon irradiation of light (> 400 nm) for 3 min (see ***Fig. S16a***), (b) a mixture of the sample (a) and **A** (0.50 mM), (c) [4+2]-*anti*-$\mathbf{2}_{CC}$, (d) a mixture of [4+2]-*anti*-$\mathbf{2}_{CC}$ (0.50 mM) and **A** (1.0 mM), (e) [4+4]-*anti*-$\mathbf{2}_{CC}$, and (f) a mixture of [4+4]-*anti*-$\mathbf{2}_{CC}$ (0.20 mM) and **A** (0.40 mM). ∗ denotes the peak of 1,1,2,2-tetrachloroethane used as an internal standard.

11-2. Photoreaction of $\mathbf{1}_C$ in Degassed and Undegassed $CDCl_3$ in the Presence of Template $\mathbf{T}_{AA}$

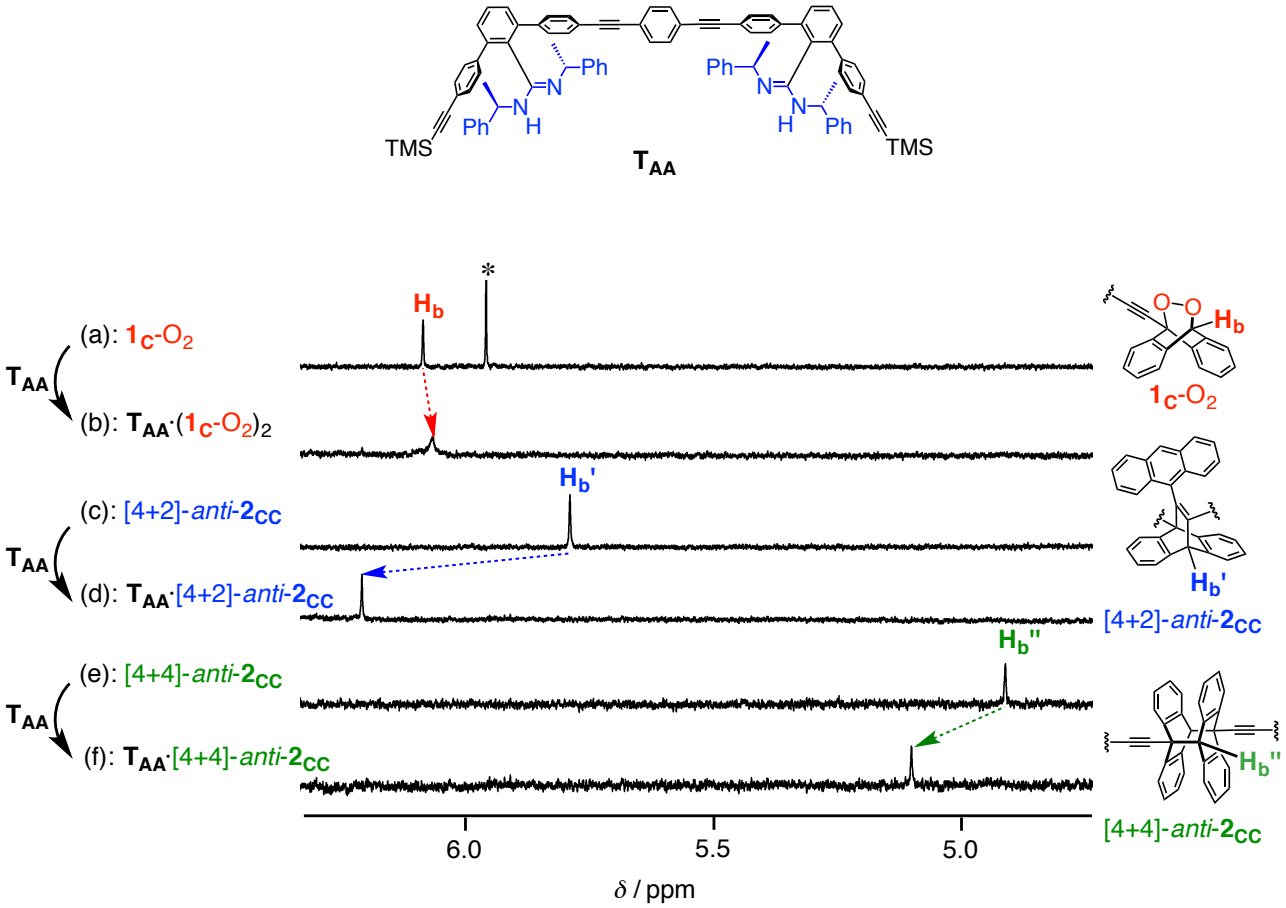

Fig. S28. ^{1}H NMR spectra (500 MHz, 25 °C) of (a) $\mathbf{1}_C$-O_2 prepared in a undegassed $CDCl_3$ solution of $\mathbf{1}_C$ (0.50 mM) upon irradiation of light (> 400 nm) for 3 min (see ***Fig. S16a***), (b) a mixture of the sample (a) and $\mathbf{T}_{AA}$ (0.25 mM), (c) [4+2]-*anti*-$\mathbf{2}_{CC}$, (d) a mixture of [4+2]-*anti*-$\mathbf{2}_{CC}$ (0.36 mM) and $\mathbf{T}_{AA}$ (0.36 mM), (e) [4+4]-*anti*-$\mathbf{2}_{CC}$, and (f) a mixture of [4+4]-*anti*-$\mathbf{2}_{CC}$ (0.20 mM) and $\mathbf{T}_{AA}$ (0.20 mM). ∗ denotes the peak of 1,1,2,2-tetrachloroethane used as an internal standard.

12. Photoreaction of Di-9-Phenylethynylanthracene-Bound Carboxylic Acid Monomer in the Presence of Oxygen

12-1. Photoreaction of 3_C in Undegassed $CDCl_3$

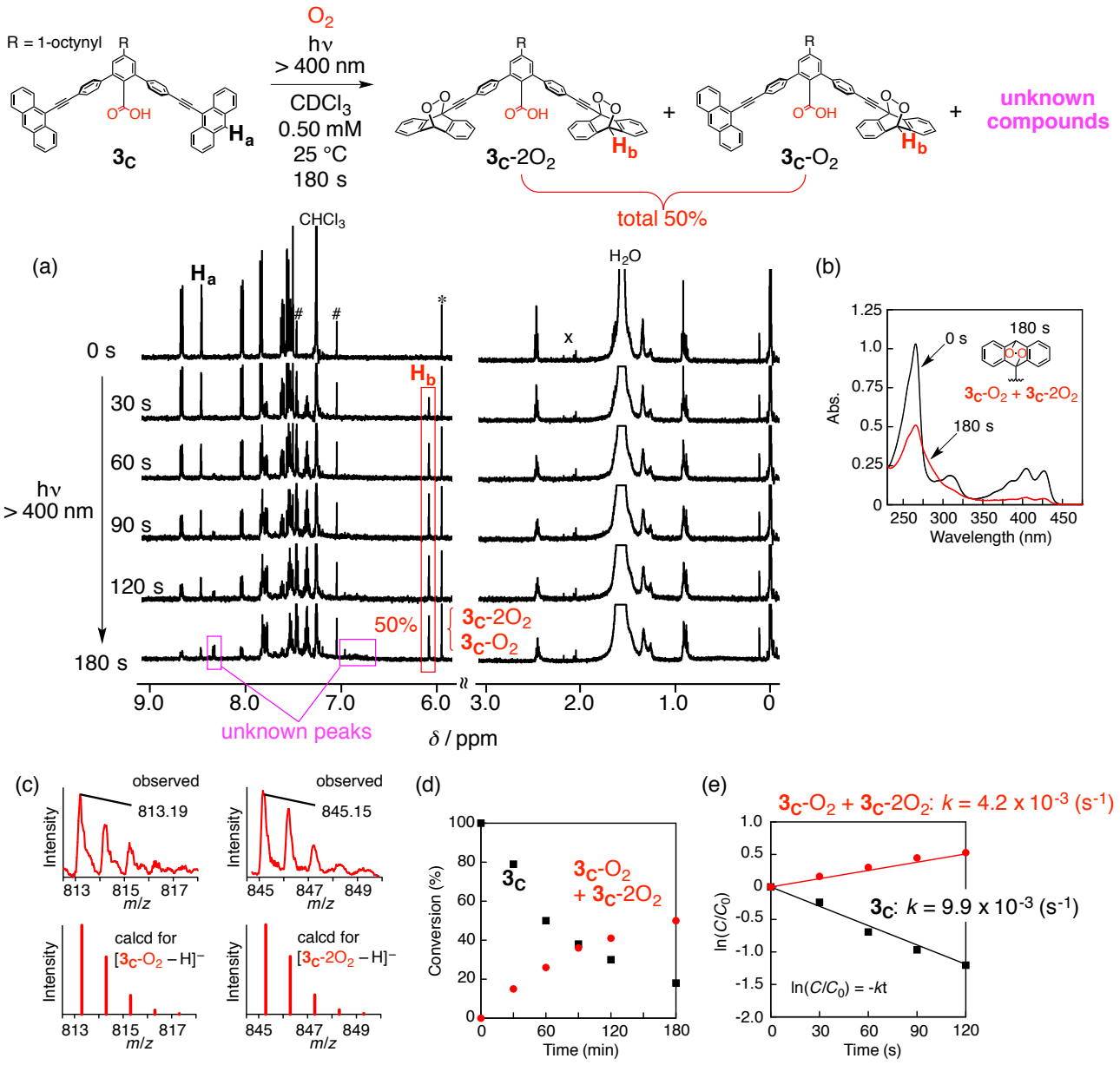

Fig. S29. (a) Time-dependent ^{1}H NMR spectral changes of $\mathbf{3}_C$ (500 MHz, undegassed $CDCl_3$, 25 °C, 0.50 mM) upon irradiation of light (> 400 nm). #, ∗, and x denote the ^{13}C satellite peaks of the solvent, the peak of 1,1,2,2-tetrachloroethane (0.10 mM) used as an internal standard, and impurities contained in $CDCl_3$, respectively. The unknown peaks are probably due to photolysis products of $\mathbf{3}_C$-$2O_2$ and $\mathbf{3}_C$-O_2. (b) Time-dependent absorption spectral changes of $\mathbf{3}_C$ (0.50 mM) in undegassed $CDCl_3$ before (0 s) and after (180 s) irradiation of light (> 400 nm). Cell length = 0.1 mm. (c) Negative mode ESI-MS spectrum (CH_3CN/CH_3OH = 1/1 (*v*/*v*)) of $\mathbf{3}_C$ after irradiation of light (> 400 nm) for 180 s in undegassed $CDCl_3$. (d) Time-conversion relationships and (e) kinetic plots of the photooxidation of $\mathbf{3}_C$ (undegassed $CDCl_3$, 25 °C, 0.50 mM) estimated from the integral ratios of the peaks for H_a ($\mathbf{3}_C$), H_b ($\mathbf{3}_C$-$2O_2$ and $\mathbf{3}_C$-O_2), and the internal standard (1,1,2,2-tetrachloroethane) based on the ^{1}H NMR spectral changes shown in (a).

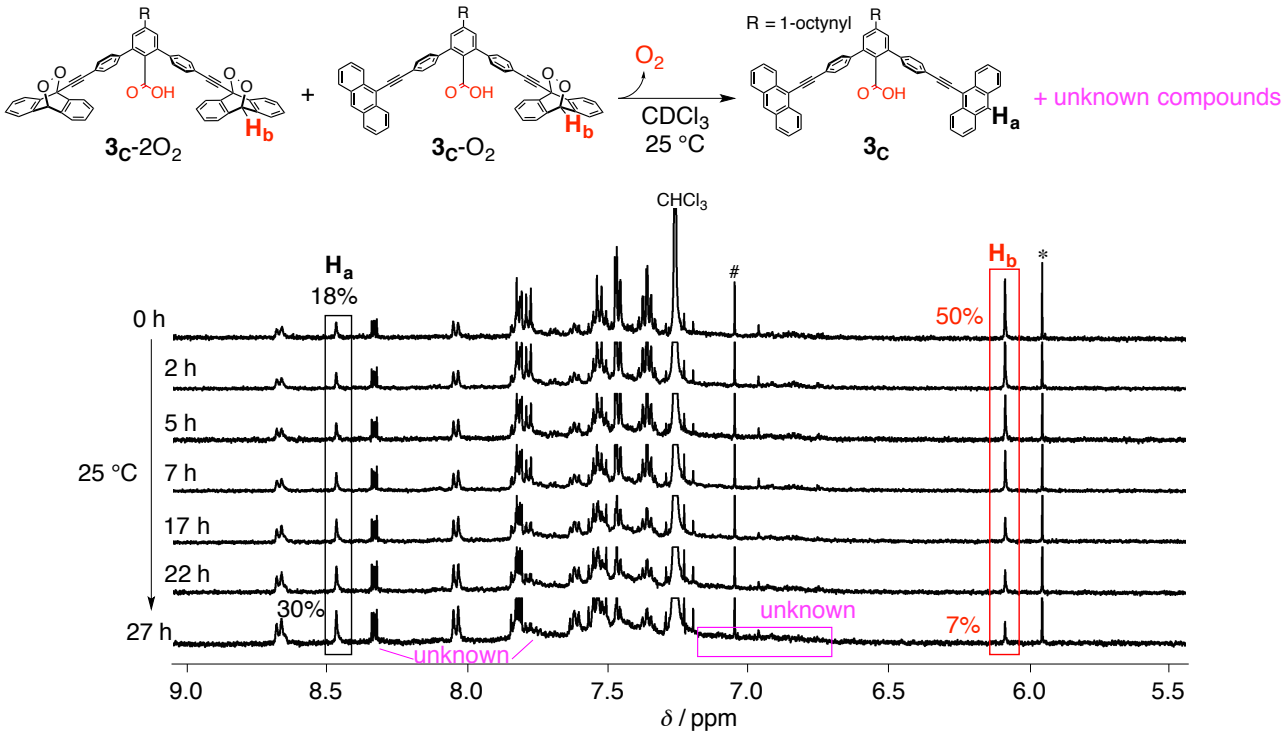

Fig. S30. Time-dependent ^{1}H NMR spectral changes of a mixture of $\mathbf{3}_{C}$-$2O_2$ and $\mathbf{3}_{C}$-O_2 under shielded light in $CDCl_3$ at 25 °C. # and ∗ denote the ^{13}C satellite peaks of the solvent and the peak of 1,1,2,2-tetrachloroethane (0.10 mM) used as an internal standard. The photooxidised mixture of $\mathbf{3}_{C}$-$2O_2$ and $\mathbf{3}_{C}$-O_2 was obtained in an undegassed $CDCl_3$ solution of $\mathbf{3}_{C}$ (0.50 mM) upon irradiation of light (> 400 nm) for 180 s (see ***Fig. S29a***). The photooxidised $\mathbf{3}_{C}$-$2O_2$ and $\mathbf{3}_{C}$-O_2 were not stable and thermally decomposed back to the monomer $\mathbf{3}_{C}$ together with a small amount of an unkown compound.

12-2. Photoreaction of 3_C in Undegassed $CDCl_3$ in the Presence of Amidine Template T_{AA}

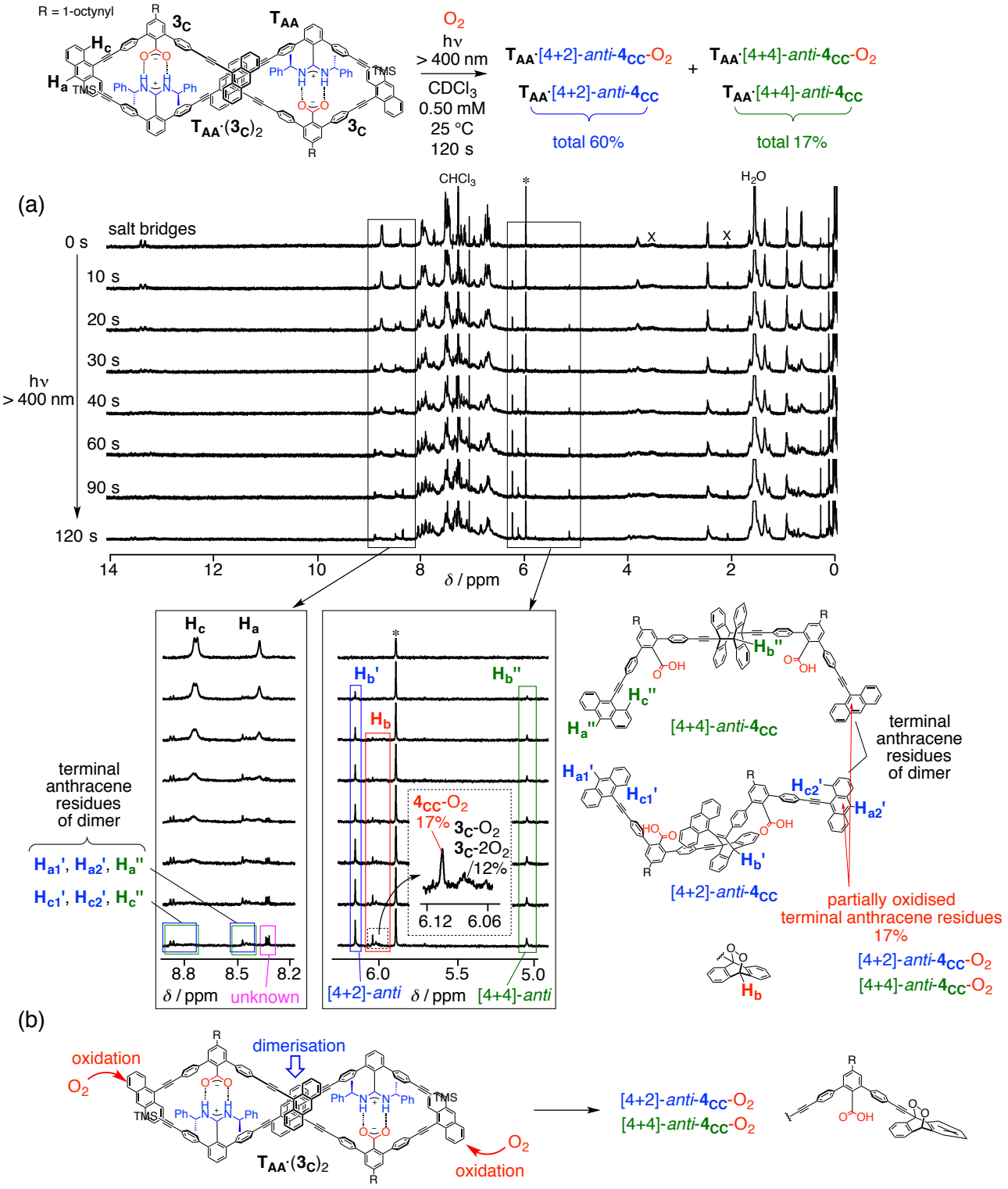

Fig. S31. (a) Time-dependent ^{1}H NMR spectral changes of $\mathbf{3}_C$ (500 MHz, undegassed $CDCl_3$, 25 °C, 0.50 mM) in the presence of $\mathbf{T}_{AA}$ (0.25 mM) upon irradiation of light (> 400 nm). ∗ and x denote the peak of 1,1,2,2-tetrachloroethane (1.1 mM) used as an internal standard and impurities contained in $CDCl_3$. (b) Possible mechanism for oxidation of terminal anthracene residues of $\mathbf{3}_C$ (0.50 mM) in the presence of $\mathbf{T}_{AA}$ (0.25 mM) in undegassed $CDCl_3$ at 25 °C. The peaks due to the complexes $\mathbf{T}_{AA}\cdot(\mathbf{3}_C\text{-}O_2)_2$ and $\mathbf{T}_{AA}\cdot(\mathbf{3}_C\text{-}2O_2)_2$ were assigned on the basis of the ^{1}H NMR spectra shown in ***Fig. S33***.

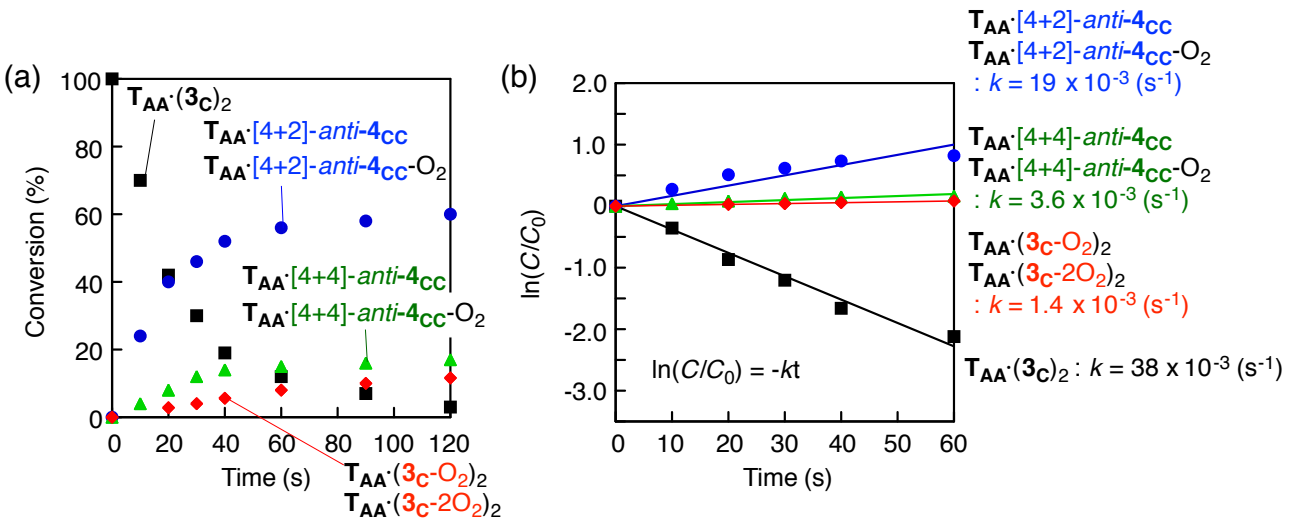

Fig. S32. (a) Time-conversion relationships and (b) kinetic plots of the photodimerisation of $\mathbf{3}_C$ (undegassed $CDCl_3$, 25 °C, 0.50 mM) in the presence of $\mathbf{T}_{AA}$ (0.25 mM) estimated from the integral ratios of the peaks for H_a ($\mathbf{T}_{AA}$·($\mathbf{3}_C$)$_2$), H_b ($\mathbf{T}_{AA}$·($\mathbf{3}_C$-$2O_2$)$_2$ and $\mathbf{T}_{AA}$·($\mathbf{3}_C$-O_2)$_2$), H_b' ($\mathbf{T}_{AA}$·[4+2]-*anti*-$\mathbf{4}_{CC}$ and $\mathbf{T}_{AA}$·[4+2]-*anti*-$\mathbf{4}_{CC}$-O_2), H_b'' ($\mathbf{T}_{AA}$·[4+4]-*anti*-$\mathbf{4}_{CC}$ and $\mathbf{T}_{AA}$·[4+4]-*anti*-$\mathbf{4}_{CC}$-O_2), and the internal standard (1,1,2,2-tetrachloroethane) based on the ^{1}H NMR spectral changes shown in ***Fig. S31a***.

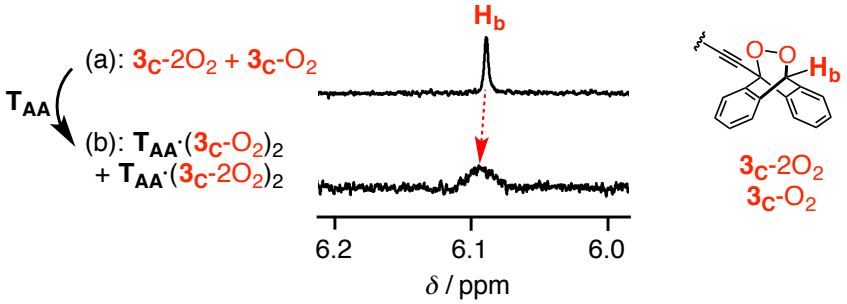

Fig. S33. ^{1}H NMR spectra (500 MHz, 25 °C) of (a) a mixture of $\mathbf{3}_C$-O_2 and $\mathbf{3}_C$-$2O_2$ prepared in a undegassed $CDCl_3$ solution of $\mathbf{3}_C$ (0.50 mM) upon irradiation of light (> 400 nm) for 3 min (see ***Fig. S29a***) and (b) a mixture of the sample (a) and $\mathbf{T}_{AA}$ (0.25 mM).

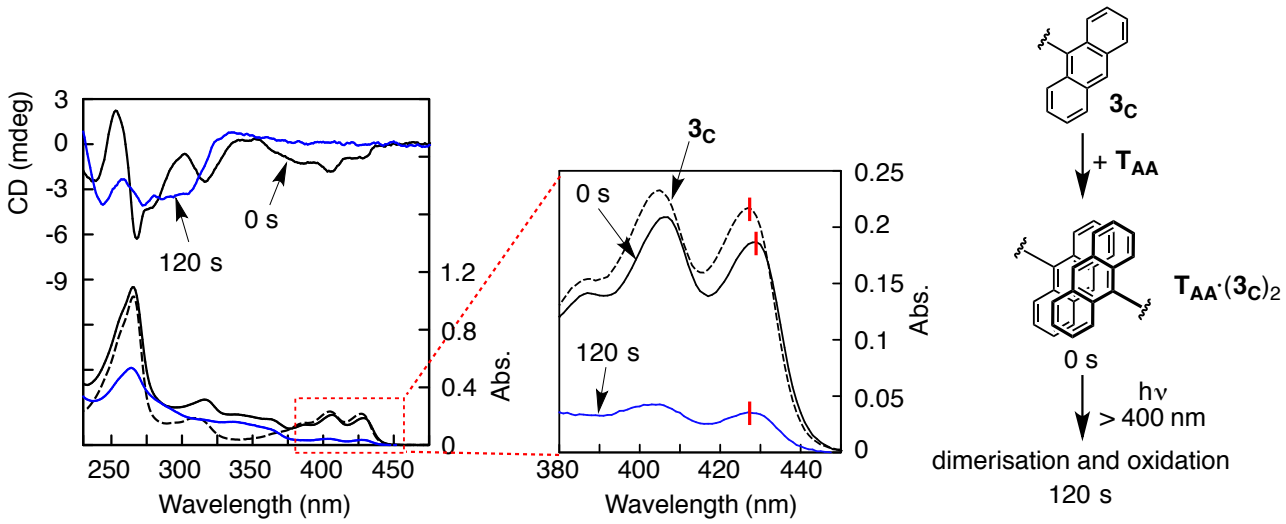

Fig. S34. Absorption spectrum of $\mathbf{3}_C$ (0.50 mM, black dotted line) in undegassed $CDCl_3$, and time-dependent absorption and CD spectral changes of $\mathbf{3}_C$ (0.50 mM) in the presence of $\mathbf{T}_{AA}$ (0.25 mM) in undegassed $CDCl_3$ before (0 s) and after (120 s) irradiation of light (> 400 nm). Cell length = 0.1 mm.

13. Photoreaction of Di-9-Phenylethynylanthracene-Bound Carboxylic Acid Monomer in the Absence of Oxygen

13-1. Photoreaction of 3_C in Degassed $CDCl_3$

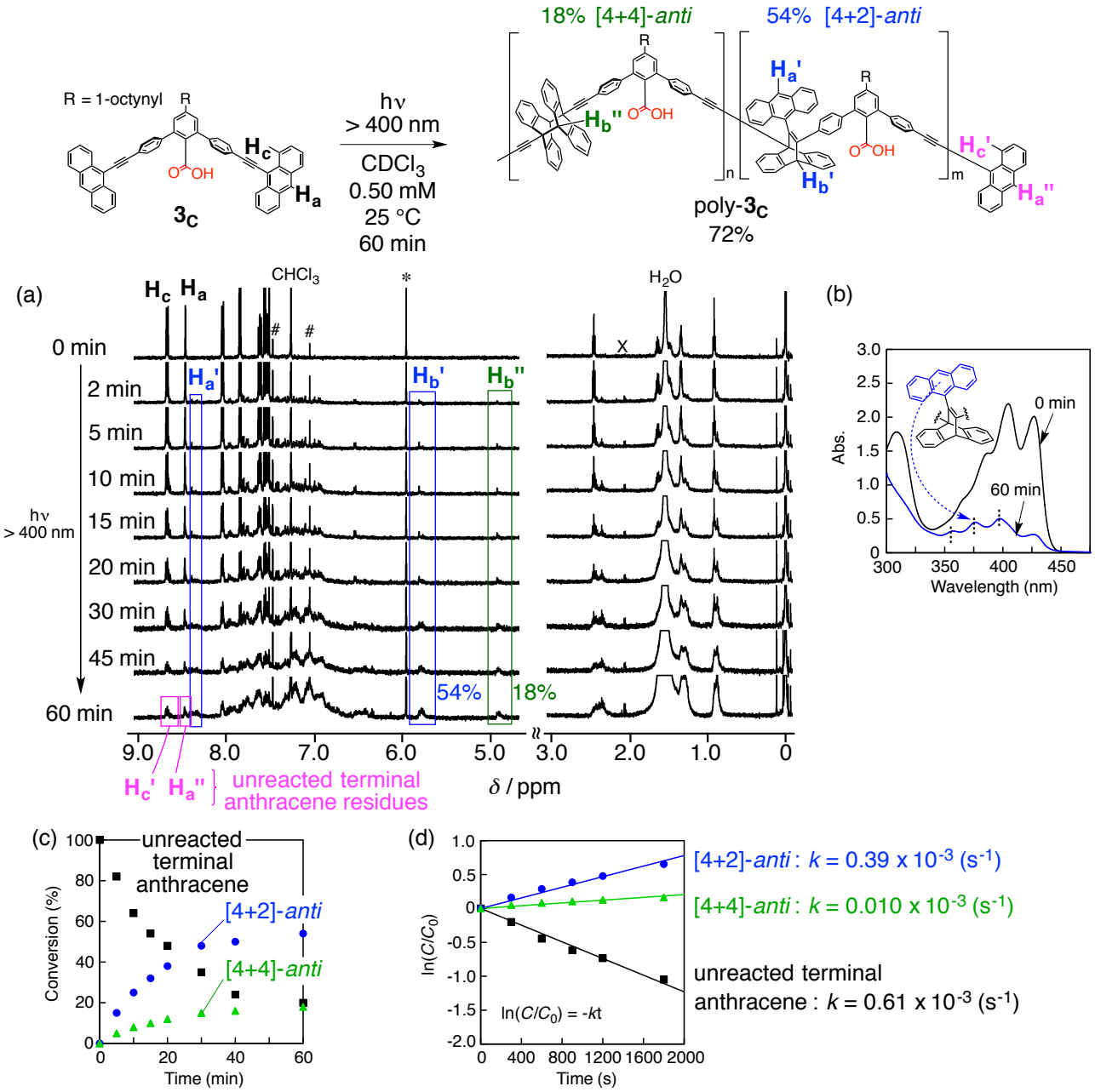

Fig. S35. (a) Time-dependent ^{1}H NMR spectral changes of $\mathbf{3}_C$ (500 MHz, degassed $CDCl_3$, 25 °C, 0.50 mM) upon irradiation of light (> 400 nm). #, ∗, and x denote the ^{13}C satellite peaks of the solvent, the peak of 1,1,2,2-tetrachloroethane (0.34 mM) used as an internal standard, and impurities contained in $CDCl_3$. (b) Time-dependent absorption spectral changes of $\mathbf{3}_C$ (0.50 mM) in degassed $CDCl_3$ before (0 min) and after (60 min) irradiation of light (> 400 nm). Cell length = 1 mm. (c) Time-conversion relationships and (d) kinetic plots of the photodimerisation of $\mathbf{3}_C$ (degassed $CDCl_3$, 25 °C, 0.50 mM) estimated from the integral ratios of the peaks for H_a and H_a'' (unreacted terminal anthracene), H_b' ([4+2]-*anti*), H_b'' ([4+4]-*anti*), and the internal standard (1,1,2,2-tetrachloroethane) based on the ^{1}H NMR spectral changes shown in (a).

13-2. Photoreaction of 3_C in Degassed $CDCl_3$ in the Presence of Amidine Template T_{AA}

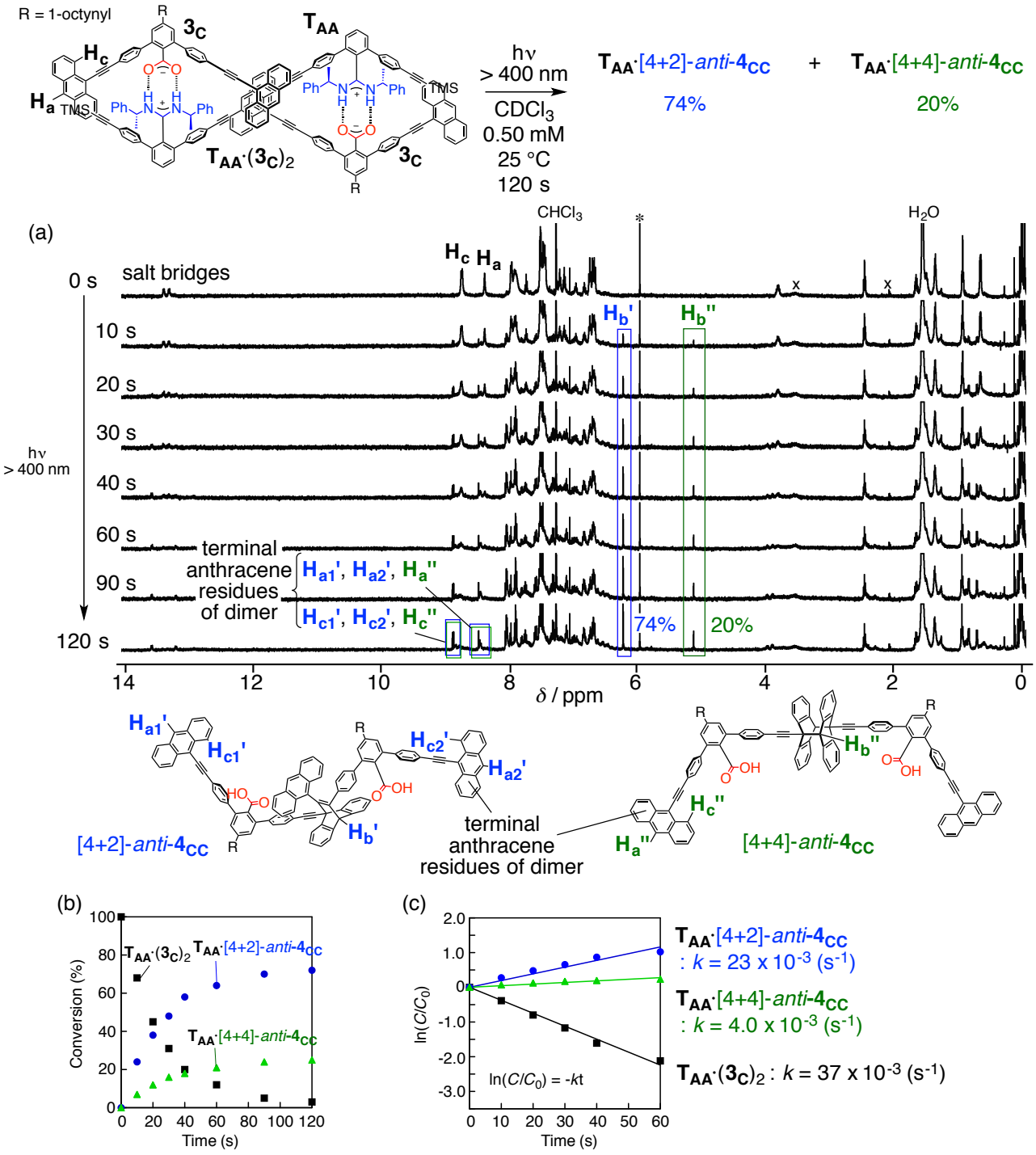

Fig. S36. (a) Time-dependent ^{1}H NMR spectral changes of $\mathbf{3}_C$ (500 MHz, degassed $CDCl_3$, 25 °C, 0.50 mM) in the presence of $\mathbf{T}_{AA}$ (0.25 mM) upon irradiation of light (> 400 nm). ∗ and x denote the peak of 1,1,2,2-tetrachloroethane (0.43 mM) used as an internal standard and impurities contained in $CDCl_3$. (b) Time-conversion relationships and (c) kinetic plots of the photodimerisation of $\mathbf{3}_C$ (degassed $CDCl_3$, 25 °C, 0.50 mM) in the presence of $\mathbf{T}_{AA}$ (0.25 mM) estimated from the integral ratios of the peaks for H_a ($\mathbf{T}_{AA}$·($\mathbf{3}_C$)$_2$), H_b' ($\mathbf{T}_{AA}$·[4+2]-*anti*-$\mathbf{4}_{CC}$), H_b'' ($\mathbf{T}_{AA}$·[4+4]-*anti*-$\mathbf{4}_{CC}$), and the internal standard (1,1,2,2-tetrachloroethane) based on the ^{1}H NMR spectral changes shown in (a).

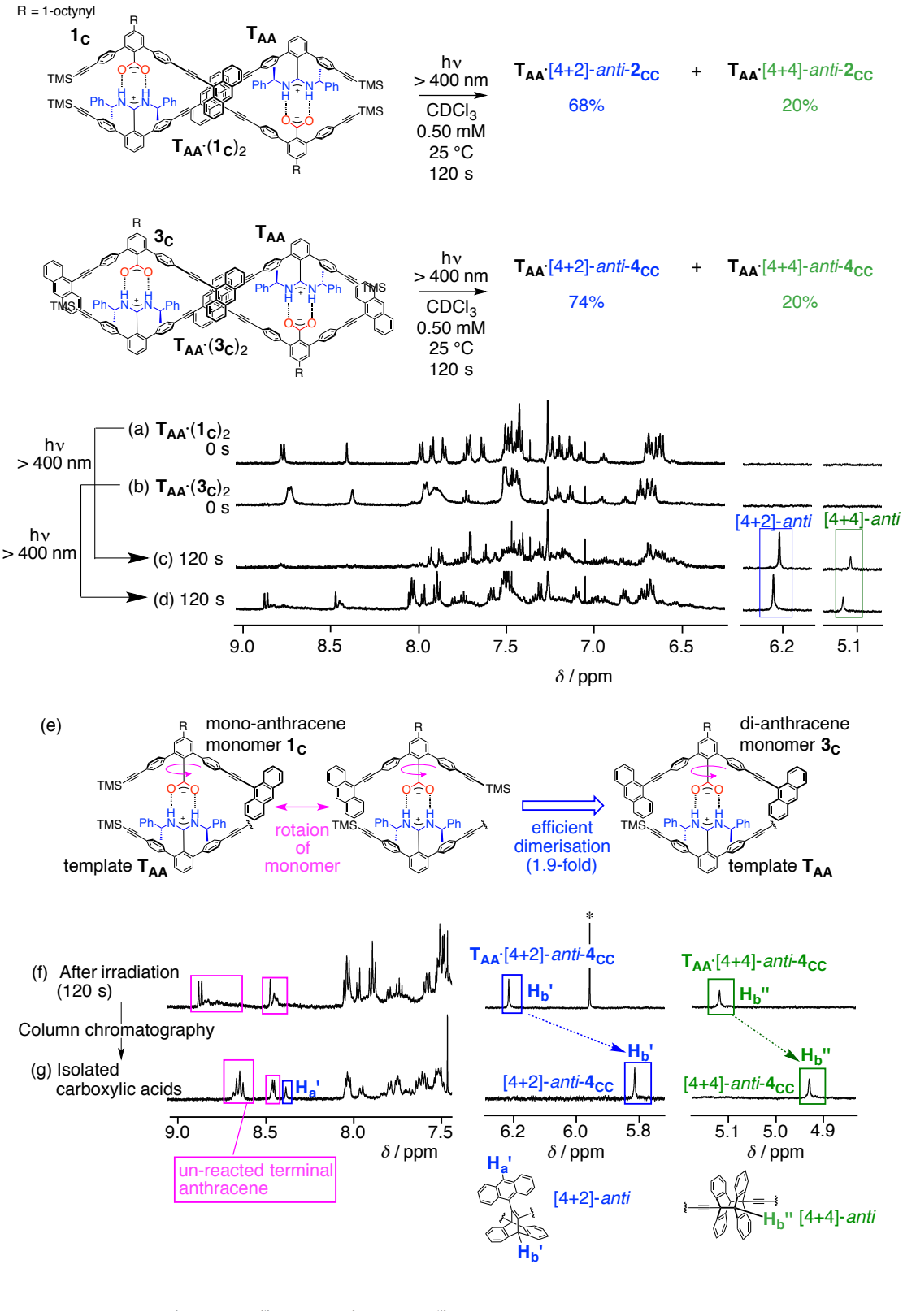

Fig. S37. (a-d) Time-dependent ^{1}H NMR spectral changes of (a) $\mathbf{1}_C$ and (b) $\mathbf{3}_C$ (500 MHz, degassed $CDCl_3$, 25 °C, 0.50 mM) in the presence of $\mathbf{T}_{AA}$ (0.25 mM) upon irradiation of light (> 400 nm) for 120 s (c and d), respectively. (e) Possible mechanism for fast photodimerisation of $\mathbf{3}_C$ (0.50 mM) in the presence of $\mathbf{T}_{AA}$ (0.25 mM) in $CDCl_3$ at 25 °C. (f-g) ^{1}H NMR spectra (500 MHz, $CDCl_3$, 25 °C) of (f) $\mathbf{T}_{AA}\cdot(\mathbf{3}_C)_2$ after irradiation of light (> 400 nm) for 120 s (see ***Fig. S36a***) and (g) isolated carboxylic acid mixtures. The isolation procedure is described in the general procedure (3-4). ∗ denotes the peak of 1,1,2,2-tetrachloroethane used as an internal standard.

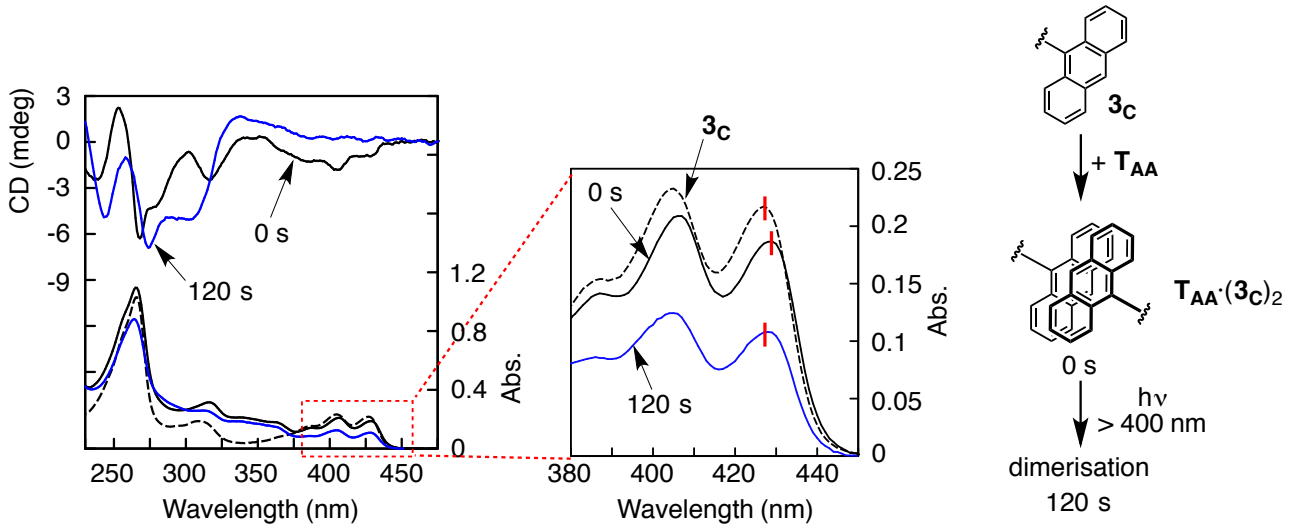

Fig. S38. Absorption spectrum of $\mathbf{3}_{\mathbf{C}}$ (0.50 mM, black dotted line) in $CDCl_3$, and time-dependent absorption and CD spectral changes of $\mathbf{3}_{\mathbf{C}}$ (0.50 mM) in the presence of $\mathbf{T}_{\mathbf{AA}}$ (0.25 mM) in degassed $CDCl_3$ before (0 s) and after (120 s) irradiation of light (> 400 nm). Cell length = 0.1 mm.

14. Supporting References

S1 C.-W. Wan, A. Burghart, J. Chen, F. Bergstrom, L. B.-Å. Johansson, M. F. Wolford, T. G. Kim, M. R. Topp, R. M. Hochstrasser and K. Burgess, *Chem. - Eur. J.*, 2003, **9**, 4430-4441.

S2 T. Maeda, Y. Furusho, S.-i. Sakurai, J. Kumaki, K. Okoshi and E. Yashima, *J. Am. Chem. Soc.*, 2008, **130**, 7938-7945.

S3 Y. Tanaka, H. Katagiri, Y. Furusho and E. Yashima, *Angew. Chem., Int. Ed.*, 2005, **44**, 3867-3870.

S4 CrystalClear, Version 1.36; Molecular Structure Corporation: The Woodlands, TX, 2000 and Rigaku Corporation: Tokyo, Japan.

S5 M. C. Burla, R. Caliandro, M. Camalli, B. Carrozzini, G. L. Cascarano, L. De Caro, C. Giacovazzo, G. Polidori and R. Spagna, *J. Appl. Crystallogr.*, 2005, **38**, 381-388

S6 G. M. Sheldrick, SHELXL-97: Program for the Refinement of Crystal Structures; University of Göttingen, Göttingen, Germany, 1997.

S7 G. M. Sheldrick, *Acta Crystallogr.,* 2008, **A64**, 112-122.

S8 K. Wakita, *Yadokari-XG,* Program for Crystal Structure Analysis, 2000.

S9 C. Kabuto, S. Akine and E. Kwon, *J. Cryst. Soc. Jpn.*, 2009, **51**, 218-224.

S10 M. Thompson, ArgusLab, Planaria Software LLC, Seattle, WA, 1996.

S11 J. J. P. Stewart, *Mol. Model.*, 2007, **13**, 1173-1213.

S12 J. J. P. Stewart, *MOPAC2012*, Stewart Computational Chemistry, Colorado Springs, CO, USA, http://openmopac.net/, 2012.

S13 M. J. Frisch, G. W. Trucks, H. B. Schlegel, G. E. Scuseria, M. A. Robb, J. R. Cheeseman, G. Scalmani, V. Barone, B. Mennucci, G. A. Petersson, H. Nakatsuji, M. Caricato, X. Li, H. P. Hratchian, A. F. Izmaylov, J. Bloino, G. Zheng, J. L. Sonnenberg, M. Hada, M. Ehara, K. Toyota, R. Fukuda, J. Hasegawa, M. Ishida, T. Nakajima, Y. Honda, O. Kitao, H. Nakai, T. Vreven, J. A. Montgomery, Jr., J. E. Peralta, F. Ogliaro, M. Bearpark, J. J. Heyd, A. Brothers, K. N. Kudin, V. N. Staroverov, R. Kobayashi, J. Normand, K. Raghavachari, A. Rendell, J. C. Burant, S. S. Iyengar, J. Tomasi, M. Cossi, N. Rega, N. J. Millam, M. Klene, J. E. Knox, J. B. Cross, V. Bakken, C. Adamo, J. Jaramillo, R. Gomperts, R. E. Stratmann, O. Yazyev, A. J. Austin, R. Cammi, C. Pomelli, J. W. Ochterski, R. L. Martin, K. Morokuma, V. G. Zakrzewski, G.A. Voth, P. Salvador, J. J. Dannenberg, S. Dapprich, A. D. Daniels, Ö. Farkas, J. B. Foresman, J. V. Ortiz, J. Cioslowski, D. J. Fox, D. J. *Gaussian 09* Gaussian, Inc., Wallingford CT, 2009.

15. Spectroscopic Data

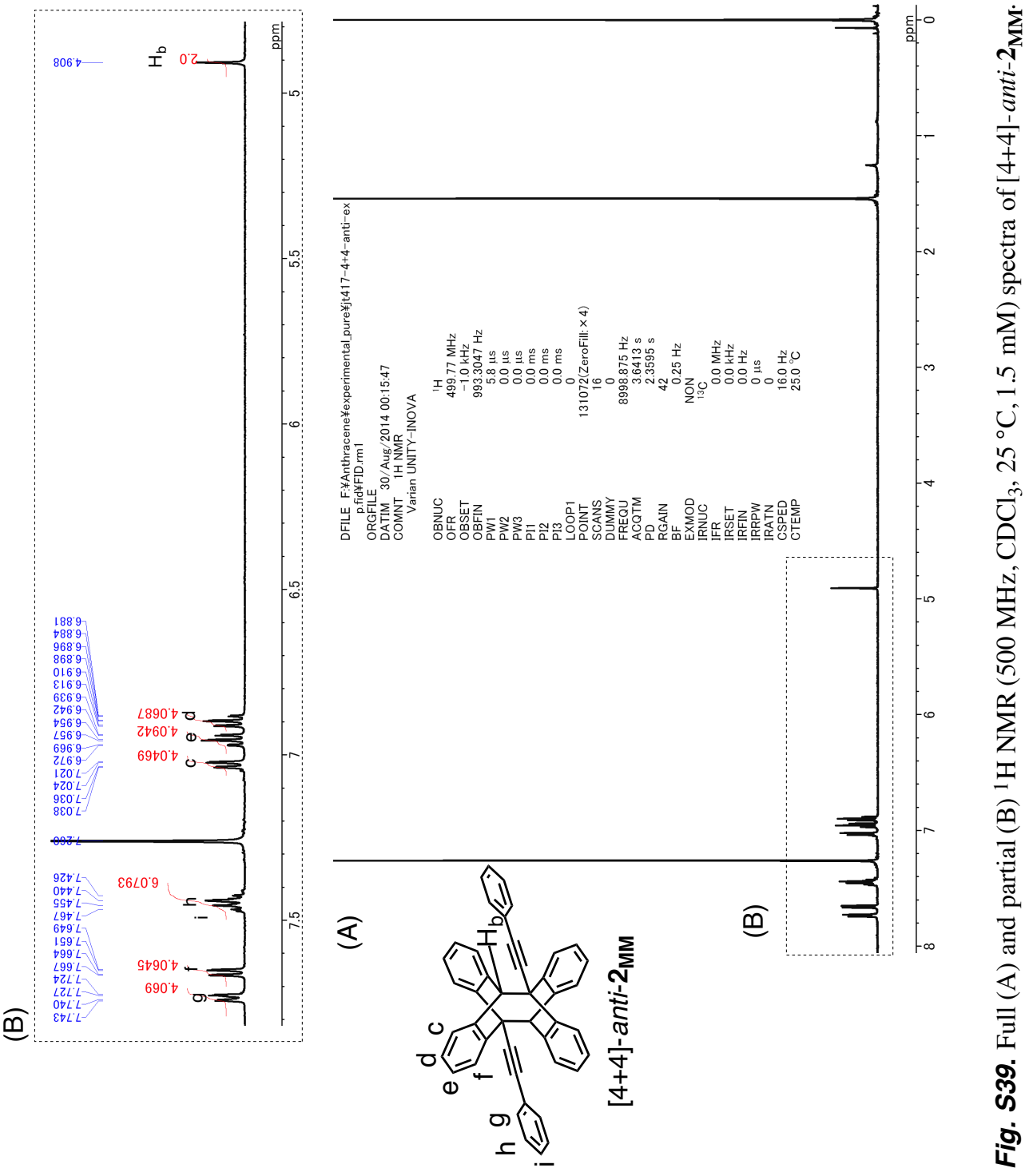

Fig. S39. Full (A) and partial (B) ^{1}H NMR (500 MHz, $CDCl_3$, 25 °C, 1.5 mM) spectra of [4+4]-*anti*-$\mathbf{2_{MM}}$.

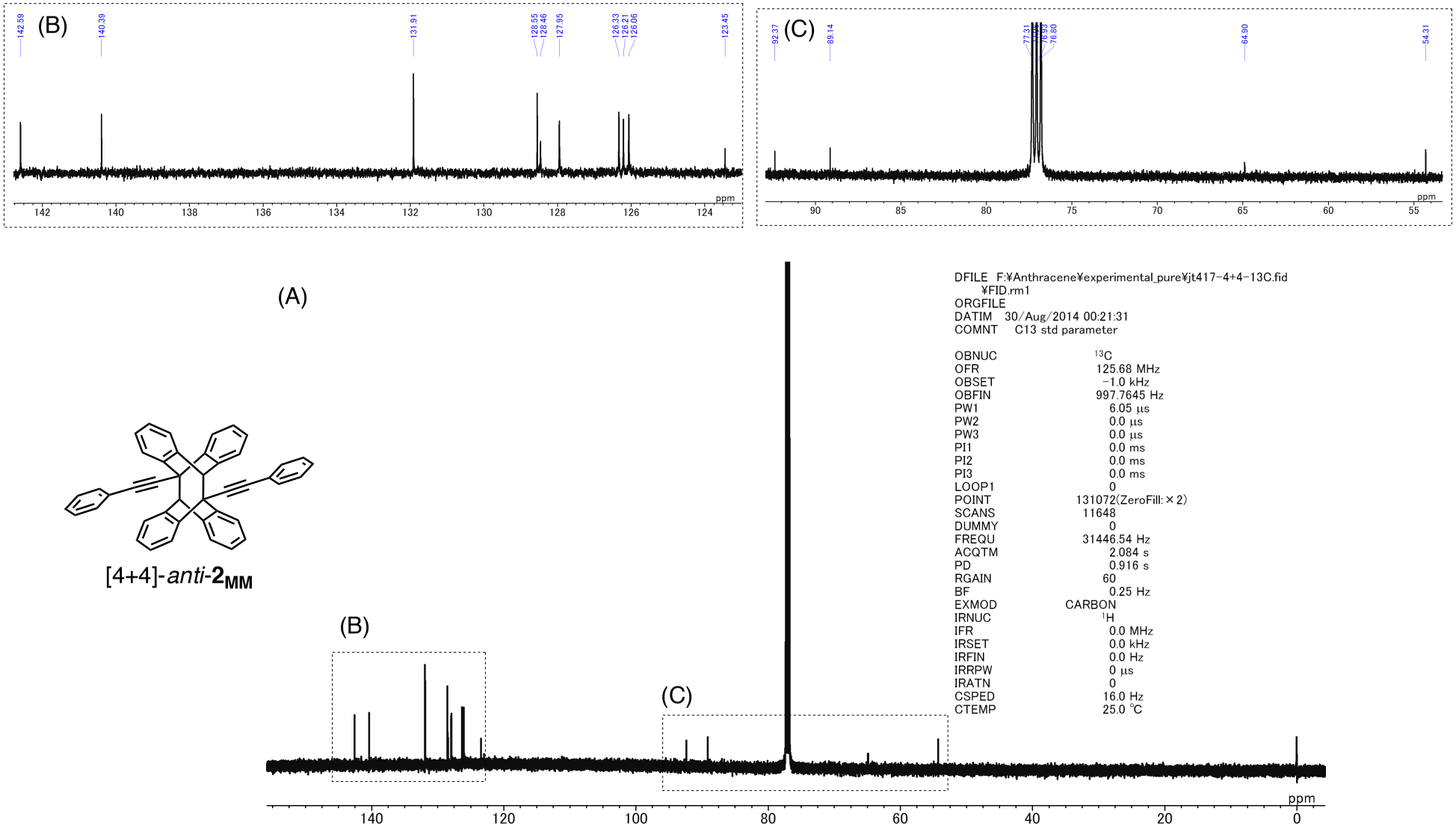

Fig. S40. Full (A) and partial (B and C) ^{13}C NMR (125 MHz, $CDCl_3$, 1.5 mM) spectra of [4+4]-*anti*-$\mathbf{2_{MM}}$.

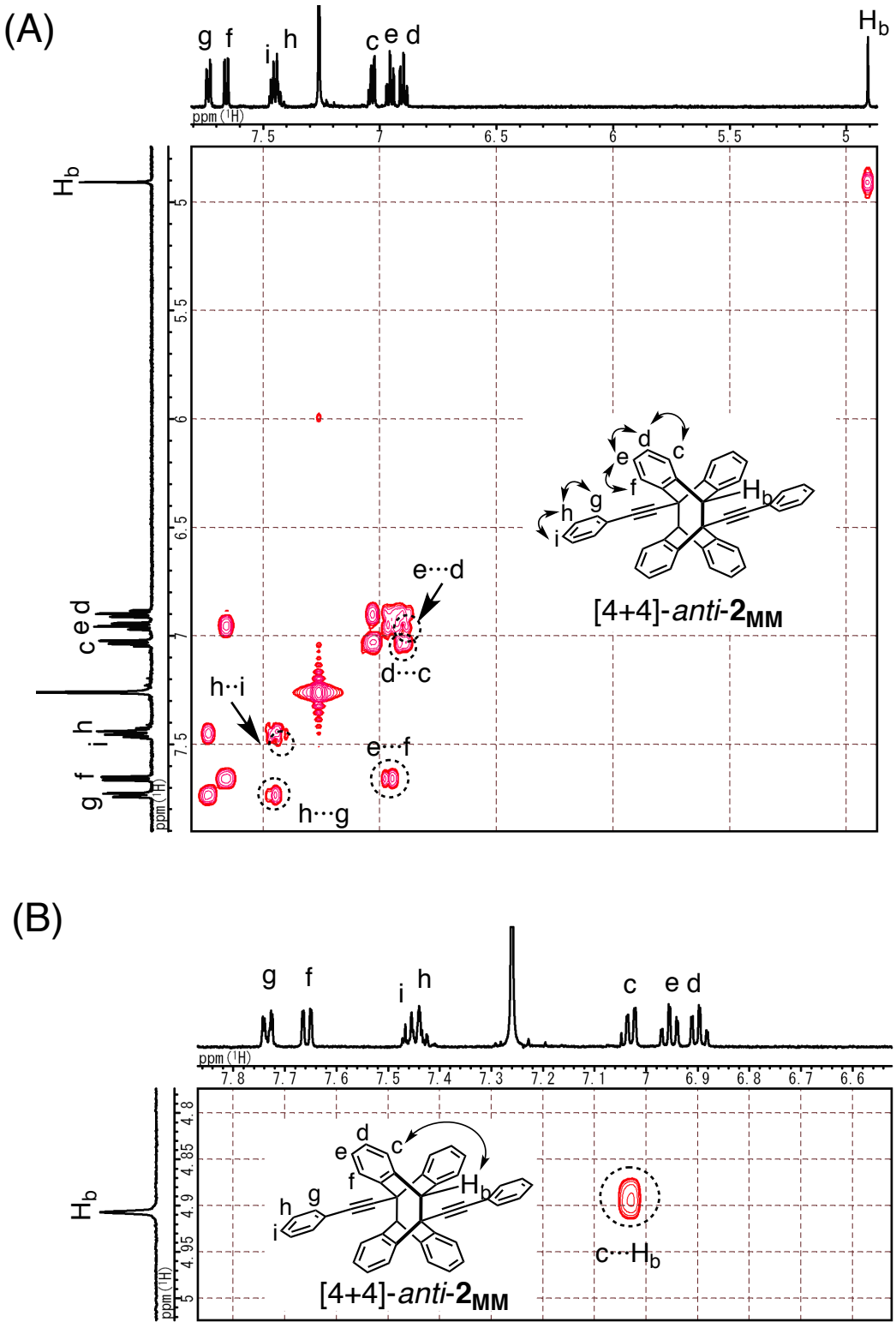

Fig. S41. (A) *g*COSY and (B) partial NOESY (mixing time = 500 ms) spectra of [4+4]-*anti*-$\mathbf{2_{MM}}$ (500 MHz, $CDCl_3$, 25 °C, 2.4 mM).

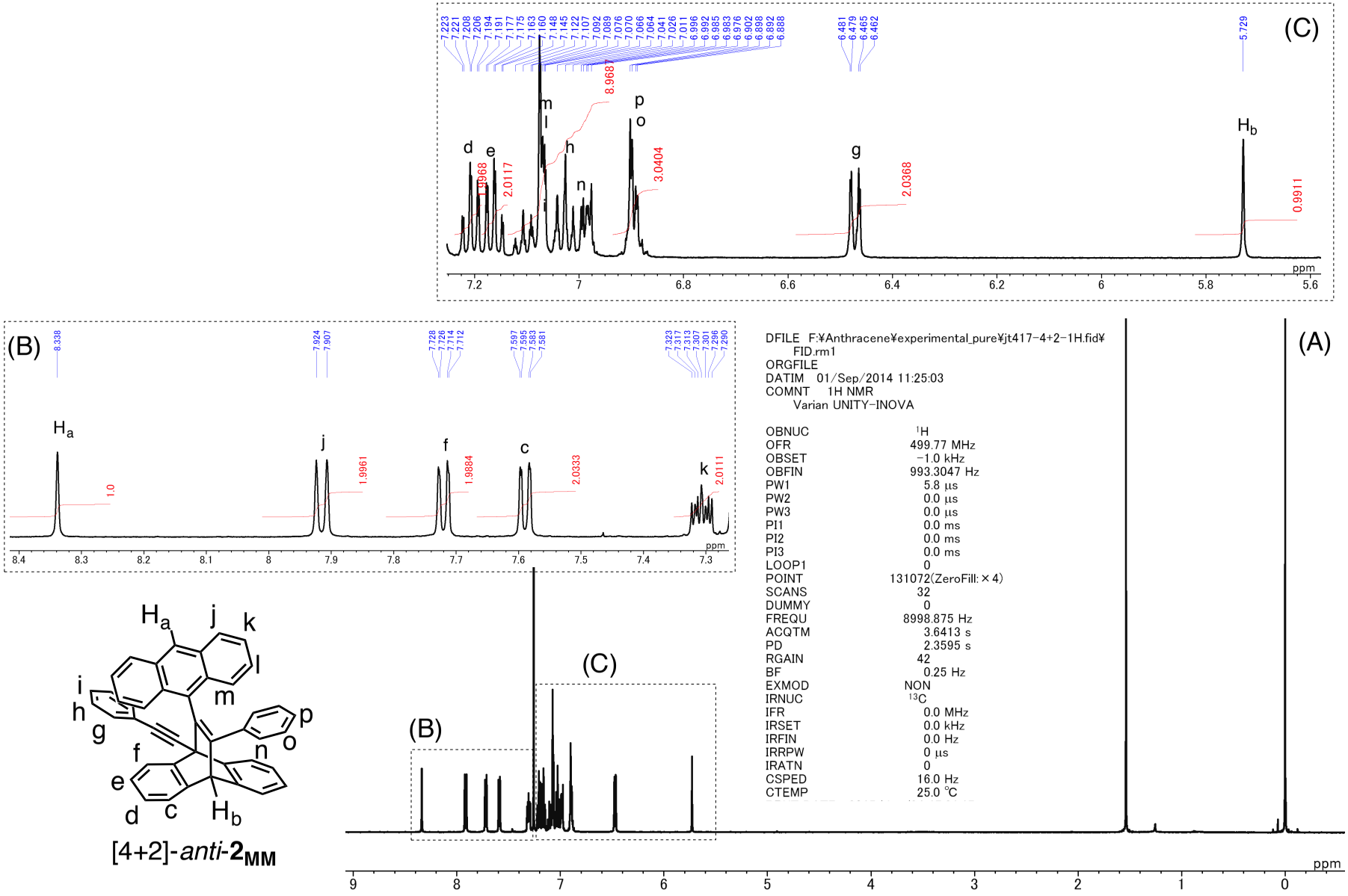

Fig. S42. Full (A) and partial (B and C) ^{1}H NMR (500 MHz, $CDCl_3$, 25 °C, 5.0 mM) spectra of [4+2]-*anti*-$\mathbf{2_{MM}}$.

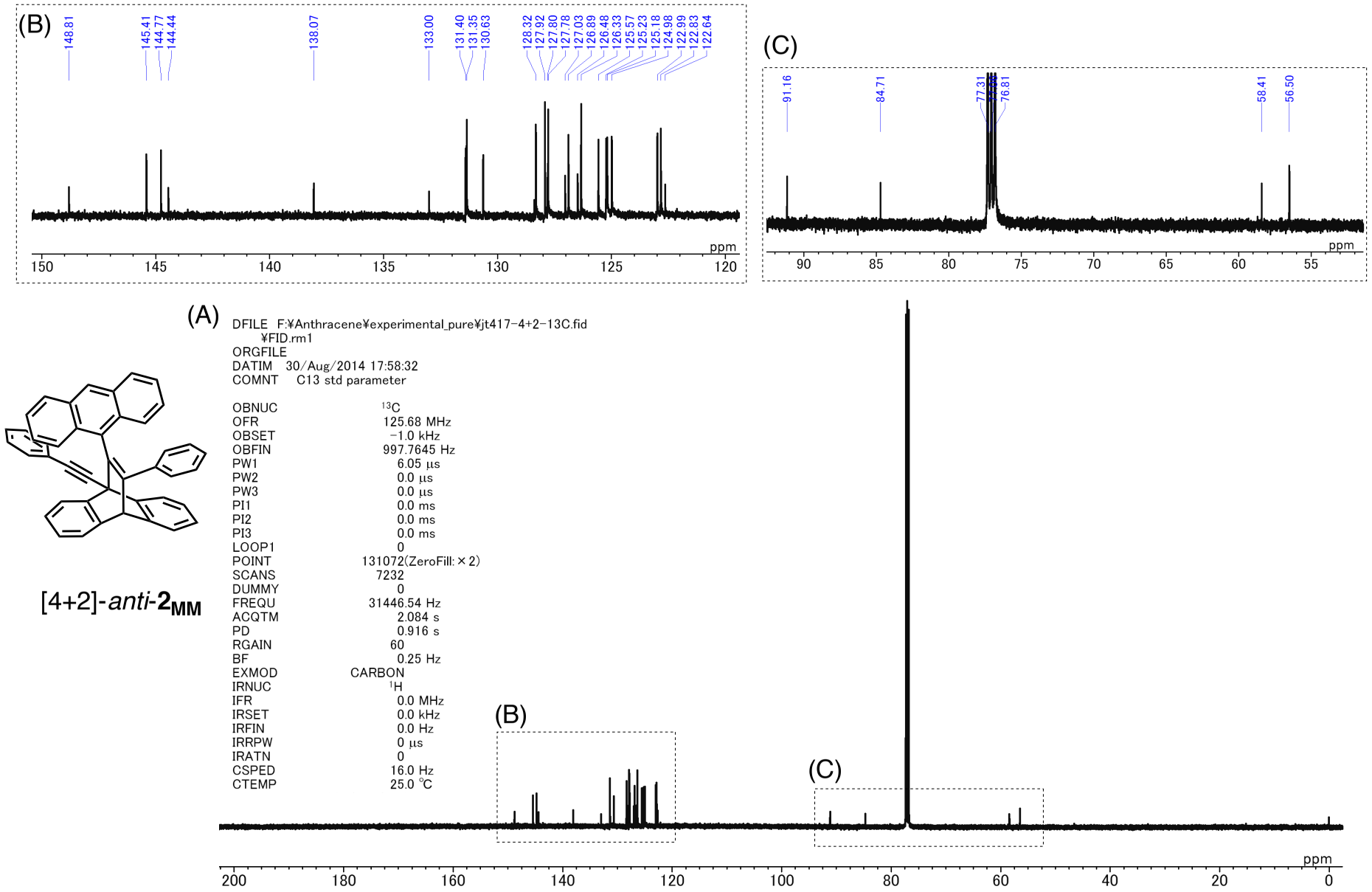

Fig. S43. Full (A) and partial (B and C) ^{13}C NMR (125 MHz, $CDCl_3$, 25 °C, 5.0 mM) spectra of [4+2]-*anti*-**2**$_{\mathbf{MM}}$.

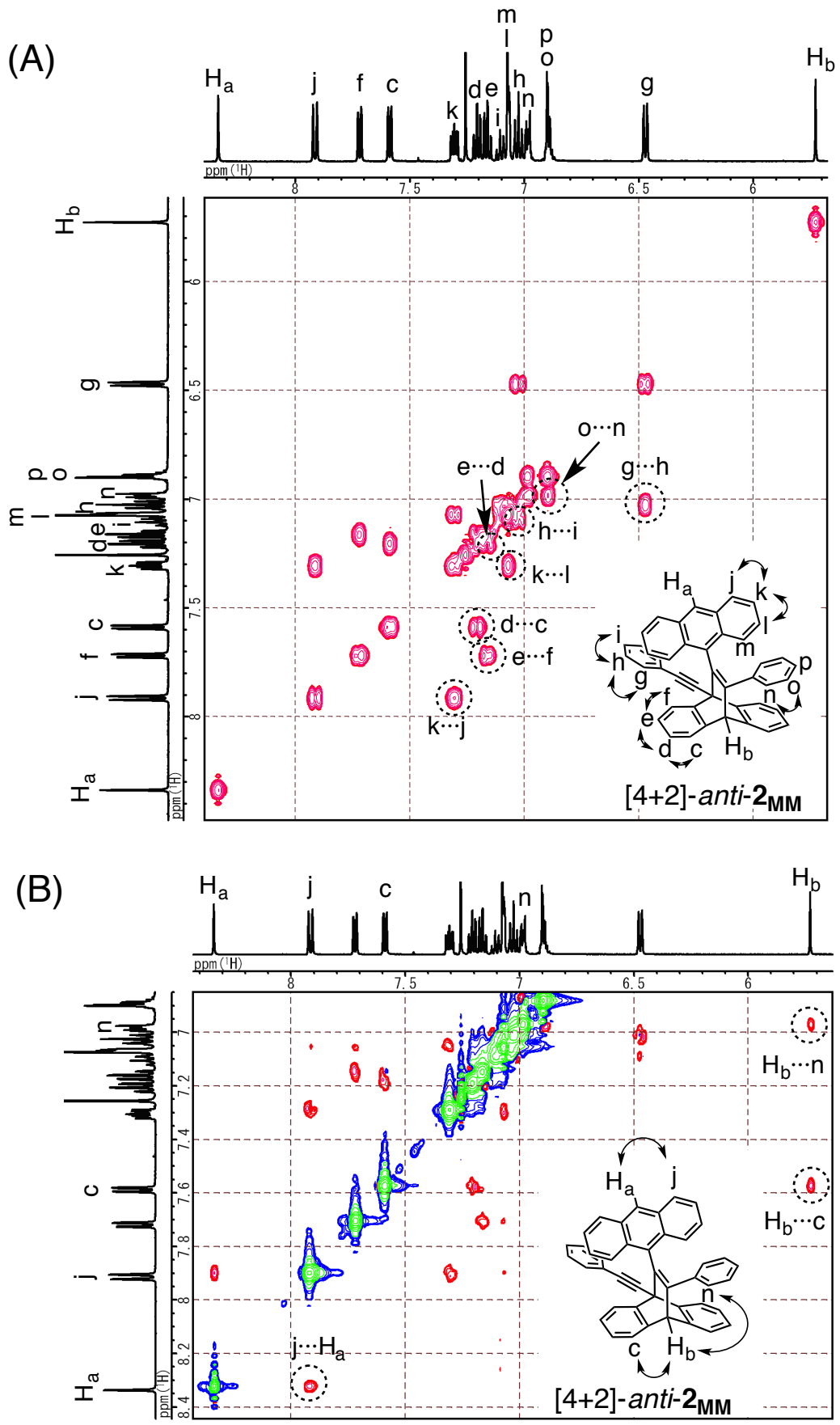

Fig. S44. (A) *g*COSY and (B) partial NOESY (mixing time = 500 ms) spectra of [4+2]-*anti*-$\mathbf{2_{MM}}$ (500 MHz, $CDCl_3$, 25 °C, 4.1 mM).

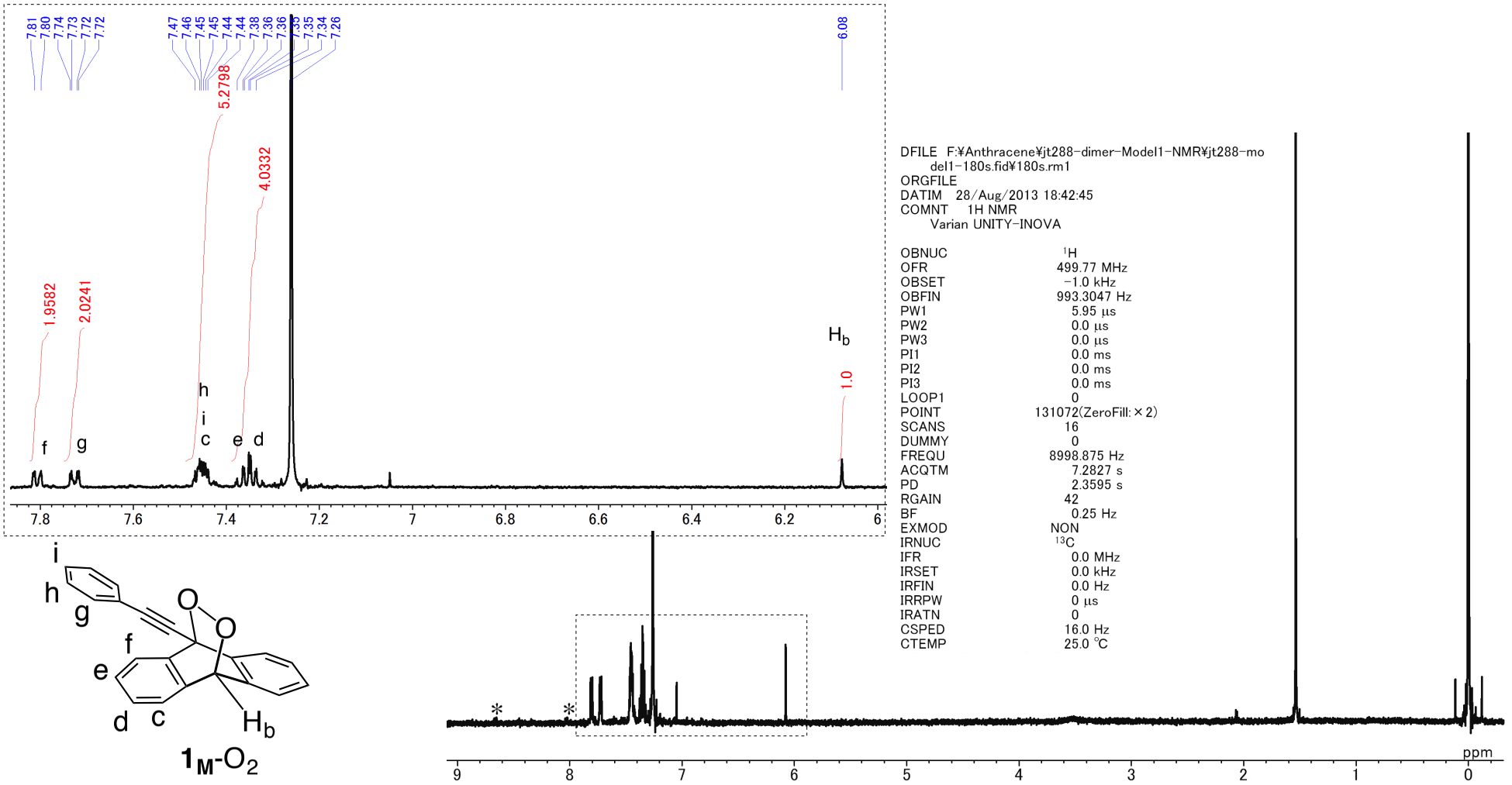

Fig. S45. Full and partial ^{1}H NMR (500 MHz, $CDCl_3$, 25 °C) spectra of a mixture of $\mathbf{1_M}$-O_2 (0.47 mM) and $\mathbf{1_M}$ (0.030 mM). * denotes peaks due to $\mathbf{1_M}$.

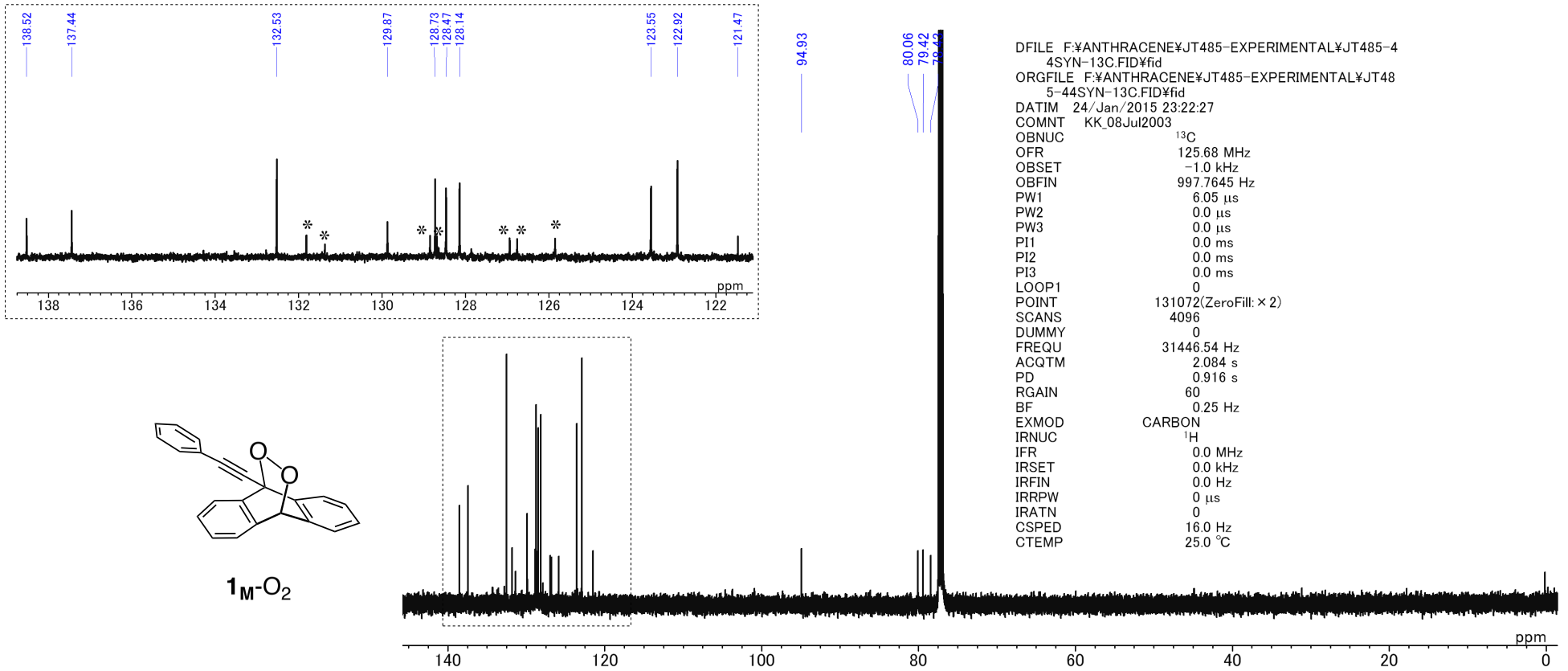

$\mathbf{1_M}$-O_2

Fig. S46. Full and partial ^{13}C NMR (125 MHz, $CDCl_3$, 25 °C) spectra of a mixture of $\mathbf{1_M}$-$\mathbf{O_2}$ (6.0 mM) and $\mathbf{1_M}$ (0.40 mM).
∗ denotes peaks due to $\mathbf{1_M}$ (see ***Fig. S48***).

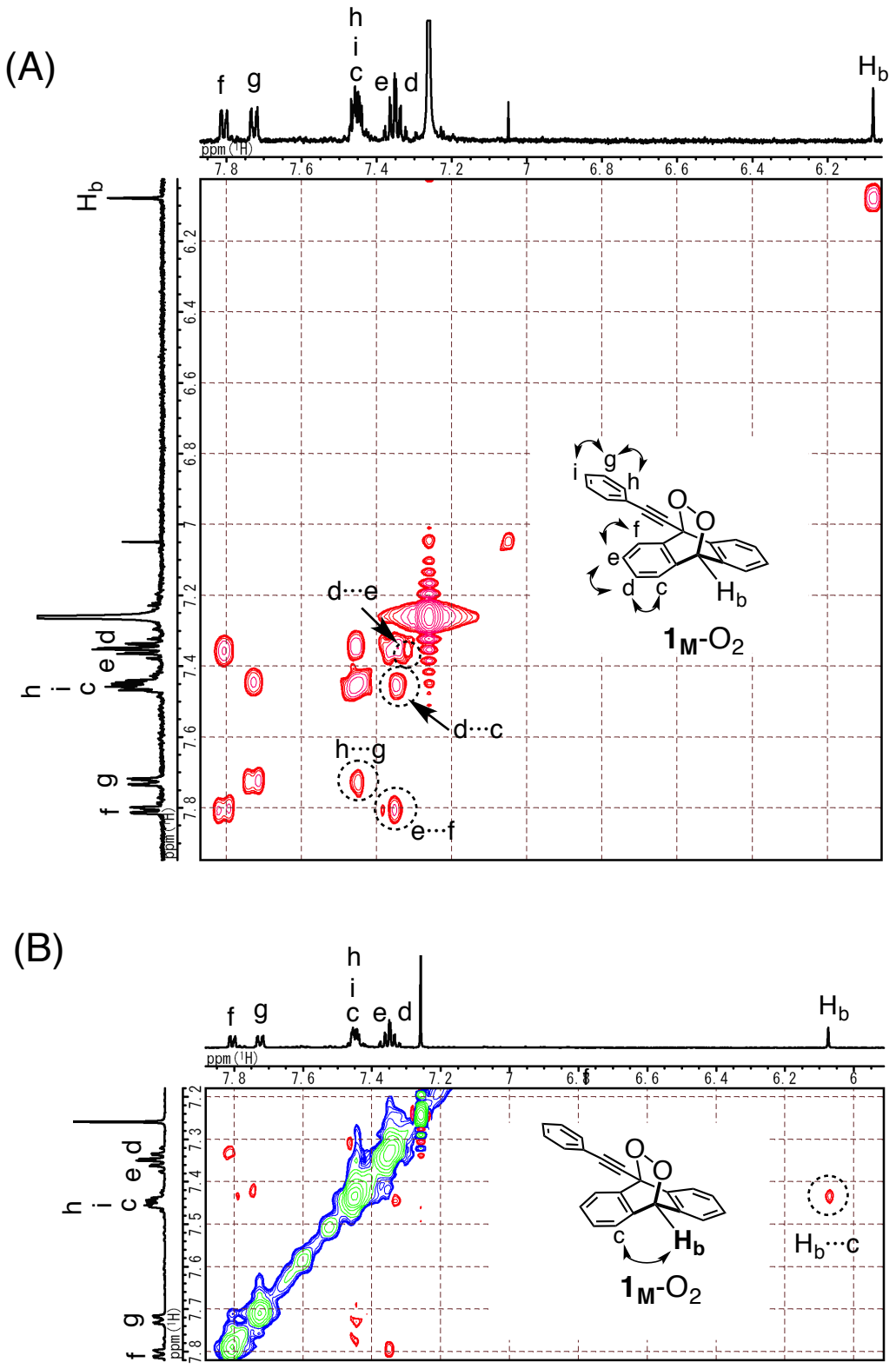

Fig. S47. (A) *g*COSY spectrum of a mixture of $\mathbf{1_M}$-O_2 (0.47 mM) and $\mathbf{1_M}$ (0.030 mM), and (B) partial NOESY (mixing time = 500 ms) spectrum of a mixture of $\mathbf{1_M}$-O_2 (6.6 mM) and $\mathbf{1_M}$ (0.40 mM) in $CDCl_3$ at 25 °C.

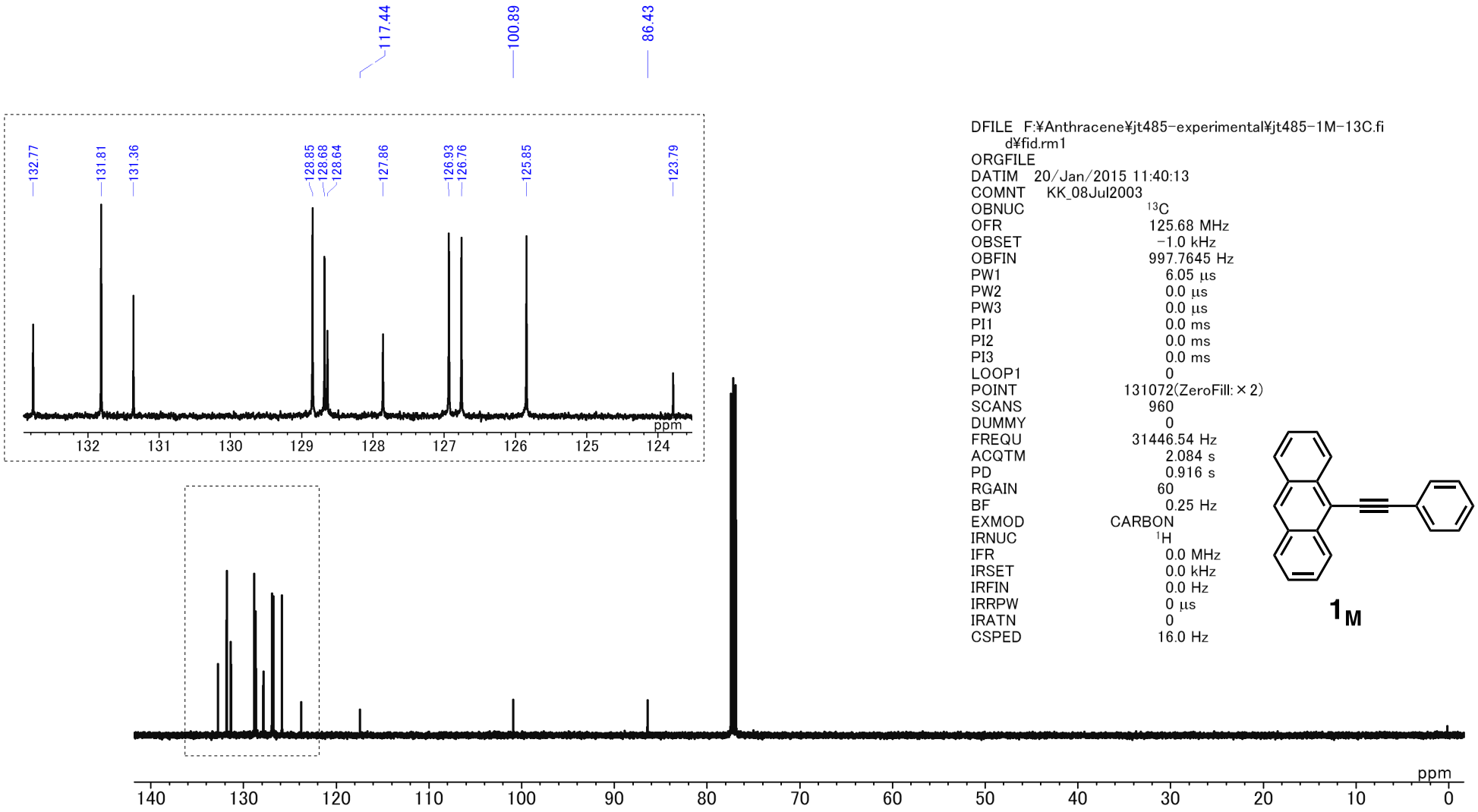

Fig. S48. Full and partial ^{13}C NMR (125 MHz, $CDCl_3$, 25 °C, 20 mM) spectra of $\mathbf{1_M}$.

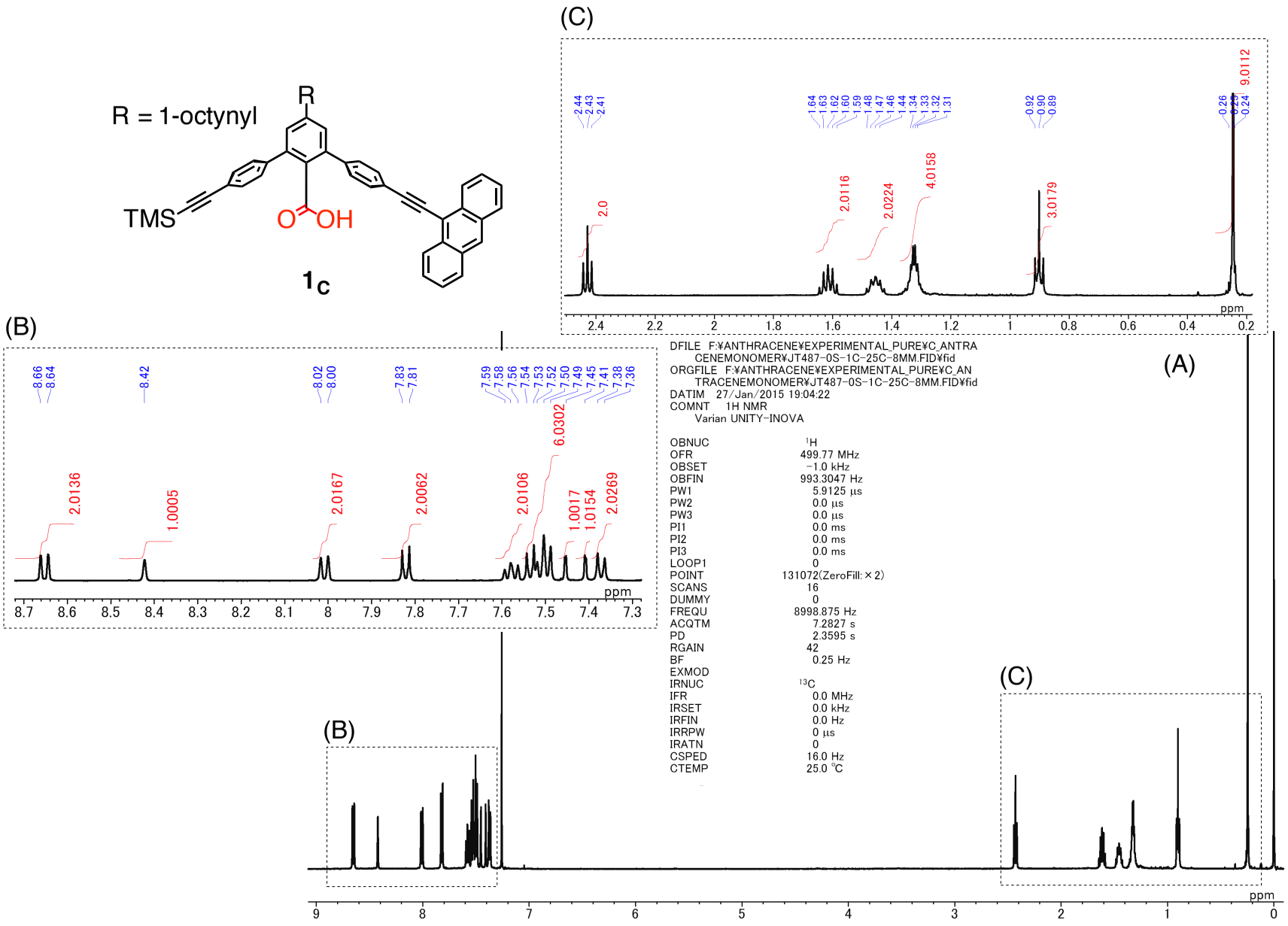

Fig. S49. Full (A) and partial (B and C) ^{1}H NMR (500 MHz, $CDCl_3$, 8.0 mM, 25 °C) spectra of $\mathbf{1_C}$.

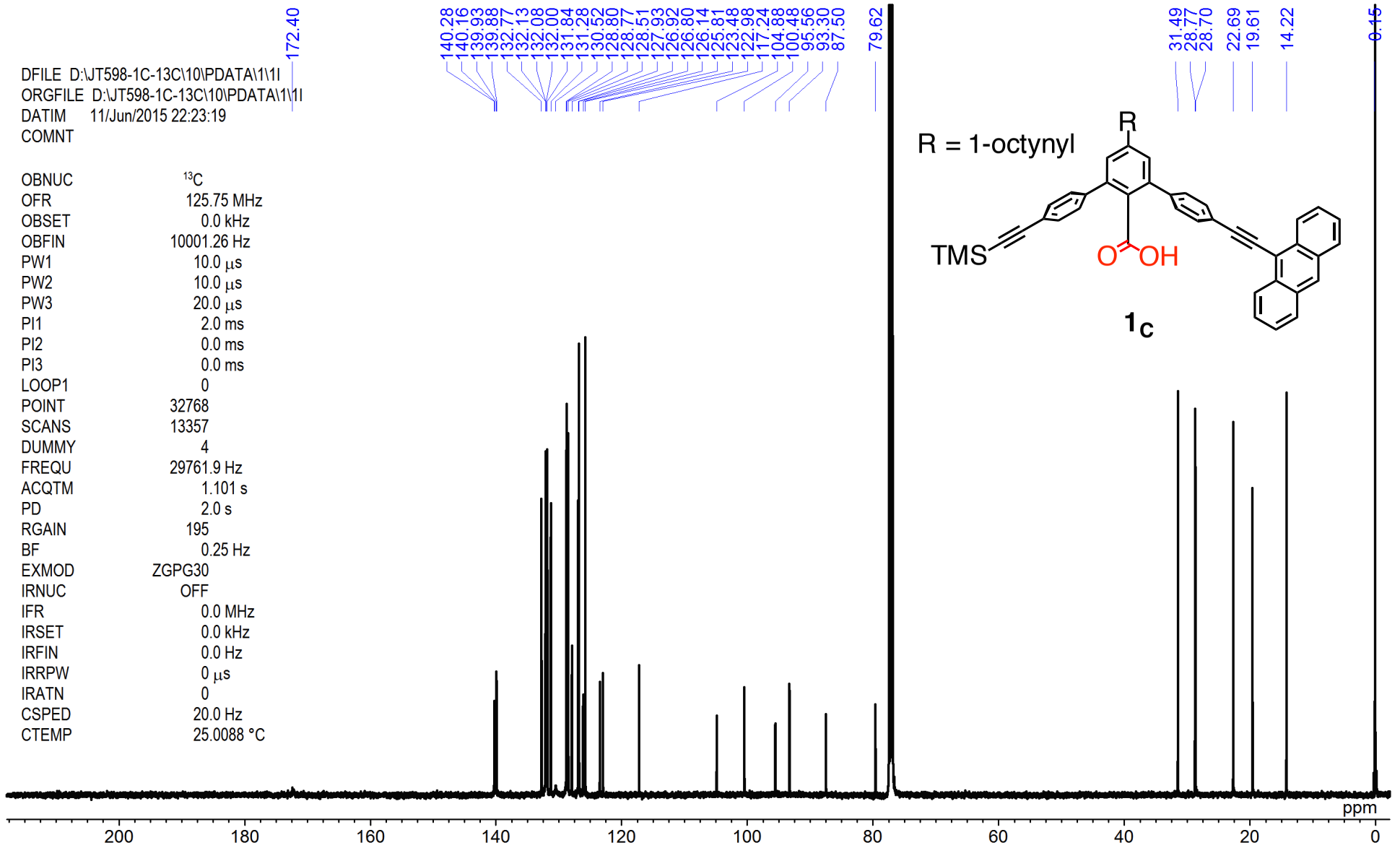

Fig. S50. Full ^{13}C NMR (125 MHz, $CDCl_3$, 25 °C, 8.0 mM) spectrum of $\mathbf{1_C}$.

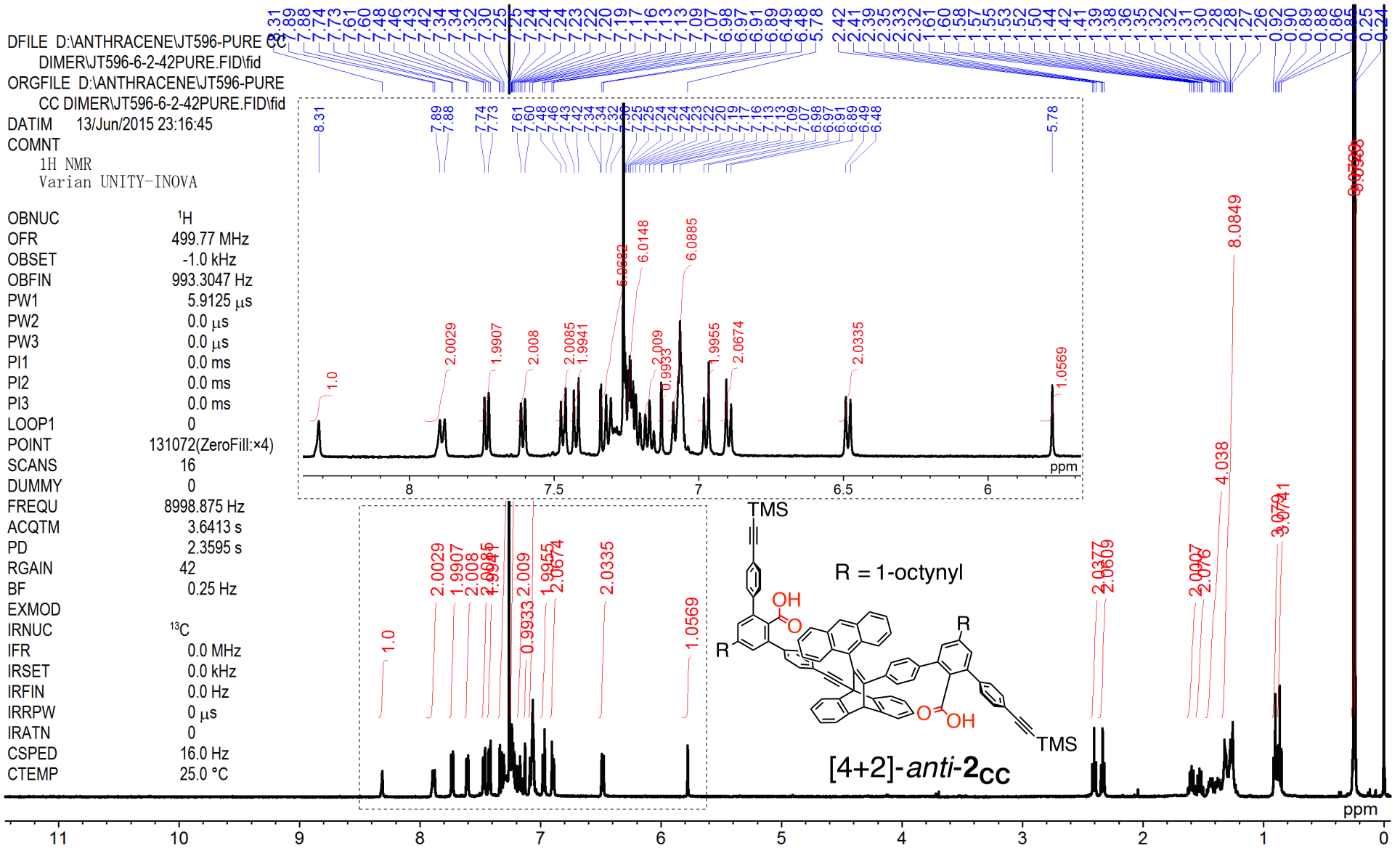

Fig. S51. Full and partial ^{1}H NMR (500 MHz, $CDCl_3$, 25 °C, 4.6 mM) spectra of [4+2]-*anti*-$\mathbf{2_{CC}}$.

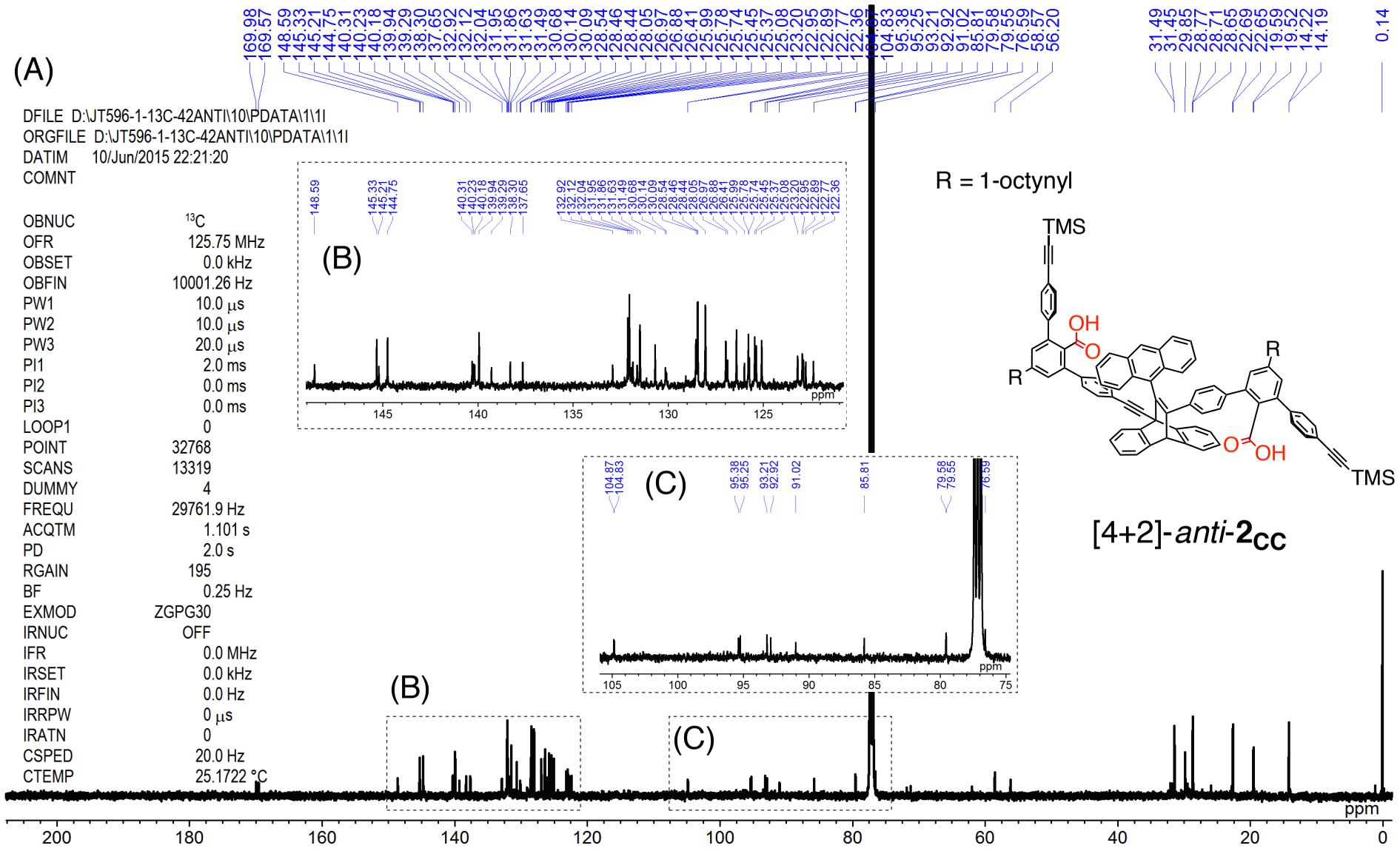

Fig. S52. Full (A) and partial (B and C) ^{13}C NMR (125 MHz, $CDCl_3$, 25 °C, 4.6 mM) spectra of [4+2]-*anti*-$\mathbf{2_{CC}}$.

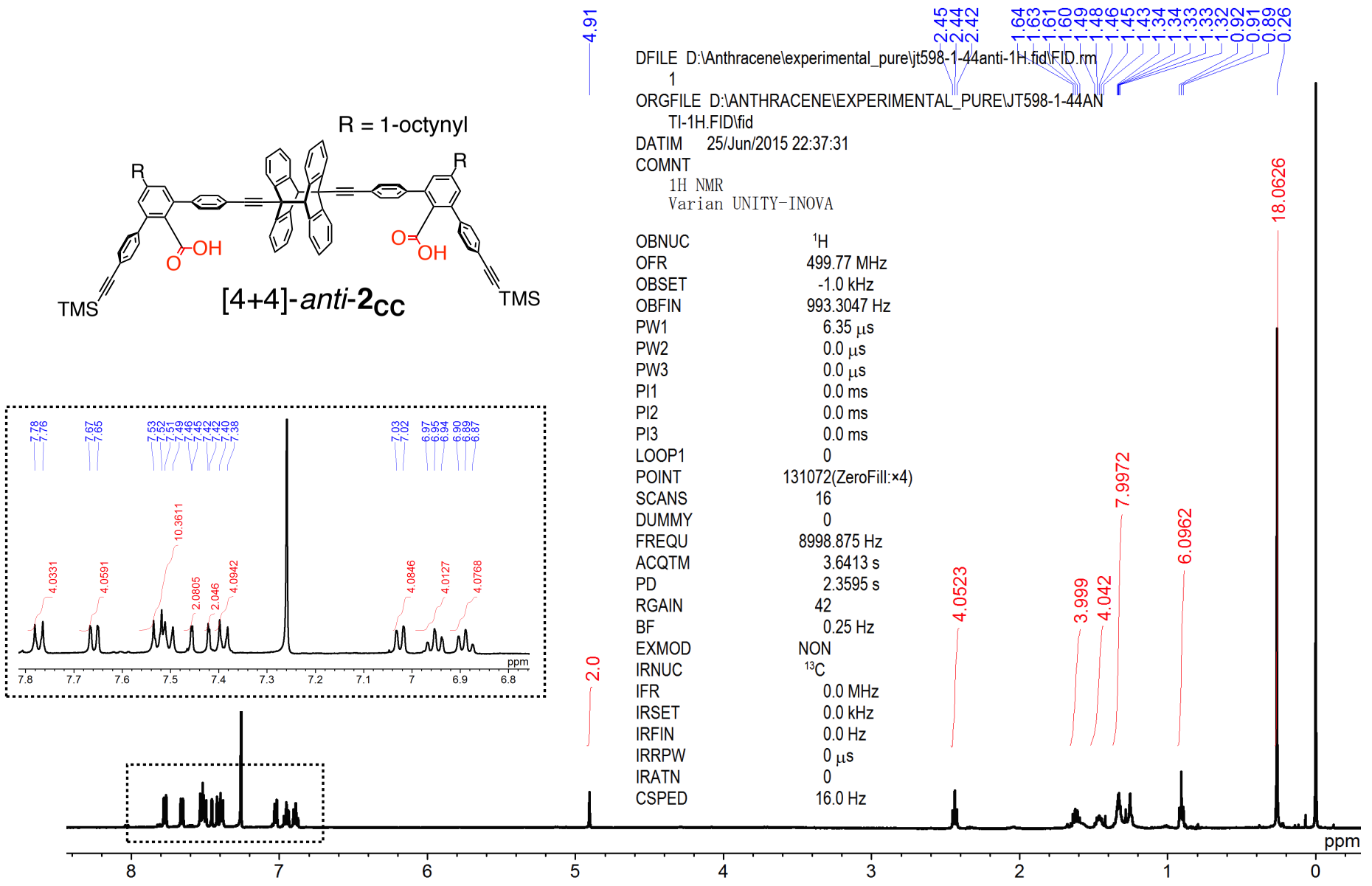

Fig. S53. Full and partial ^{1}H NMR (500 MHz, $CDCl_3$, 25 °C, 3.1 mM) spectra of [4+4]-*anti*-$\mathbf{2_{CC}}$.

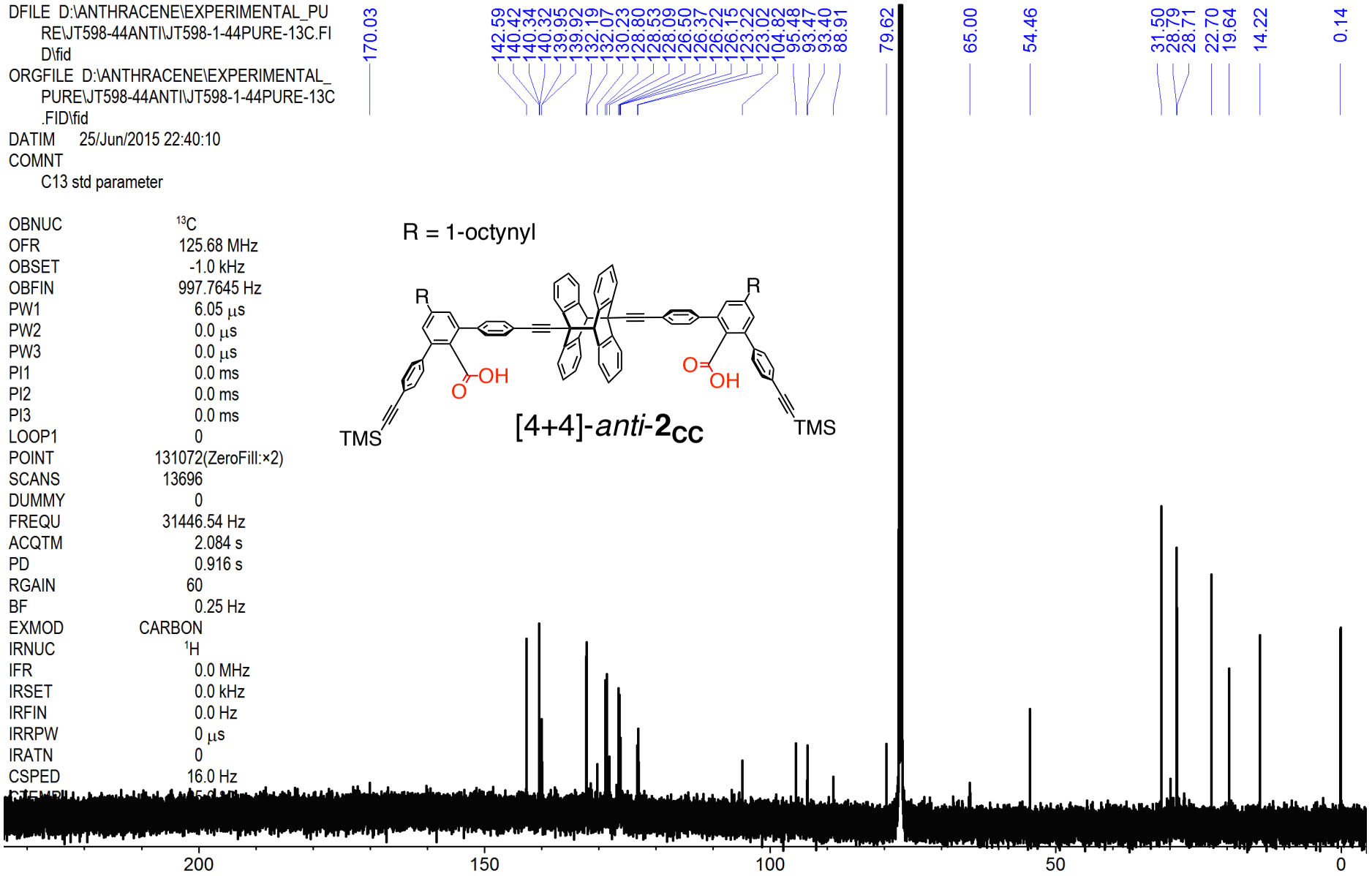

Fig. S54. ^{13}C NMR (125 MHz, $CDCl_3$, 25 °C, 3.1 mM) spectrum of [4+4]-*anti*-$\mathbf{2_{CC}}$.

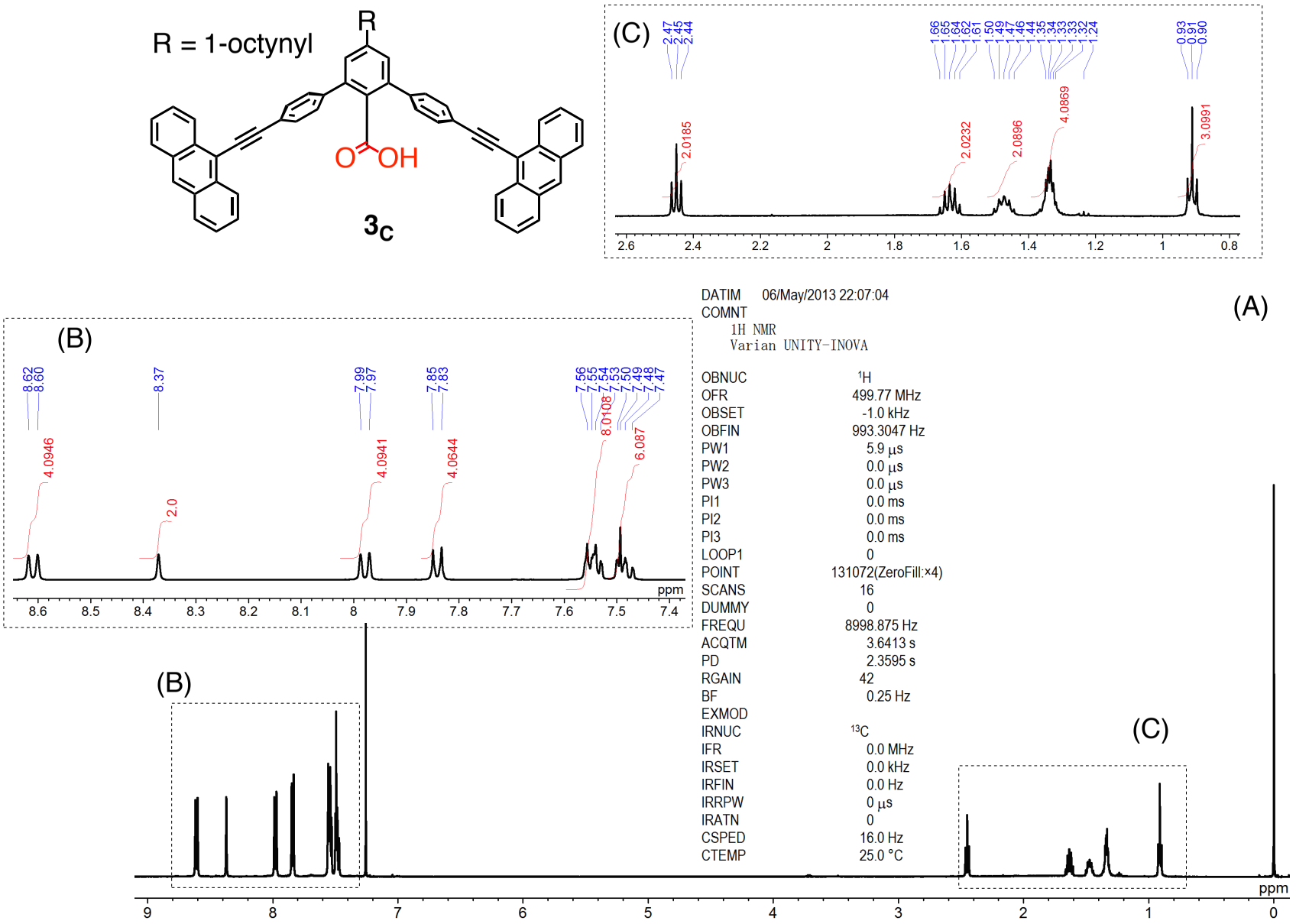

Fig. S55. Full (A) and partial (B and C) ^{1}H NMR (500 MHz, $CDCl_3$, 13 mM, 25 °C) spectra of $\mathbf{3_C}$.

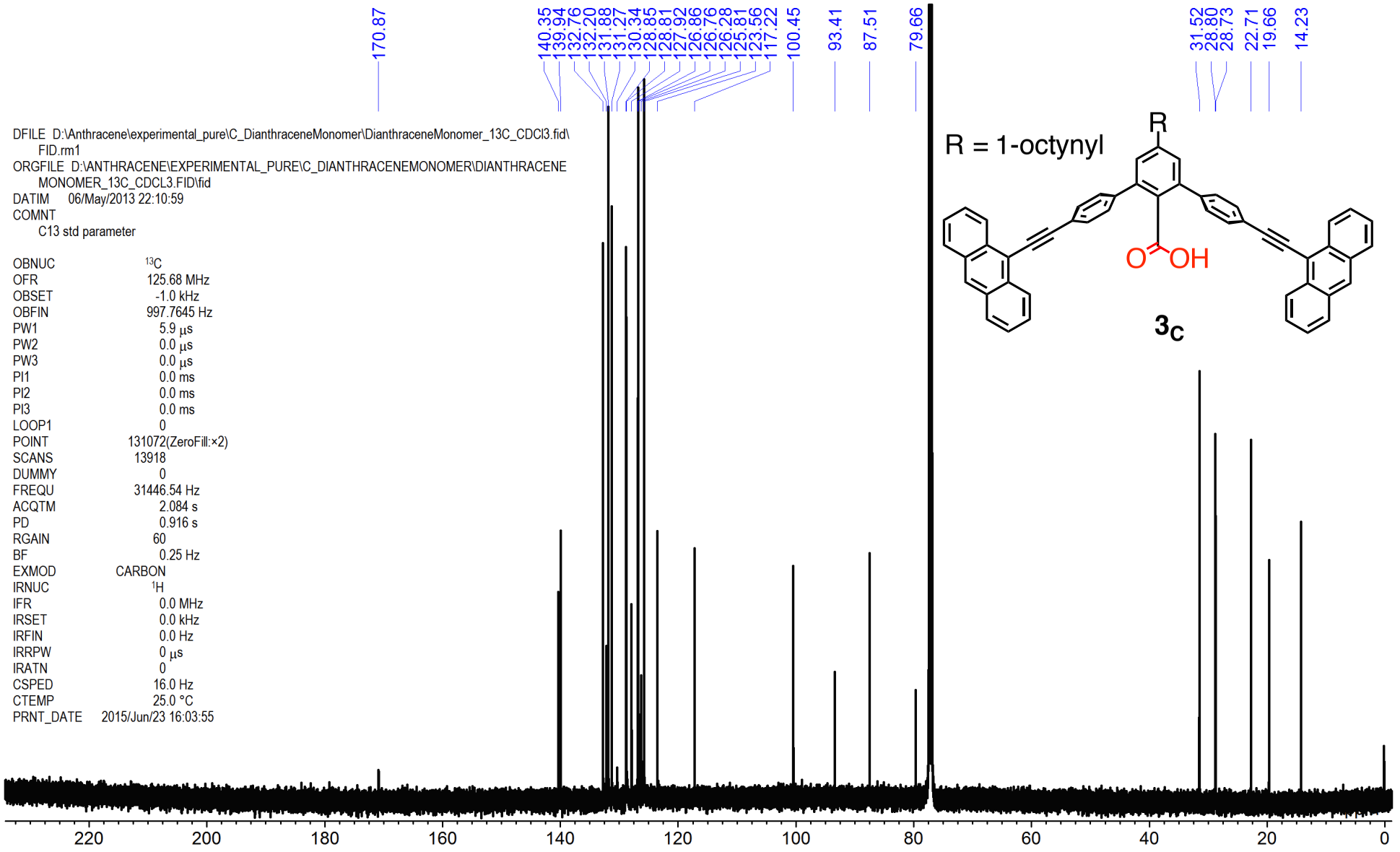

Fig. S56. ^{13}C NMR (125 MHz, $CDCl_3$, 25 °C, 13 mM) spectrum of $\mathbf{3_C}$.

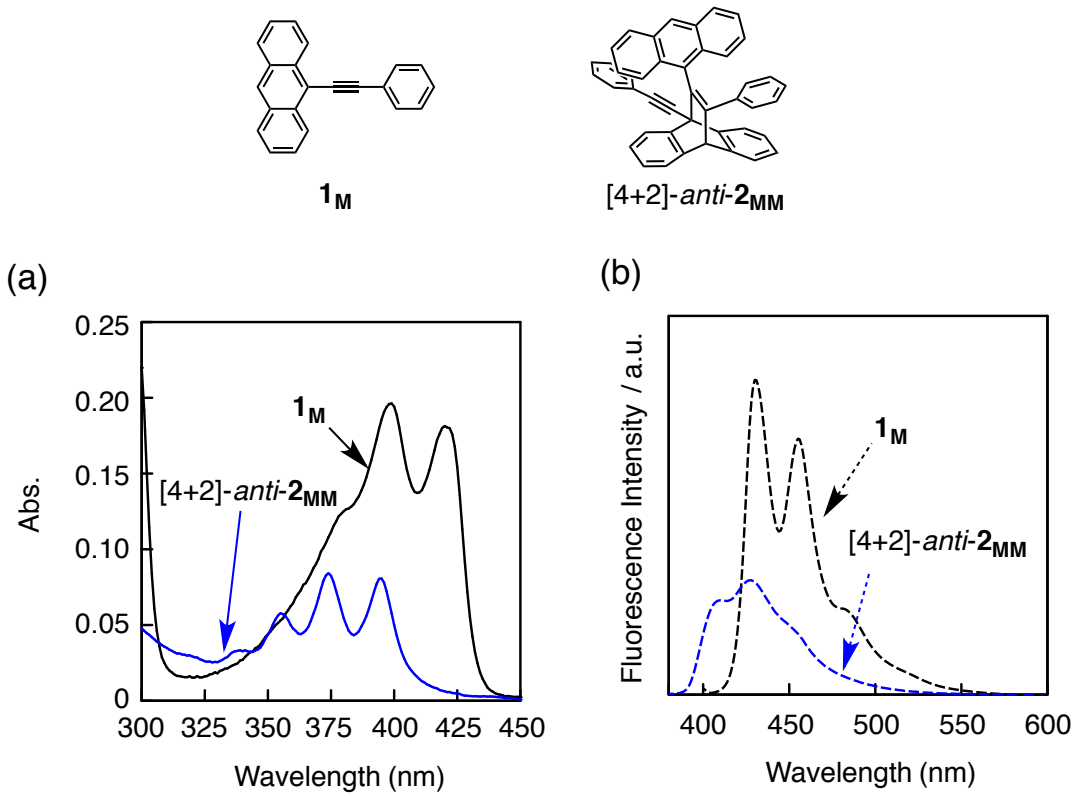

Fig. S57. (a) Absorption and (b) fluorescence spectra of $\mathbf{1}_{M}$ (12 μM) and [4+2]-*anti*-$\mathbf{2}_{MM}$ (11 μM) in $CDCl_3$ at ambient temperature. Excited wavelength: 399 nm ($\mathbf{1}_{M}$) and 374 nm ([4+2]-*anti*-$\mathbf{2}_{MM}$). Cell length = 1 cm.

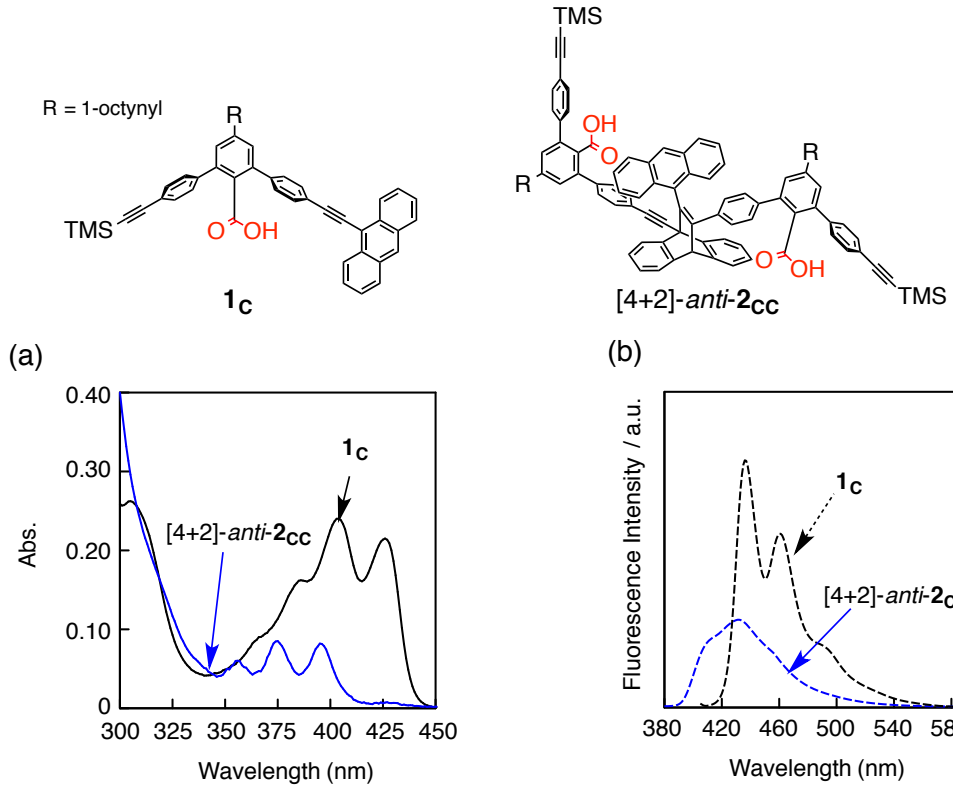

Fig. S58. (a) Absorption and (b) fluorescence spectra of $\mathbf{1}_{C}$ (10 μM) and [4+2]-*anti*-$\mathbf{2}_{MM}$ (10 μM) in $CDCl_3$ at ambient temperature. Excited wavelength: 404 nm ($\mathbf{1}_{C}$) and 375 nm ([4+2]-*anti*-$\mathbf{2}_{CC}$). Cell length = 1 cm.

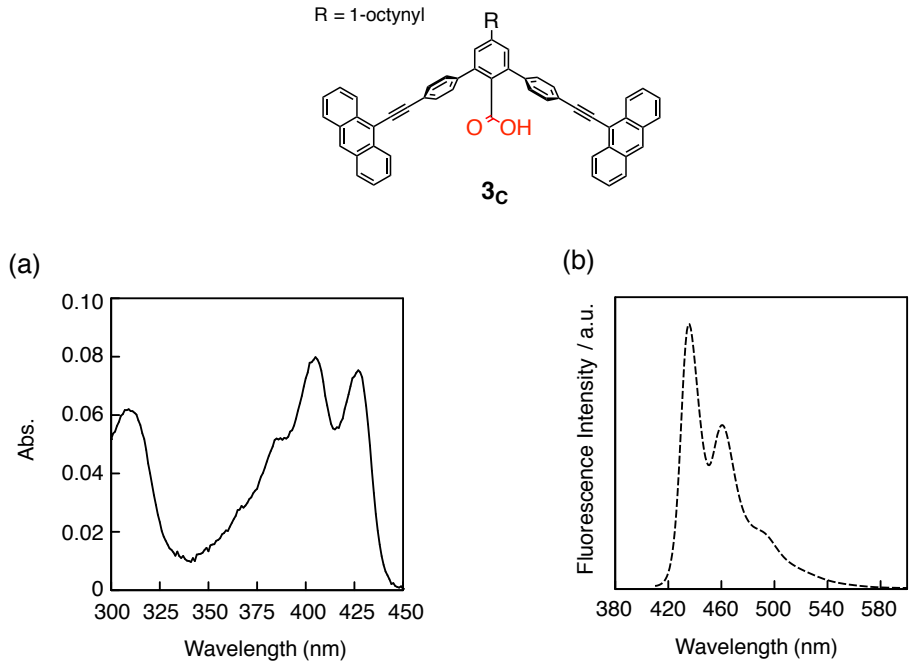

Fig. S59. (a) Absorption and (b) fluorescence spectra of $\mathbf{3_C}$ (3 μM) in $CDCl_3$ at ambient temperature. Excited wavelength: 405 nm. Cell length = 1 cm.